MEASUREMENT OF WATER CONTENT IN POROUS MEDIA UNDER GEOTHERMAL FLUID FLOW CONDITIONS

A DISSERTATION

SUBMITTED TO THE DEPARTMENT OF PETROLEUM ENGINEERING

AND THE COMMITTEE ON GRADUATE STUDIES

OF STANFORD UNIVERSITY

IN PARTIAL FULFILLMENT OF THE REQUIREMENTS

FOR THE DEGREE OF

DOCTOR OF PHILOSOPHY

by

Hsiu-Kuo Chen

November 1976

ACKNOWLEDGEMENT

The author wishes to thank his adviser, Dr. Henry J. Ramey, Jr., for his advice and encouragement. The author would also like to thank Dr. Marshall B. Standing for his counsel and assistance in many aspects of the experimental work. Thanks are also extended to Dr. William E. Brigham, Dr. Sullivan S. Marsden, Jr., and Dr. Frank G. Miller for serving on the author's reading committee.

The author wishes to express his sincere gratitude to Dr. Paul Baker and the Chevron Oil Field Research Company for contributions concerning the capacitance probe design, and Dr. S. C. Jones and the Marathon Oil Company for advice concerning the large Hassler-sleeve core holder.

Thanks are also due to Messrs. Jon Grim, Peter Gordon, Luke Meisenback, Mrs. Alice Mansourian, and Frank Peters for their assistance on the construction of the experimental apparatus.

The author is deeply grateful to his friends, Mr. Yu-Min Houng for his assistance in stabilizing the electronic circuit of the capacitance probe, and Mr. John Counsil for helpful discussions concerning this report.

The author would like to express his deepest appreciation to his wife, Yu-Mei, for constant encouragement and moral support during the years of graduate study.

This research was carried out under Research Grant No. AER-03490-A03, provided by the National Science Foundation. Financial support, provided by the National Science Foundation, is gratefully acknowledged.

ABSTRACT

The objectives of this study were: (1) to investigate methods for the in-situ measurement of water content in porous media, expressed as a volume fraction of the pore space; (2) to measure water content in the two-phase geothermal fluid flow and depletion experiments, and (3) to investigate salt deposition in boiling brine flow systems. Neither the measurement of water saturation in steam-water flow experiments nor salt deposition in porous media caused by boiling have received extensive study.

A review of available methods for measuring water content indicates that the capacitance probe is the most promising tool for measuring water saturation during high temperature steam-water flow in porous media. The capacitance probe designed by Baker[1] was selected for intensive study. Calibrations were made in two sand packs of different sand grain size filled with a steam-water mixture at high temperatures. Calibrations were also made in short synthetic consolidated sandstone cores filled with air-water mixtures at room temperature. The calibration curves led to conclusions that the capacitance probe readings were nearly independent of porous media type and operating temperature.

The water saturations in steady two-phase flow and depletion experiments were measured successfully with the capacitance

probe. From the mass flow rate, inlet water temperature, and temperature profiles for steady two-phase flow experiments, the relative permeabilities of steam and water were calculated. To demonstrate the technique, a portion of a steam-water relative permeability curve was constructed using the experimental saturation data.

Finally, a preliminary brine depletion study was conducted by producing water and steam from a core initially filled with a hot, compressed 12,000 ppm sodium chloride solution. The conclusions reached were: (1) salt deposition increased with distance from the closed end of the core, (2) the permeability of the core to nitrogen gas did not appear to be affected by the salt deposition for the given system, and (3) brines of higher concentration should be studied in future experiments.

I certify that I have read this thesis and that in my opinion it is fully adequate, in scope and quality, as a dissertation for the degree of Doctor of Philosophy.

(Principal Advisor)

I certify that I have read this thesis and that in my opinion it is fully adequate, in scope and quality, as a dissertation for the degree of Doctor of Philosophy.

(Petroleum Engineering)

I certify that I have read this thesis and that in my opinion it is fully adequate, in scope and quality, as a dissertation for the degree of Doctor of Philosophy.

(Petroleum Engineering)

I certify that I have read this thesis and that in my opinion it is fully adequate, in scope and quality, as a dissertation for the degree of Doctor of Philosophy.

(Petroleum Engineering)

Approved for the University Committee on Graduate Studies:

Dean of Graduate Studies

TABLE OF CONTENTS

LIST OF FIGURES

FIGURE

LIST OF TABLES

TABLE

1. INTRODUCTION

The determination of liquid saturation* in laboratory multiphase flow experiments is discussed extensively in the petroleum engineering literature. In addition, the measurement of water content in soil has been discussed thoroughly in soil science publications. The measuring devices reported to date are based on: resistivity, x-ray absorption, microwave attenuation, neutron scattering, nuclear magnetic resonance, magnetic susceptibility, refractive index, or dielectric constant (capacitance). However, the problem of measuring water saturation in laboratory steam-water flow systems typical of geothermal energy recovery has not received extensive study. All methods of measuring water content, except the capacitance probe[1], have considered measurement at room temperature. Consequently, evaluation of the feasibility of using a capacitance probe at geothermal system temperatures became the most important

*The word "saturation" is used in the petroleum engineering sense to mean volume fraction of the pore space occupied by a specific fluid phase--liquid water, in this case. Unfortunately, "saturation" may also refer to "saturated solutions (brines)," and to "saturated water and steam," in the thermodynamic sense as phases in phase equilibrium along a vapor pressure curve. All three usages are possible in this report. An attempt will be made to insure a minimum of confusion in the use of the term "saturation" in this report.

objective of this study. No quantitative data on use of a capacitance probe for steam systems was available.

After assembling a capacitance probe, the probe was calibrated in two to three-inch-long synthetic consolidated sandstone cores filled with an air-water mixture at room temperature. Next, the probe was calibrated in two sand packs filled with a steam-water mixture at temperatures varying from 300 to 310°F. The probe was then used to measure water saturation in steady two-phase flow and depletion experiments. With the exception of the room temperature calibration, all experiments were performed with a bench scale linear flow model designed and constructed by Arihara[2].

Finally, in order to investigate salt deposition in porous media and its effect on reservoir permeability, a preliminary experinent was performed. Water and steam were produced from a synthetic consolidated sandstone core initially containing a hot, compressed brine solution of 12,000 ppm sodium chloride. The details and results of all experiments are presented in the following.

2. LITERATURE SURVEY

A review of methods available for measuring liquid content (saturation) in porous media indicated that the capacitance probe method was the best candidate. The capacitance probe is easy to use in a metal core holder at high temperatures. The merits and limitations of each method considered is discussed in the following.

Once the decision was made to use the capacitance probe, the dielectric properties of the media surrounding the probe were collected.

The literature survey was completed by reviewing the theoretical and experimental information available on two-phase boiling flow in porous media.

2-1 Saturation Yeasurement

"Saturation" is defined here in the petroleum sense as fraction of tne pore volume occupied by liquid or gas. The techniques which have been used to measure liquid saturation in the laboratory include the use of: (1) electrical resistivity or conductivity, (2) X-ray absorption, (3) neutron scattering, (4) microwave attenuation, (5) nuclear magnetic resonance, (6) magnetic susceptibility, (7) refractive index, and (8) dielectric constant (capacitance). Much of the theoretical background, instrumentation, uses, and disadvantages

of these techniques have been described by Arihara[2] and Denlinger[3]. For this reason, the following discussion will concentrate on the limitations and merits of these methods.

2-1-1 Resistivity (Conductivity) Method. Muskat, et al.[4], and Botset[5] used appropriately-spaced piezometer rings for electrical conductivity (resistivity) neasurements. The liquid or gas content was found by using a conductive liquid with an A.C. bridge to measure the resistance of the medium between two rings. Conductivity decreases as free gas bubbles form in the porous media. The relationship between saturation and conductivity was determined by calibration tests. The measured conductivity was normalized with respect to the original conductivity of the sand saturated with the conductive liquid. The calibration curve so found was obtained for three different unconsolidated sands, and for a consolidated Berea sandstone. They found that the calibration curve was nearly independent of the porous medium. Leverett[6] also found that the conductivity-saturation relationship determined for several different porous media fell satisfactorily on the same curve.

The resistivity method can be used to measure gas or oil saturation in gas-water or oil-water flow experiments by using conductive water. This method is not useful for boiling steam-water flow experiments. The main drawback is that the electrical conductivity of the liquid phase will change as the water starts boiling. Consequently, the change of vapor saturation will tend to be masked by changing water conductivity.

2-1-2 X-Ray Absorption Method. Boyer, et al.[7], Morgan, et al.[8], and Laird, et al.[9], measured the absorption of an X-ray beam by the core and its liquid content to determine liquid saturation. The X-ray method can be used to determine the saturation of oil-water and gas-water systems when an X-ray absorbing tracer is added to the water. An X-ray beam is strongly absorbed and scattered by a steel shell. Therefore, the X-ray method is not useful for measuring liquid saturation in high-pressure and temperature experiments because a steel core holder is required.

2-1-3 Neutron-Scattering Method. Brunner, et al.[10], used neutron scattering for measuring liquid saturation in porous media. Neutrons are uncharged particles with a mass nearly equivalent to a hydrogen nucleus. Because a fast neutron is scattered by a hydrogen nucleus, it loses about half of its kinetic energy in an average collision. Therefore, the number of slow neutrons exiting a core irradiated by fast neutrons indicates the quantity of hydrogen in the core. In other words, the neutron scattering method measures water saturation by detecting the content of hydrogen atoms. An additional property of neutrons is their high penetration capability with respect to steel. Because the quantity of hydrogen atoms in the mixture depends on the mass of water, this method appears useful for measuring the water content in steam-water flow experiments. However, complex instrumentation, shielding, and operating procedures make the method difficult. Visvalingam, et al.[11], presented a comprehensive review of using the neutron-scattering method for measuring soil moisture content. Their

review included. the theory of neutron scattering, field methods, calibration, and factors influencing the neutron count.

2-1-4 Microwave Attenuation. Parson[12] applied microwave attenuation for measuring saturations in laboratory flooding experiments. Microwaves are electromagnetic waves with a wavelength of 1 mm to 1 m. The principle of this method is based on the absorption of microwave energy by high dielectric constat materials, such as water. The main advantages of this method are: (1) no physical contact with the test sample, and (2) a nearly linear correlation between probe signal and water saturation. The main disadvantage is that the microwave attenuation probe requires a nonmetallic core holder.

2-1-5 Nuclear Magnetic Resonance. Saraf, et al.[13], employed the Nuclear Magnetic Resonance (NMR) method to measure oil saturation in two-phase and three-phase relative permeability measurements. They used kerosene as the oil phase, heavy water (D_2O) as the aqueous phase, and nitrogen as the gas phase. The intensity of the NMR signal is proportional to the concentration of hydrogen nuclei in the sample. The intensity also changes with changing electrolyte concentration. This method also requires a non-magnetic core holder, and the accuracy of the saturation measurements decreases as solid material leaching increases at high temperatures. The NMR method becomes impractical at high pressures and temperatures.

2-1-6 Magnetic Susceptibility. Whalen[14] developed a magnetic susceptibility method for measuring liquid saturation in porous media. The saturation of the liquid having greater magnetic

susceptibility is determined by aid of induced voltage in the secondary of a transformer. The transformer includes the core and its containing fluid as part of the magnetic flux path. If the magnetic susceptibility of the fluids contained in the core is weak, some magnetic tracer should be added to one of the fluids. The magnetic susceptibility method also requires a nonmagnetic core holder. A change in the concentration of magnetic tracer due to boiling could mask a change in liquid saturation. For these reasons, this method does not appear useful for high temperatures and boiling flow experiments.

2-1-7 Refractive Index Method. McDonald[15] used the refractive index method to monitor water saturation while studying boiling flow through porous media. The water saturation was determined by a calibrated meter consisting of a light on one side of a flow conduit packed with spherical glass beads. A photodiode was placed on the other side of the conduit. The intensity of light transmitted through the translucent media and detected by the diode was a function of the number of bubble interfaces encountered by the light. Because the index of refraction for nitrogen and water vapor is almost identical, nitrogen was used as water vapor to eliminate the problem of condensation during calibration. This method can not be used to measure liquid saturation in natural sand packs or consolidated sandstones. This is due to anisotropic optical properties of quartz, the chief constituent of a sand grain. Also, the clay contained in the sandstone adds another complexity.

2-1-8 Dielectric Constant (Capacitance) Method. The dielectric constant of a material is its specific inductive capacity. It is the ratio of the capacitance of a capacitor containing the material between the plates to the capacity when air or a vecuum is used as the dielectric.

Water has a high dielectric constant of about 78 at 25°C. Most gases have low dielectric constants of about unity, and are constant over wide temperature ranges. The capacitance method for measuring saturation in porous media depends on the difference in dielectric constants between liquids and gases.

A study of the capacitance of plaster of paris blocks as an indicator of moisture content was reported by Anderson, et al.[16], in 1942. They found that the capacitance of the blocks decreased with a decrease in moisture content. There was no time lag in capacitance response to changes in moisture content. In 1943, Anderson[17] developed an electrical condenser (capacitor) or "probe" to determine soil moisture content in field surveys. The probe was a metal cylinder embedded in a circular insulating rod. A metal rod, serving as the other plate of the condenser, passed through the center of the insulating rod. The capacitance was measured with an A.C. Wheatstone bridge at a frequency of 1000 Hz. Anderson found that the shape of the curve showing the relation between capacitance (p.f.) of the probe and moisture content (in gms of water per c.c. of soil) over a range from 0.05 to 1.0 grams of water per c.c. of soil did not depend significantly on soil texture when the "permanent wilting percentage" was taken as

the origin. The "permanent wilting percentage" of a soil is the moisture content above which the surface tension of water plays the dominant role in holding the water.

In 1945, Willihan[18] reviewed the dielectric method for soil moisture determination. He pointed out that the concentric arrangement of the condenser plates and proper shielding of the capacity bridge are important to this method. Later in 1960, Leach[19] discussed the important factors affecting the design of a single-electrode capacitor for measuring the moisture content of textile packages. These important factors are: (1) the effect of height above ground, (2) the effect of the length and radius of the electrode, (3) the volume of the dielectric surrounding the probe, (4) density of the dielectric, and (5) the conductivity of the dielectric.

Thomas[20] designed a probe with an electrode having a large fringe capacitance for in-situ measurement of moisture content in soil, and similar substances. The probe was constructed from a 1 in. square insulating rod, wedge-shaped at Fts lower end. Strips of stainless steel were attached by screws to the wsdge side of the rod to form a co-planar condenser. Thomas also presented the electric field map of this probe. According to the field map of the electrode with a 1.68 in. mean length, the media surrounding the probe, within a radius of 1.25 in., contributed 75 percent of the measured capacitance. In other words, the probe could "see" at least 1.25 in. outside of the probe. From the experimental results, he found that the relationship between moisture content (volume of water in 1 c.c. of moist soil) and capacitance change

(air to soil in p.f.) did not depend appreciably on the type of the soil. For moisture content in the range of 0 to 10%, the relationship was linear. For moisture content in the range of 4.5% to 45%, the relationship was linear on a semi-logarithmic graph.

Gregory and Mattar[21] described the development of an inaxpensive capacitance sensor for continuous monitoring of the volume fraction of a two-phase (nonelectrolyte) mixture flowing in pipes. They also discussed the limitations of some existing methods for saturation measurement. For example, they indicated that the capacitance method should not work if an electrically conductive fluid forms a continuous phase. The sensor which they recommended was a capacitor with a continuous helix pair exactly facing each other. Each electrode had. an integral number of spirals to eliminate liquid distribution effects. Typical results of static calibration tests showed that the relationship between sensor vapor-liquid meter reading and the actual percent volume of liquid was linear in the range from 0 to 100% liquid saturation.

Baker[1] developed a radio-frequency capacitance probe to monitor water saturation in the steam zone during steam-flooding experiments. He found that the probe was sensitive to changes in water saturation. His data showed good agreement between the steam saturation front and the steam temperature front. Baker indicated that satisfactory calibration at the steam temperature had not been achieved. Nevertheless, this probe seems to be. the most promising device €or measuring

water saturation in steam-water boiling experiments. The probe is not limited by the use of a metal core holder or by high temperature and pressure conditions. The preliminary evaluation of this probe as a device for measuring liquid saturation in laboratory flow experiments was carried out in early phases of the subject study and has been reported by Denlinger[3]. The probe uses the difference in dielectric constant between materials and phases surrounding it. A detailed description of the instrumentation and operating principles of this capacitance probe is presented in "Experimental Apparatus," Section 4 of this report.

Based on the unique dielectric properties of water, Meadar, et al.[23], described an open hole dielectric logging method for estimating formation water saturation with unknown salinity. They reported that this method was independent of water salinity for estimating formation water content. Both laboratory and field test results were reported. The sonde of this logging tool consists of four main parts: a transnitter power source (battery), two transmitters, two receivers, and receiver electronics. Two receivers with a multiple-twin coil wound on a fiberglass mandrel operate at frequencies of 16 and 30 MHz. On the transmitter top, two single-turn receiver coils feed the signal to the receiver electronics. All coils in the transmitter and receiver are electrostatically shielded. Temperature compensation of the downhole electronics was made for operation to about 300°F.

In view of the preceding, the Baker capacitance probe appears most adaptable for determining water saturation in high-temperature steam-water flow experiments.

2-2 Dielectric Properties and Constants

In the following, the dielectric properties of water, steam, and rocks will be presented.

2-2-1 Dielectric Constants of Water and Steam. Akerlof and Oshry[24] measured the dielectric constant of water in equilibrium with its vapor over temperatures ranging from the boiling point (100°C) to the critical point (373°C). The following equation matches their data:

$$= 5321\,T^{-1} + 233.76 - 0.9297\,T + 0.1417 \times 10^{-2}\,T^{2} - 0.8292 \times 10^{-6}\,T^{3} \qquad (2\text{-}1)$$

where T is absolute temperature in °K.

The calculated values for the dielectric constant of water at high temperatures from 100°C to 240°C are shown in Fig. 2-1.

Warren[25] indicated that the effect of pressure on dielectric constant is relatively small. The dielectric constant of water changes less than 0.5% for each 100 psi change in pressure.

The dielectric constant of a saline solution increases with the salinity. The dielectric constant of a binary electrolyte can be calculated by the Falkenhagen formula[26]:

$$\varepsilon = \varepsilon_{o} + 3.79\sqrt{n} \qquad (2\text{-}2)$$

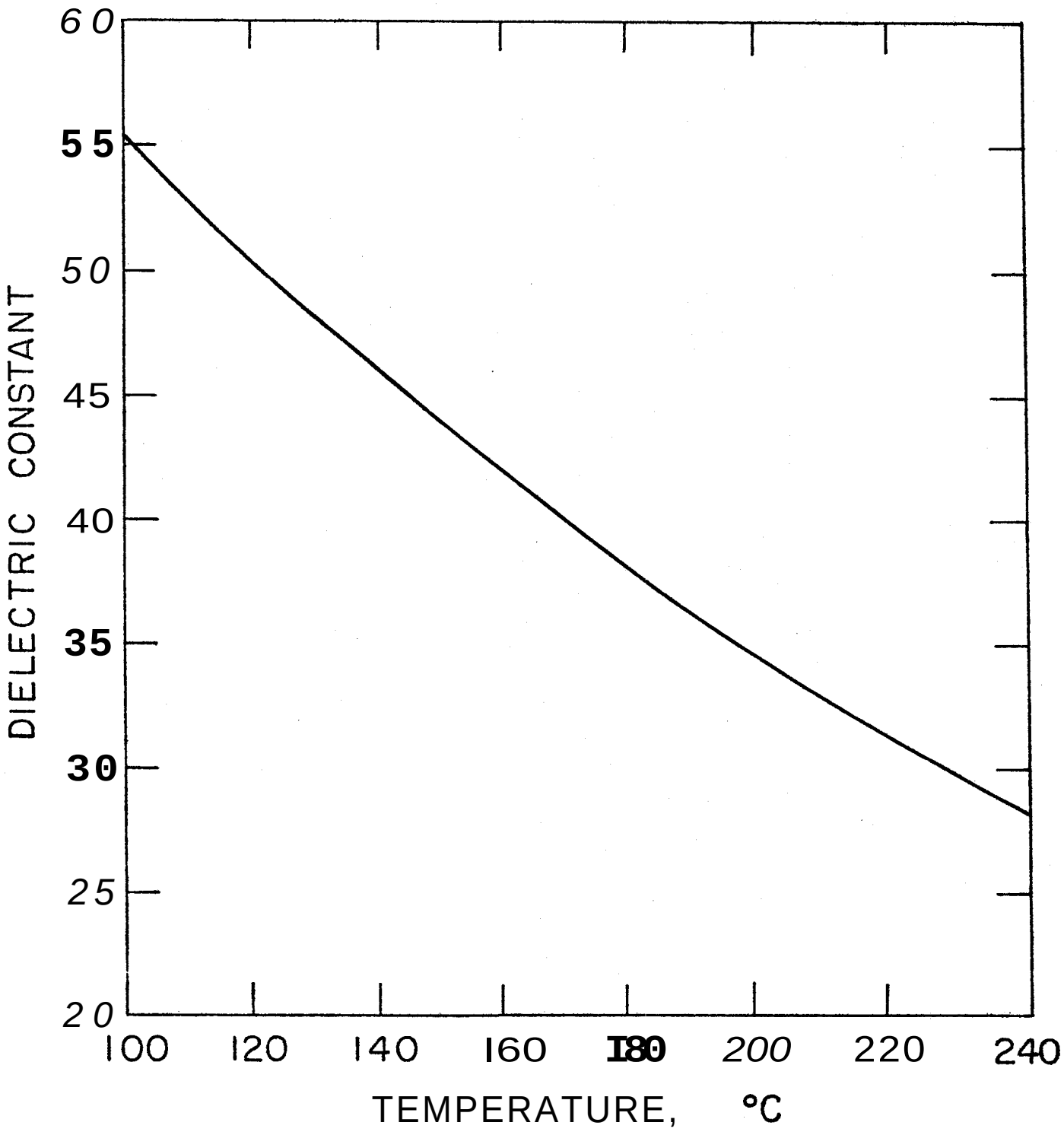

FIGURE 2-1. COMPUTED VALUES FOR DIELECTRIC CONSTANT OF WATER VS. TEMPERATURE (REF. *24*)

where ε = dielectric constant of the electrolyte

ε_o = dielectric constant of pure water

n = concentration of the electrolyte, moles per liter

According to this formula, the increase in dielectric constant for a low concentration electrolyte is very small. For example, the dielectric constant of water at 25°C increases 2% with 12,000 ppm NaCl in solution.

The dielectric constants of steam and air are nearly identical over a wide temperature range. Steam has a dielectric constant of 1.0126 and 1.00785, at 100°C and 140°C, respectively[27].

Thus it appears that the dielectric properties of steam-water and steam-brine mixtures are nearly ideal for the purposes of this study.

2-2-2 Dielectric Constants of Rocks. The dielectric constants of several dry rocks are shown in Table 2-1. The data show that the dielectric constant of dry rock depends on the type of rock. For dry sandstone, the dielectric constant ranges from 4.7 to 5.9 at a measuring frequency of 10 MHz.

The dielectric constant of some water-bearing porous media is shown in Table 2-2. The dielectric constants of all porous media tabulated increase with water content. Keller and Licastro[29] also found a high dielectric constant associated with high water content in 27 cores from the Morrison formation, Colorado. The dielectric constant ranged from 4 to 106 for frequencies between 50 Hz and 30 MHz.

Table 2-1. Dielectric Constants of Dry Rocks and Soils[28]

	Source	Dielectric Constant 1 MHz	10 MHz
1. Sedimentary Rocks			
Dolomite	Pennsylvania	7.90	7.72
Kaolinite	Georgia	4.55	4.49
Lowville Linestone	Pennsylvania	8.69	8.56
Carlin Limestone	Pennsylvania	9.40	9.22
Arkose Linestone	New Jersey	5.34	5.31
Graywacke Sandstone	Pennsylvania	6.12	5.87
Quartzite Sandstone	Pennsylvania	4. 88	4.72
Sandstone, Korrison Formation, Water Content 0.7%	Colorado	5.55	5.20
2. Soils			
Sandy Soil		2.59	2.56
Loamy Soil		2.53	2.43
Clayey Soil		2.56	2.44
3. Igneous Rocks			
Aworthosite	Minnesota	9.93	9.03
Diabase	USSR	9.09	8.50
Diabase	New Jersey-.	**8.31**	7.76

Table 2-2. The Effect of Water Content on the Dielectric Constants of Sedimentary Rock and Soil[28]

	Dielectric Constant at Radio Frequencies
1. Sandstone, dry	4.69-4.99
1.5% water*	7.40
2.8% water	12.1
4.2% water	10.9
2. Packed Sand	
dry	2.93
1.5% water	5.0
3.0% water	11.0
4.5% water	39.1
6.0% water	105.
3. Soil (Dacca, India)	
7.78% water	3.95
19.9% water	4.75
25.8% water	5.23
32.1% water	7.93
36.8% water	21.9
41.4% water	29.4

*Water percentages were not specified in Ref. 28. They may be percent by weight.

No data for the dielectric constants for rocks containing water of high salinity were found in the literature. However, it has been reported that the effect of water salinity on the dielectric constant of rock containing a brine with less than 5,000 ppm salt can be neglected[27].

2-3 Steady, Two-Phase, Boiling Flow

The mechanics and governing differential equations of mass and heat transfer in capillary-like porous media have been described by Luikov[30]. A detailed discussion of this model can be found in Reference 2.

Until recently, only a few experiments appear to have been run to study the thermodynamic and fluid dynamic character of single-component, steady, two-phase, boiling flow in sandstone to our knowledge. The studies are those of Miller[31] and Arihara[?]. In 1951, Miller[31] injected liquid propane in a linear sand pack under nearly adiabatic conditions. Although the thermodynamic properties of propane are different from water, the governing flow equation derived by Miller can be applied directly to the present steam-water flow experiments. Under adiabatic and steady flow conditions, the flow process is nearly isenthalpic. Thus, the enthalpy of the vapor-liquid mixture passing any transverse section in the sand pack per unit time can be written as:

$$w_\ell h_\ell + w_g h_g = wh = \text{constant} \qquad (2\text{-}3)$$

where w_ℓ = weight rate of liquid

w_g = weight rate of vapor

w = total weight rate of vapor and liquid mixture

h_ℓ = enthalpy of liquid

h_g = enthalpy of vapor

h = enthalpy of inlet liquid

Define the mass flow fraction of vapor, f, at any arbitrary transverse section as follows:

$$f = \frac{w_g}{w} \tag{2-4}$$

then

$$1 - f = \frac{w_\ell}{w} \tag{2-5}$$

Introducing Eqs. .2-4 and 2-5 into Eq. 2-3:

$$f = \frac{h-h_\ell}{h_g-h_\ell} \tag{2-6}$$

For steady, two-phase flow, the mass balance equation is given by:

$$w_\ell + w_g = w = \text{constant} \tag{2-7}$$

Applying Darcy's law to each phase of the mixture;

$$w_\ell = -\frac{Ak_\ell}{\mu_\ell v_\ell}\frac{dp_\ell}{dx} \tag{2-8}$$

$$w_g = - \frac{Ak_g}{\mu_g v_g} \frac{dp_g}{dx} \qquad (2\text{-}9)$$

where A = cross sectional area of the core

k_ℓ = effective permeability to the liquid

k_g = effective permeability to the vapor

μ_ℓ = viscosity of liquid

μ_g = viscosity of vapor

p_ℓ, p_g = pressure in liquid and gas phases, respectively

v_ℓ, v_g = specific volume of liquid and gas

Introducing Eqs. 2-8 and 2-9 into Eq. 2-7 and also neglecting the capillary forces:

$$\frac{k_\ell/k}{\mu_\ell v_\ell} + \frac{k_g/k}{\mu_g v_g} = - \frac{w}{Ak \frac{dp}{dx}} \qquad (2\text{-}10)$$

Dividing Eq. 2-8 by Eq. 2-9, and combining with Eqs. 2-4 and 2-5, leads to

$$\frac{k_\ell}{k_g} = \frac{\mu_\ell v_\ell}{\mu_g v_g} \left(\frac{1-f}{f}\right) \qquad (2\text{-}11)$$

For a given inlet liquid temperature, mass flow rate, core absolute permeability and cross sectional area, and knowing the temperature profile in the two-phase region, the relative permeabilities of liquid and vapor can be obtained by combining Eqs. 2-4, 2-10, and 2-11.

In 1974, Arihara[2] conducted several steady, two-phase (steam-water) flow experiments in synthetic consolidated sandstone and Berea sandstone cores. The hot, compressed water was injected into the core at a rate such that a boiling front would form in the core leading to an obvious two-phase flow region. He found that the flow closely followed an isenthalyic process, and approached steady state. From experiments, he drew the following important conclusions regarding steady, steam-water boiling flow in a linear model:

(1) It is possible to develop in-situ, two-phase boiling flow with a wide range of temperature and pressure drops in consolidated cores.

(2) The total mass flow rate for a series of experiments decreases with increasing pressure and temperature drop in the two-phase region.

(3) It is possible to have a wide range of liquid saturations in the two-phase flow region.

2-4 Depletion (Batch) Experiments

Kruger and Ramey[32] presented a mathematical model (developed by P.G. Atkinson) to simulate bench-scale depletion experiments. Their model did not simulate the transition from compressed water to saturated, two-phase boiling flow very well. Typical results showed that boiling occurred at the outlet end and gradually extended to the closed end. Finally, the liquid saturation became uniform along the core as the liquid saturation reached its residual value.

Garg, et al.[33], discussed the governing equations and a method of solution for two-phase (steam and water) flow in porous media. This theoretical model has been applied to study mass and energy transport in bench scale linear models, The assumptions of their model are: (1) the rock matrix is rigid, (2) water and vapor are in local thermodynamic equilibrium, (3) fluid and rock matrix are in local thermal equilibrium, and (4) Darcy's law is valid. The governing differential equations are as follows; The mass balance equations are:

$$\text{liquid phase: } \nabla[\phi(1-s_g)\rho_\ell u_\ell] - \dot{m} = -\frac{\partial}{\partial t}[\phi(1-s_g)\rho_\ell] \qquad (2\text{-}12)$$

$$\text{vapor phase: } \nabla[\phi s_g \rho_g u_g] + \dot{m} = -\frac{\partial}{\partial x}[\phi s_g \rho_g] \qquad (2\text{-}13)$$

where $\dot{m}$ = mass transfer rate from liquid to vapor phase

u_ℓ = velocity of liquid phase

u_g = velocity of vapor phase

The energy balance is:

$$\frac{\partial}{\partial t}[(1-\phi)\rho_s E_s + \phi(1-s_g)\rho_\ell E_\ell + \phi s_g \rho_g E_g] + \nabla[\phi(1-s_g)\rho_\ell E_\ell u_\ell + \phi S_g \rho_g E_g u_g] - \nabla[k_m \nabla T] = 0 \qquad (2\text{-}14)$$

where k_m = thermal conductivity of the rock, liquid and vapor mixture

The first term is the energy storage in the mixture, the second term is energy transport by convection, and the last term represents the energy transport by conduction.

The rate equations are:

$$\text{liquid: } u_\ell = -\frac{k_{r\ell}\, k}{\phi(1-s_g)\mu_\ell}\,[\nabla p - \rho_\ell g] \qquad (2\text{-}15)$$

$$\text{vapor: } u_g = -\frac{k_{rg}\, k}{\phi s_g \mu_g}\,[\nabla p - \rho_g g] \qquad (2\text{-}16)$$

where $k_{r\ell}$, k_{rg} = relative permeability of liquid and vapor, respectively

k = absolute permeability of liquid flow in the core

An implicit iterative finite difference method was employed to solve these non-linear governing equations, and to solve for long time results. These sdlutions have been used to match laboratory experiments.

Two types of experiments performed in this laboratory were simulated. One involves injecting cold water into a core filled with hot water. The other involves producing hot water and steam from a core initially filled with compressed distilled water. The calculation results showed close agreement with the measured pressure and temperature history from the experiments. The calculated saturation history showed that boiling seems to start at both ends of the core. After long time periods, the closed end becomes dry. The water saturation becomes uniform for the remaining four-fifths of the core. Garg, et al., gave no explanation for this behavior.

Because their objective was to study vapor pressure lowering in porous media, Cady[34], Bilhartz[22], Strobel[35], and Chicoine[36] performed depletion experiments with a small pressure drop across their vertical cores produced from the top. Cady performed his experiment in an unconsolidated sand pack with a permeability of 4.5 daycys. Bilhartz reproduced the Cady experiment. Strobel performed his experiment with a natural consolidated sandstone with a permeability of 550 md. During their production runs, both Cady's and Strobel's temperature results showed that a dry steam zone formed at the producing end (top of the core) and gradually spread down to the closed end of the core. The region below the dry zone was a two-phase zone in which temperature and pressure followed the usual vapor pressure curve.

In order to have obvious two-phase flow, Arihara ran his experiments in a different way. A large pressure drop was introduced by high rate flow through the outlet valve of a closed system initially filled with compressed hot water. Typical results of temperature, pressure, and mass production history were reported. The Arihara experiments were performed with horizontal cores.

3. STATEMENT OF THE PROBLEM

Relative permeability-saturation relations for multiphase flow through reservoir rocks is important for forecasting the behavior and the ultimate recovery of oil and gas reservoirs. Relative permeability is generally defined as the ratio of the effective permeability to a given phase (in multiphase flow) to the permeability of a rock with single-phase flow of that fluid through it. The methods of measuring relative permeability and fluid content (saturation) in the laboratory are described exhaustively in the petroleum engineering literature.

In the same manner, relative permeability-saturation relations are also needed for forecasting energy recovery from a geothermal reservoir. Steam-water relative permeability-water saturation data have not been presented in the literature. To our knowledge, no actual measurements have been made. In addition, the technique of measuring water saturation in steam-water flow experiments has not been studied. Therefore, the objectives of this study are to develop a probe for measuring water saturation in laboratory steam-water flow experiments and to construct preliminary relative permeability curves for steam and water vs. water saturation. A secondary objective involved investigation of certain effects of salt in solution upon geothermal experiments.

Because hot brine geothermal fields are common, the problem of salt deposition in the reservoir is of interest to geothermal engineers. Some interesting questions are as follows. Where does salt deposit in the reservoir when boiling occurs? Does the salt deposition affect the rock permeability? The answers to these questions do not appear in the literature to our knowledge. To answer these questions, fluid will be produced from a closed, hot brine system in the laboratory, simulating a depletion geothermal system.

4. EXPERIMENTAL APPARATUS

A schematic diagram of the bench-scale linear flow model is shown in Fig. 4-1, and photographs of the apparatus are shown in Fig. 4-2(a) and (b). To deaerate the feed-water, the water was boiled in an open flask and cooled by passing through a heat exchanger. The boiled water was then pumped into the core. An accumulator was located at the outlet of the pump to reduce pumping pulsation. A flowrator was connected in the line for coarse adjustment of the flow rate. The water was then raised to the desired temperature by passing the injection flowline through an electric furnace. The core holder was located in a controlled temperature air bath. A second pump was used to pressurize the confining water outside the Hassler sleeve to the desired pressure when a consolidated core was used. A microregulating value in the outlet line was located outside the air bath. The produced hot water and steam were condensed in a heat exchanger. The mass flow rate and cumulative mass production were measured by timed weighing of the produced fluid on mass balance. Liquid saturation measurement will be described later in this section.

A pressure gauge and. thermocouple were Located in the flow line following the electric furnace but before the air bath. They served to measure the state of the feed-water as compressed hot water or a steam-water mixture. Two pressure

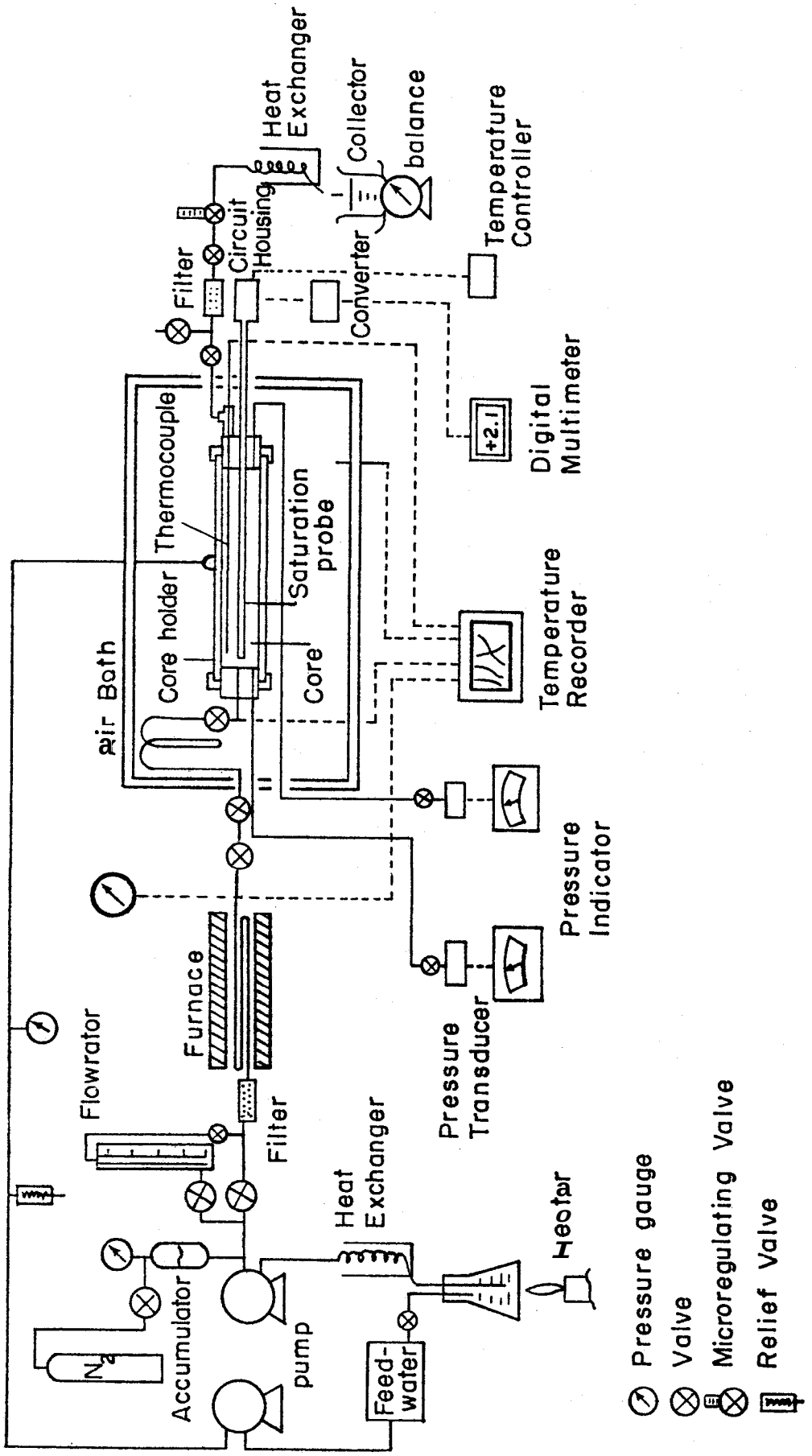

FI WRE 4-1. SCHEMATIC DIAGRAM OF APPARATUS

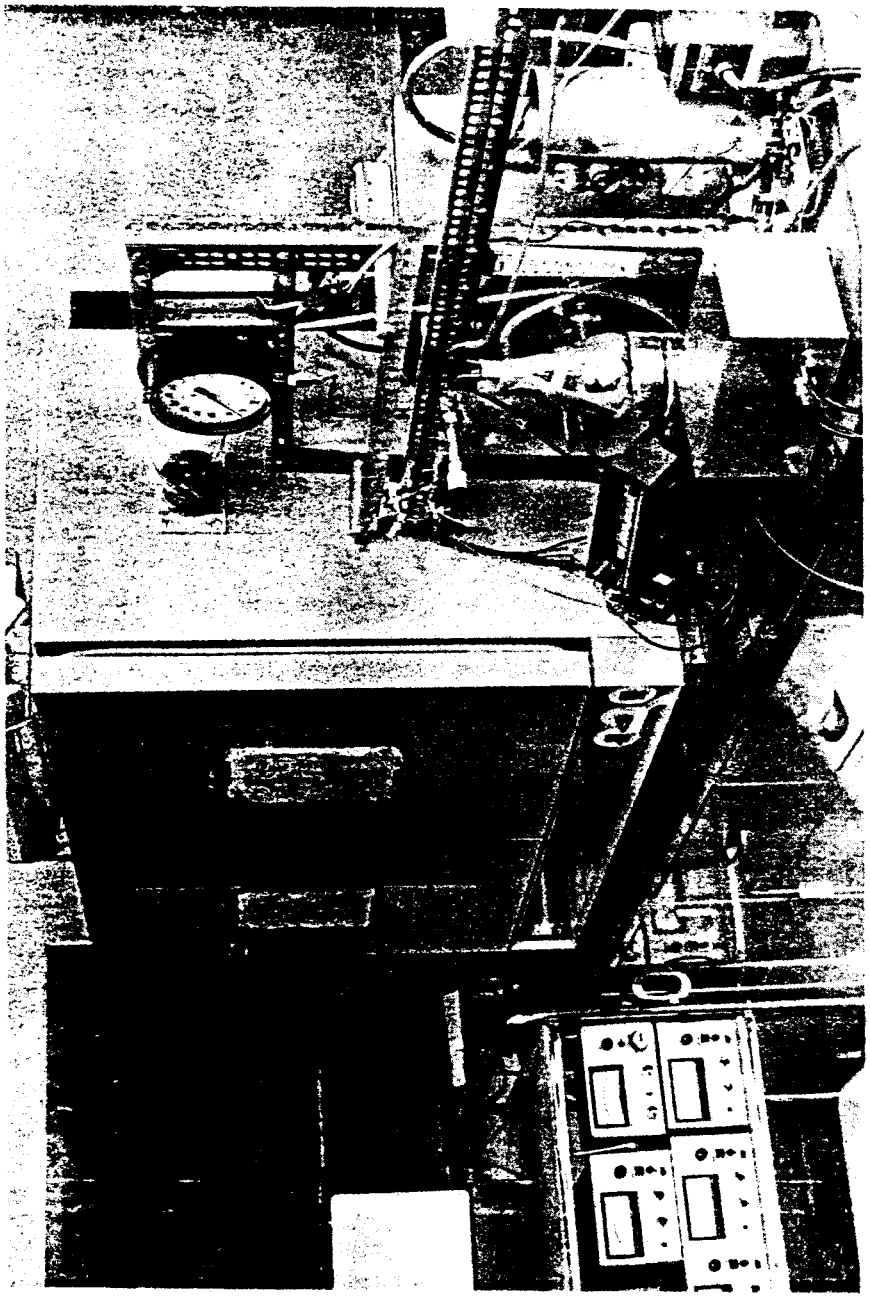

Figure 4-2(a): Photograph of Apparatus

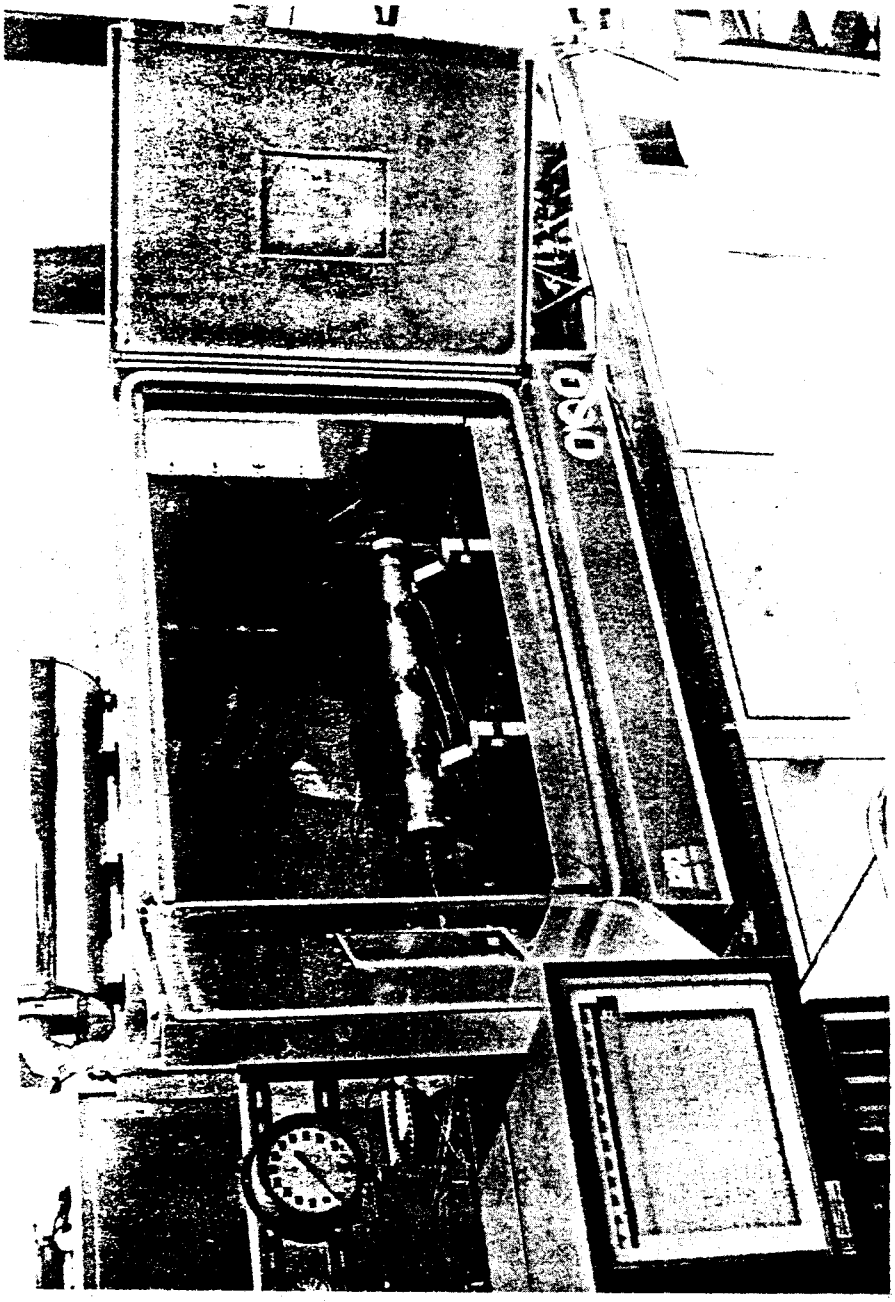

Figure 4-2(b): Photograph of Apparatus

transducers were used to monitor the inlet and outlet core pressures. A traversing thermocoupl-e was used to measure the core temperature during experiments. The temperature of the air bath was also monitored by a thermocouple.

The major components of the apparatus are described in the following.

4-1 Pump

An adjustable volume pump was used to deliver the de-aerated water *to* the core. The pumping action was created by actuating a flexible Teflon diaphram as the plunger of the pump reciprocated at a fixed stroke rate. Although a fixed volume of hydraulic fluid was displaced, the pumping czpacity could be adjusted by the volume control knob.

4-2 Electric Furnace and Temperature Controller

The injection tubing made three passes through the tubular furnace to heat the feed water. Because the tempera-tare controller regulated the time percentage that the load current was on, the fluid temperature at the outlet end of the furnace depended on the flow rate. Hence, the current load time was adjusted to maintain the desired constant tem-per-ture at the flow rate of interest.

4-3 Air Bath

The air bath was used to maintain a constant ambient temperature for the reservoir model. A uniform temperature

inside the air bath was achieved by operating a fan and directing the air flow with a louver. The maximum temperature of the air bath was sensitive to the position of the louver blades, and was about 400°F. About five hours were required to obtain uniform elevated temperature in a water-saturated core contained in the core holder.

4-4 Core Holder

Two types of core holders were used in this study. The 2.73 inch ID x 24 inch long stainless steel tube with a flange at both ends was used as the core holder for unconsolidated sand packs. A detailed drawing of the core holder with probe guide and thermocouple well is shown in Fig. 4-3.

A modified Hassler-type core holder, after a design by Jones[37], was employed for consolidated sandstones. To make the core holder more convenient for loading and unloading the core, an adjustable plug was used at both ends. A detailed drawing of the core holder is shown in Fig. 4-4. The core holder included a stainless steel shell, either a viton or a silicone rubber sleeve, stainless steel compression ring, and an adjustable end plug and cap at both ends. The stainless steel shell had four ports. One served for admitting confining pressure. The other three ports could be used for core pressure measurement. The inlet plug had taps for inlet flow and pressure measurement. The outlet plug had taps for exit flow, pressure measurement, and an opening for the saturation probe guide. A heat exchanger type tubing fitting was used to pass the thermocouple well through the exit flow tap.

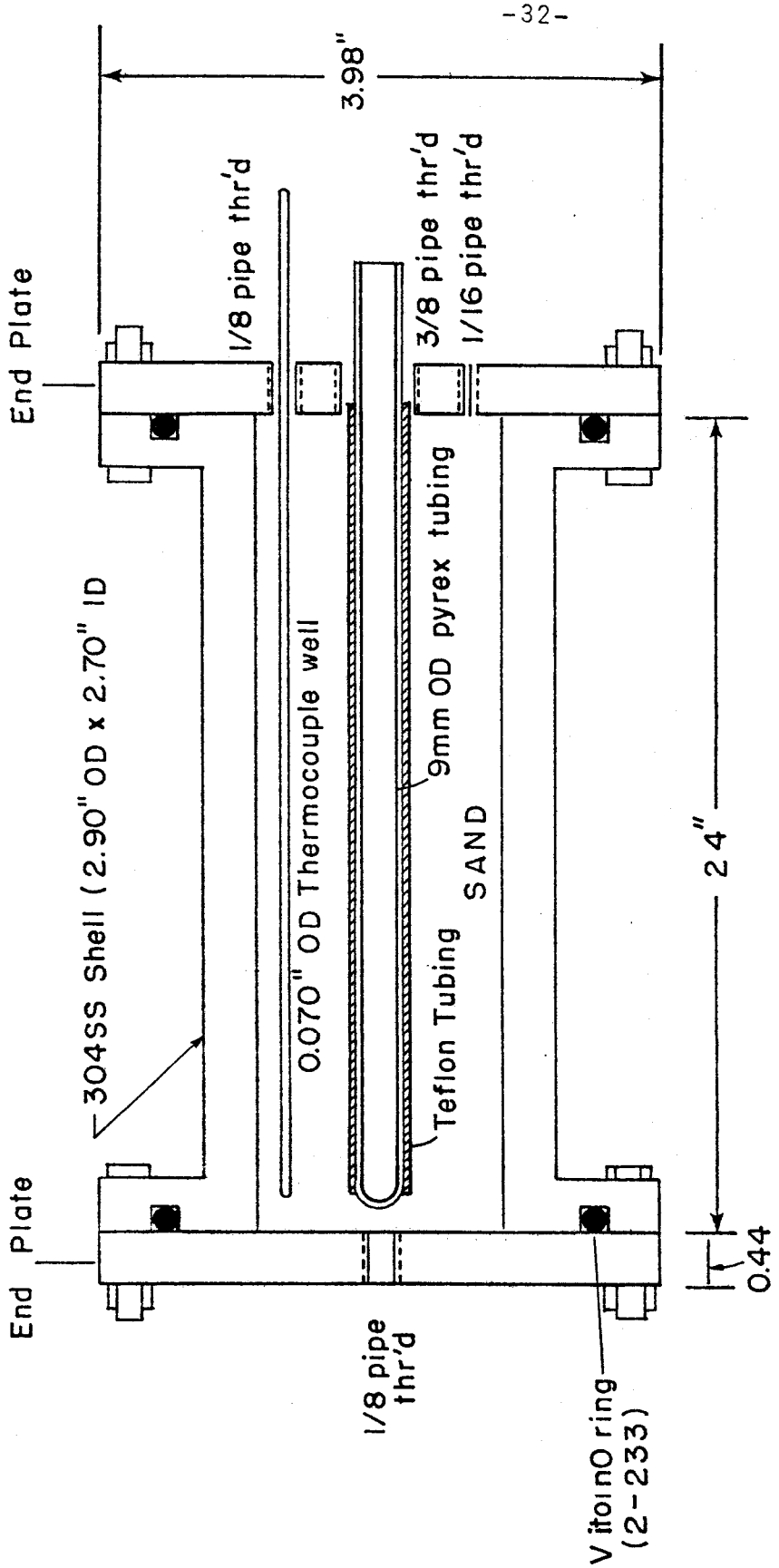

FIGURE 4-3. CORE HOLDER FOR UNCONSOLIDATED SAND PACK

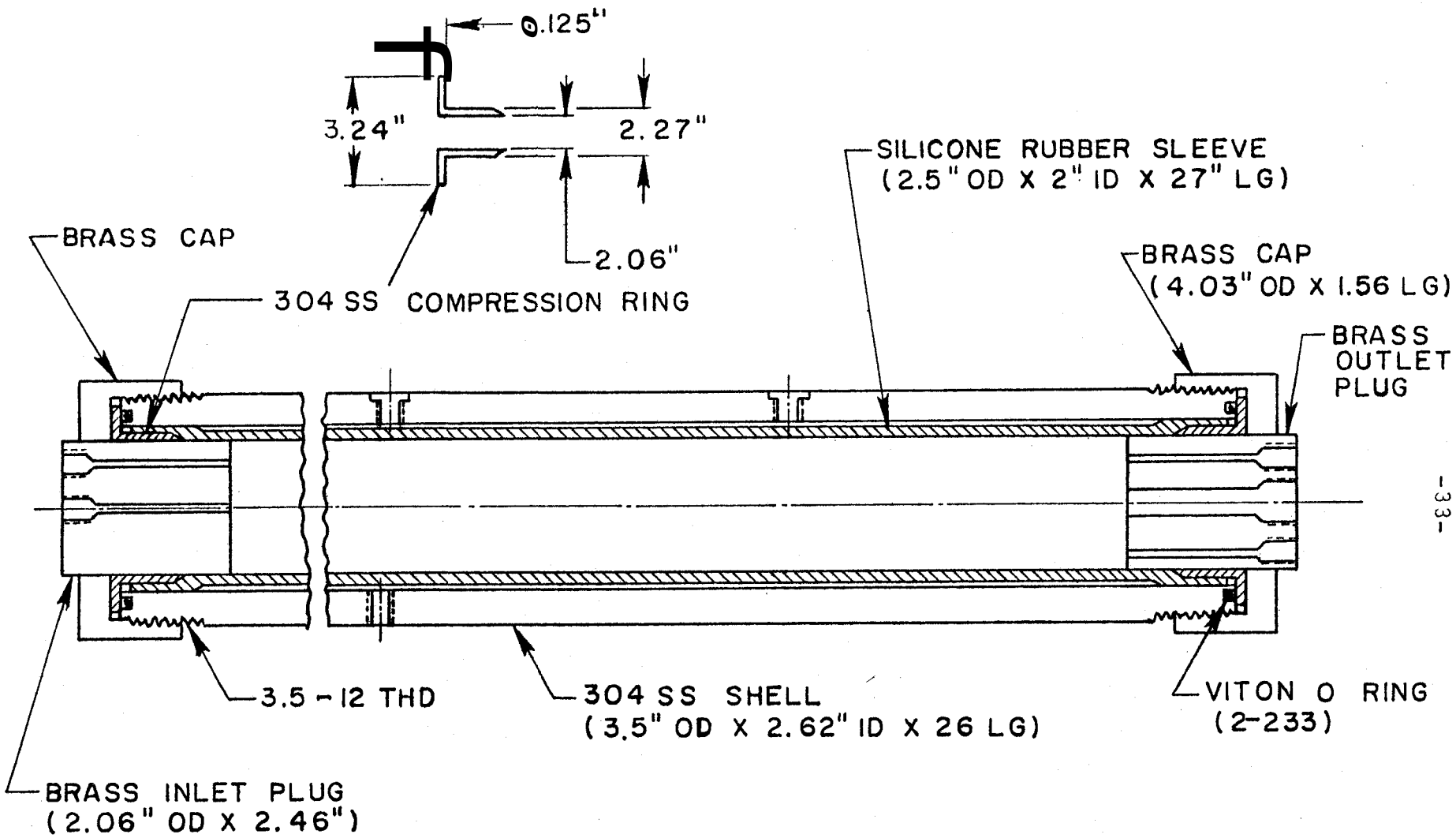

FIGURE 4-4. CORE HOLDER FOR CONSOLIDATED SANDSTONE CORE

4.5 Porous Media

This study involved two types of porous media--unconsolidated sand packs and synthetic consolidated sandstones. The calibration of the capacitance probe in a steam-water system at high temperatures was made in two unconsolidated sand packs of different grain size. Other experiments were performed in the synthetic consolidated sandstone. The properties of the porous rnedia are presented in Appendix A.

A 9 mm 03 pyrex tubing coated with a 0.015 inch thick Teflon tubing was used as a guide for the liquid saturation probe. The probe guide was cast in the center of the synthetic consolidated sandstone. A 0.070 inch OD stainless steel tubing was used as a guide for the traversing thermocouple, and was cast 0.75 inches from the center of the synthetic consolidated core. Prior to coating the pyrex tubing with the Teflon tubing sleeve, bare pyrex tubing was used, and usually broke due to thermal stress, and terminated the experiment.

The technique of fabricating a synthetic consolidated sandstone has been described by Wygal[38], Heath[39], Evers40, and Arihara[2]. However, to keep the long synthetic consolidated care from cracking, two important precautions were found in this study. The first precaution is to cure the core under a wet condition to minimize volume reduction during hardening. This step can be done by spraying the core with water and covering with a plastic sheet. The second precaution is to preheat the long synthetic consolidated core to a moderate temperature (about 160°F) for several hours before elevating the core to the desired higher temperature.

4-6 Pressure Measurement

Pressure was measured by a calibrated diaphragm-type pressure transducer. The capacity of the transducer depended on the design pressure rating of the stainless steel diaphragm. The pressure ranges of the plate included 0 to 1, 5, 25, 100, and 500 psi. The pressure reading could be obtained either from a 5 inch analog meter with ± 1% full scale accuracy, or from a 3 digit reading using the meter as a null balance indicator. The indicator meter served for 10%, 30%, and 100% of the capacity of the transducer plate by selecting a meter sensitivity. Therefore, for a 500 psi plate being used in this study, the sccuracy of reading was ± 5 psi for pressure above 150 psi, ± 1.5 €or pressure between 150 psi and 50 psi, and was ± 0.5 psi for pressure below 50 psi.

4-7 Temperature Measurement

All temperatures were measured by J-type iron-constantan sheathed thermocouples. The core temperature was measured with a 0.040 inch OD thermocouple traversing inside 0.070 inch G3 stainless steel tubing in the core. All temperatures were recorded by a 24 channel temperature recorder. Temperatures were measured with an estimated accuracy of ±1oF.

4-8 Saturation Measurement

The dielectric constant capacitance probe was used to measure water saturation in steam-water flow experiments. The operating principles and instrumentation of this probe are as follows.

4-8-1 Operating Principles of the Probe. The probe utilizes the dielectric constant difference between solid materials and fluid phases. The probe changes the resonant frequency difference between two oscillators by changing the capacitance of a capacitor in one of the oscillators. The capacitance of the capacitor changes by changing the dielectric constant of the media surrounding the gap of the capacitor. The dielectric constant of the medium increases with increase in water content in the medium. The water content can be measured by relating the probe signal to a given reference point such as a steam-filled core, or a water-saturated core.

4-8-2 Main Components of the Probe. A schematic diagram of the measurement of liquid water saturation in a porous medium is shown in Fig. 4-5(a), and a photograph of the capacitance probe is shown in Fig. 4-5(b). The schematic diagram of the probe in operating position is shown in Fig. 4-1. The saturation probe includes a capacitor (probe), probe circuit, digital-analog converter, temperature controller, digital multimeter, and power source. Because the major objective of this study is use of the capacitance probe to measure liquid saturation, a detailed description of tho, probe components is given in the following.

A drawing of the capacitor is shown in Fig. 4-6. The end with a closed copper tube attached to a brass rod becomes one plate of the capacitor. The other plate is a silver-plated pyrex tube. Teflon spacers were used to keep the brass rod in

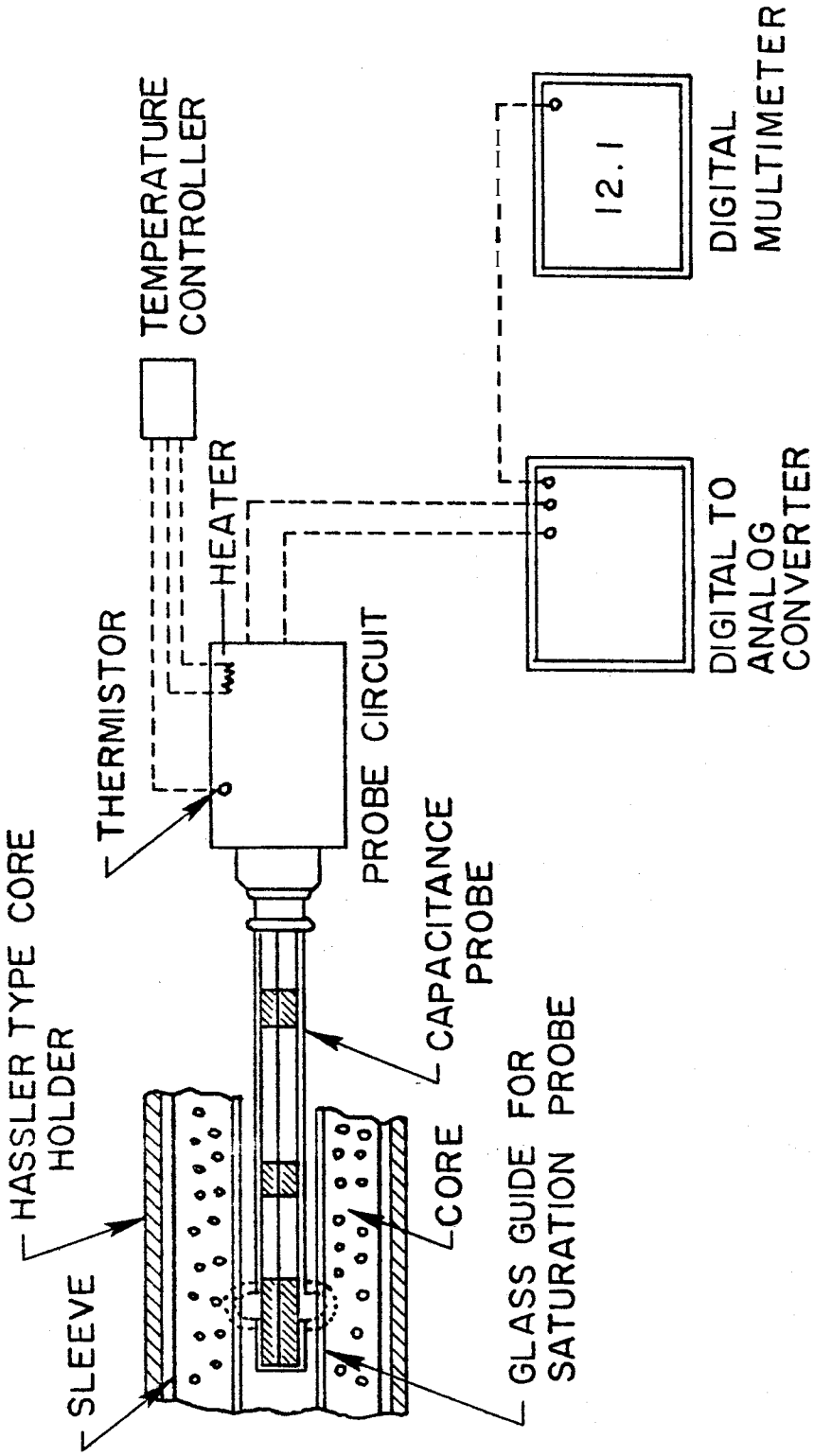

FIGURE 4-5(a). SCHEMATIC DIAGRAM FOR IN SITU MEASUREMENT OF WATER SATURATION IN STEAM-WATER FLOW IN SYNTHETIC CONSOLIDATED SANDSTONE CORE

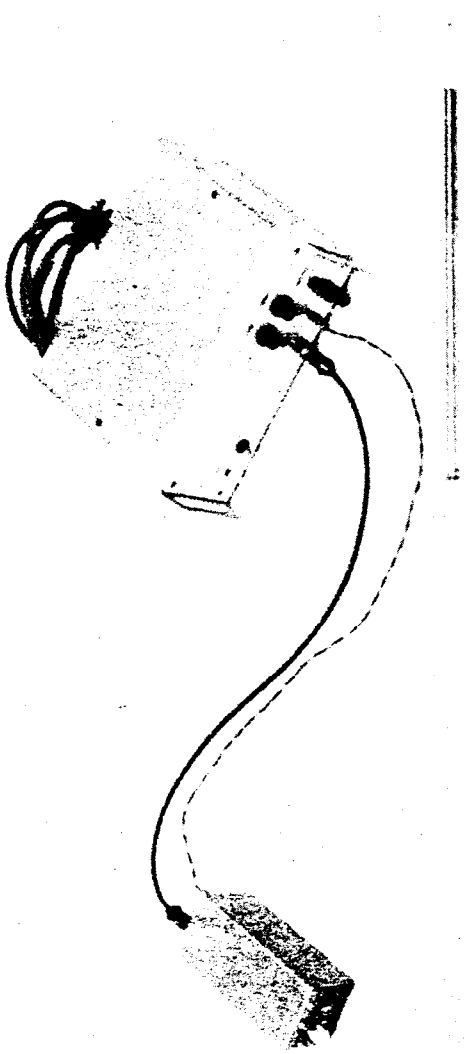

Figure 4-5(b): Photograph of Capacitance Probe

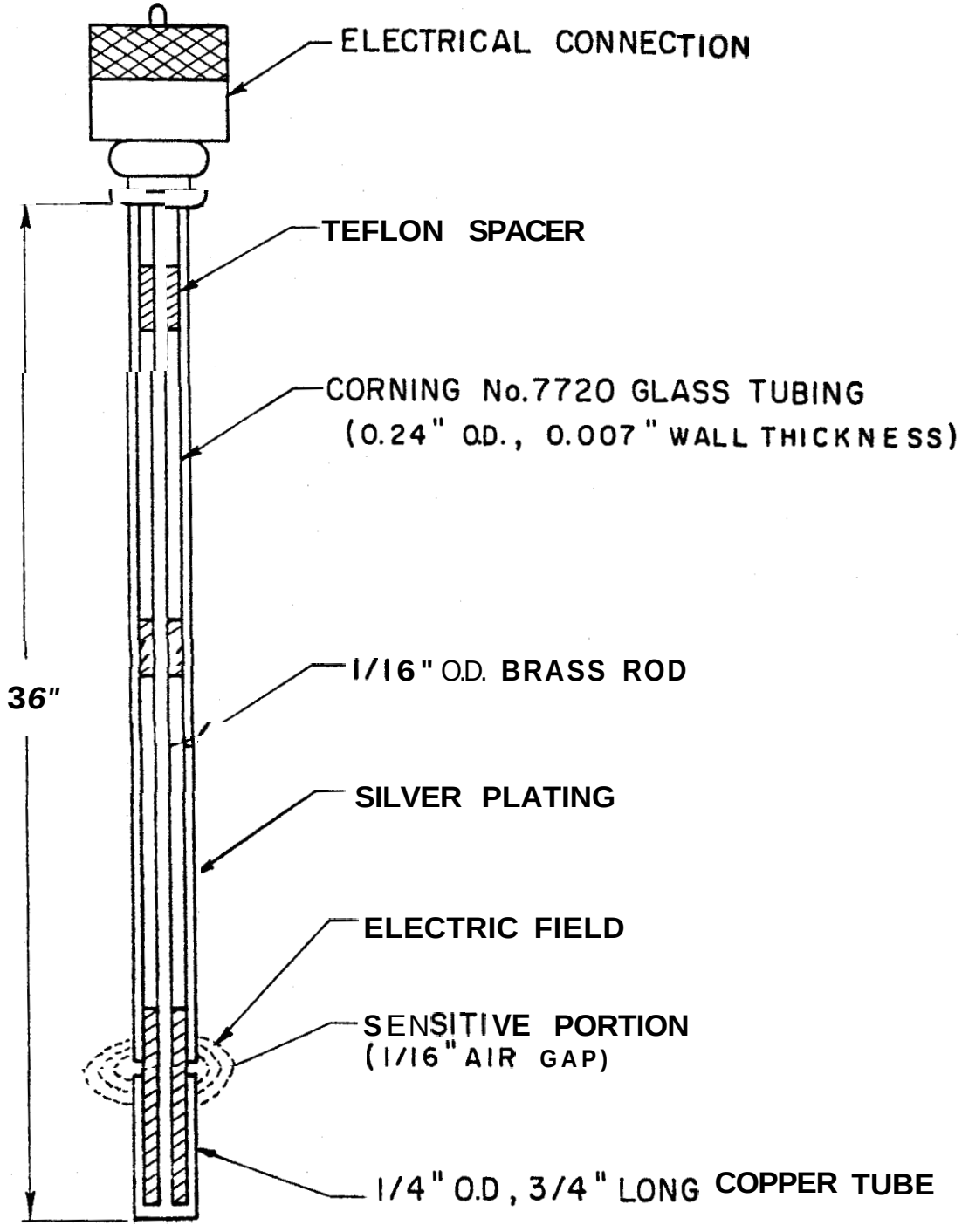

FIGURE 4-6. **CAPACITANCE** PROBE

the center of the glass tube. The sensitive portion is located at the 1/16 in. gap between the open end of the copper tube and the silver plating, because the electric field extends into the media outside the probe guide. Consequently, the capacitance of the capacitor changes as the water content in the media changes.

The main components of the capacitance probe circuit are shown in Fig. 4-7. There are three important parts. These three parts are: (1) two crystal-stabilized oscillators, (2) a detector, and (3) an amplifier. The two oscillators are identical except that one is connected to the capacitor probe. Both are tuned to about 7.5 MHz, with about 1.3 KHz difference when the capacitance probe is immersed in air. Once set, the difference is fixed unless the capacitance of the probe changes. The detailed probe circuit diagram was given in Appendix C of Arihara's dissertation2.

The digital to analog converter indicated in Fig. 4-7 was used to obtain a D.C. voltage whose magnitude was directly proportional to the frequency difference of the two oscillators. The detailed circuit diagram was shown in Appendix C of Arihara's dissertation[2].

The capacitance probe and circuitry used in this study are essentially the same as the original Baker[41,1] design. Initially, problems were experienced with stability of the detection circuit. These problems were found to he a result of temperature variation, even though the equipment was located in an air-conditioned laboratory. In fairness, there

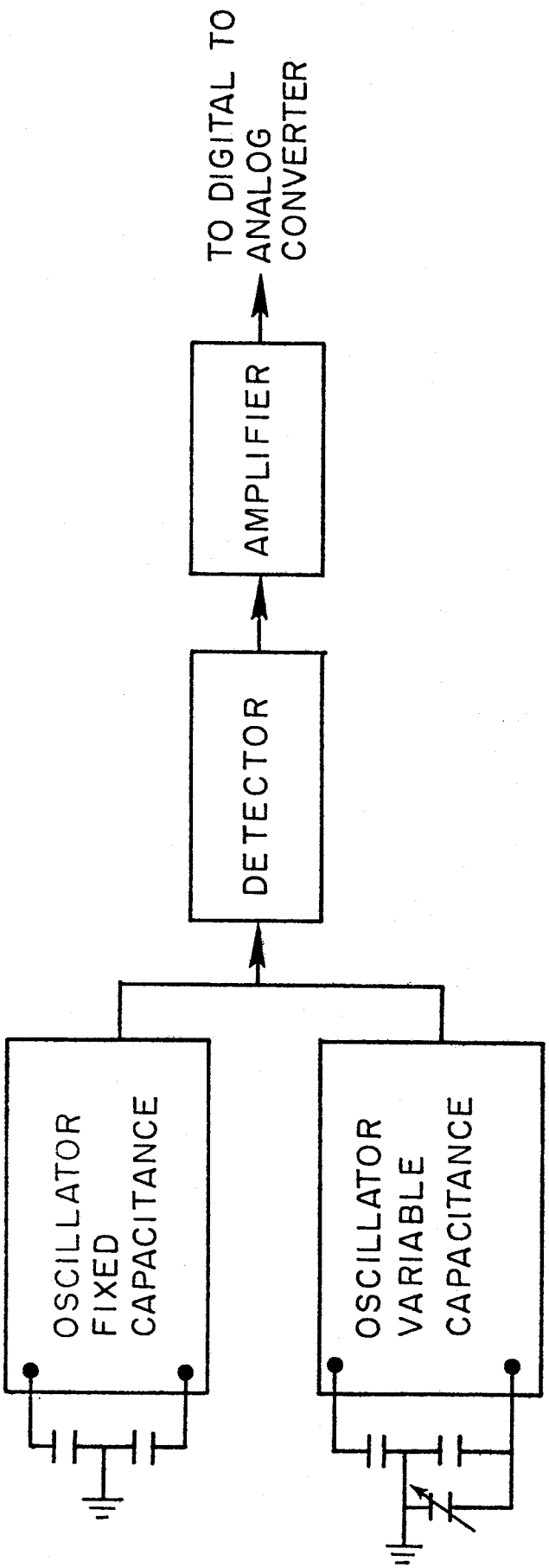

FIGURE 4-7. SCHEMATIC DIAGRAM OF THE PROBE CIRCUIT

was an unusually large heat load in the laboratory. The Kruger[32] Chimney Model is located in the same laboratory, for example. Although it was difficult to locate the source of instability in probe results in early calibration work, it was not difficult to correct the situation once the source was known. A heater-temperature controller assembly was added to the probe circuit electronic package.

Two 15 watt cartridge heaters, 3/16 inch OD by 1 3/8 inch length were fastened inside the case of the probe circuitry housing. The temperature inside the probe circuitry box was set at $38^{\circ}C \pm 0.1^{\circ}C$. A solid-state thermistor controller was used to maintain the temperature.

The purpose of maintaining a constant temperature inside the circuitry housing is as follows. Ideally, the frequency difference of two oscillators will remain constant, no matter what the ambient temperature, as long as the capacitance of the circuit does not change. This is based on the assumption that frequency shifting due to ambient temperature change will be the saxe for each oscillator. However, it is impractical to cut two crystals at exactly the same angle from their axis such that two crystals will have the same temperature coefficient. Hence, to eliminate the external temperature effect on the probe signal, it is important to maintain a fixed temperature in the circuitry housing.

Another stability problem was. solved by eliminating power supply variations. Four 12 volt D.C. batteries were used to supply a stable, constant voltage to the probe circuit.

Because the probe output signal is in the millivolt range, a constant power supply is necessary to reduce noise in the probe signal,

5. EXPERIMENTAL PROCEDURE

Four types of experiments were performed in this study. First, in order to utilize the capacitance probe as a quantitative water content measuring device, the most important objective was to study calibration of the probe. Later, the feasibility of using this probe to measure water saturation was demonstrated in steady, two-phase flow and depletion experiments. Finally, a brine experiment was performed to study the effect of salt deposition on reservoir properties and salt distribution in a geothermal reservoir.

A short, synthetic consolidated sandstone core filled with air and water was used to construct the probe signal-water saturation calibration at room temperature. Water saturation was measured by a gravimetric method.. In the steam-water calibration, a nearly equal amount of hot water and steam was produced from a sand pack initially filled with a hot, compressed distilled water. 'Following a production stage, the care was allowed to reheat. Production and reheating stages were repeated until the core was completely dry. The water saturation at each stage was determined by a mass balance.

.For steady state flow experiments, constant temperature hot water was injected into the synthetic consolidated sandstone core at a constant rate such that a boiling front would form in the core. As for depletion experiments, hot water

and steam were produced from an initially hot compressed liquid system with the injection end of the core closed.

The procedure for the brine experiment was similar to that of the calibration of the probe in the steam-water system, except that the hot water and steam were produced from a core initially containing a hot, compressed brine solution of 12,090 ppm sodium chloride.

The detailed procedure for each experiment is as follows.

5-1 Calibration of the Capacitance Probe at Room Temperature

The synthetic consolidated core is dried at 115°C for 24 hours. It was 2 to 3 inches in length, 1.93 inches in diameter, and had a 9 mm OD glass tube in the center of the core. Evacuate the core while the core is still hot. Measure the weight and probe signal of the dry core. Evacuate the core for 2 to 3 hours. Saturate the core with water while under vacuum. Weigh and record the probe signal of the fully-saturated core. Reduce the water saturation by heating the core for a specified tine. Repeat probe measurements during saturation. All probe measurements were taken after the core had cooled to room temperature.

5-2 Calibration of the Probe at High Temperatures

Evacuate the sand pack in the stainless steel core holder for 24 hours. Saturate the core with deaerated distilled water, measure the pore volume and probe signal of the saturated core. Heat the core to the desired temperature. Record the probe signal of the core with a 100 percent water saturation. Produce a desired amount of hot water and steam

to obtain different water saturations. Shut in the system. Wait until the core temperature returns to initial temperature. Record the probe signal. Repeat desaturation and measurement until the core is completely dry.

5-3 Preparation of Steam-Water Flow Experiments

One of many problems encountered in this study was to eliminate gas coming from the synthetic consolidated sandstone care during the high temperature experiments. Although the core was evacuated before the experiment and deaerated water was used as a confining medium outside the sleeve of the core holder, several hundred cc of gas had been collected during the depleticn experiments. The analysis of gas using a Gas Petitioner showed that about fifty percent of gas was air, and the rest was of unknown composition. The source of gas was found by the following simple experiment. When a piece of Viton, silicone rubber and Teflon were immersed in a deaerated hot water, gas bubbles were found on the surface of these materials. The experiment indicated that silicone rubber and Teflon start to decompose at about 180°F. The following procedures were taken to remove the gas of decomposition from the core.

Evacuate and saturate the synthetic consolidated core with water at room temperature. Gradually heat the core to about 160°F for several hours to prevent the core from cracking. Gradually elevate the core temperature to 260°F. Meanwhile, deplete the core to remove the gas produced from either

the Viton or silicon rubber and. Teflon tubing. Resaturate the core with hot water. Raise the core temperature to 295oF. Deplete the core again. Resaturate the core with hot water at 295° F. Prepare to run a steady, two-phase flow experiment.

5-4 Steady, Two-Phase Flow Experiments

The procedure for steady, two-phase flow experiments was as follows. With the outlet end maintained in the liquid region, continueusly inject hot water through the core until the core temperature was uniform. Initiate two-phase flow by decreasing the outlet pressure. Record the probe signal and temperatures along the axis of the core when the temperature becomes stable. At the same time, record the inlet and outlet pressures and the mass flow rate.

5-5 Depletion (Batch) Experiment

The procedure for the depletion experiments was as follows. Resaturate the core with water at the end of the steady, two-phase flow experiments. Close the outlet valve and pressurize the system to maintain the whole core in the compressed liquid region. Close the inlet valve. Wait until the core temperature stabilizes. Record the probe signal. Open the outlet valve for maximum flow rate. Record the inlet and outlet pressures and temperatures, and the saturation profile as functions of time. Record the probe signal throughout the experiment.

5-6 Brine Experiment

The procedure for the brine experiment was as follows. Inject a hot brine solution of 12,000 ppm sodium chloride through a core saturated with hot distilled water until the resistivity of the effluent reaches the resistivity of the inlet brine. Close the outlet valve and pressurize the system to 200 psig. Close the inlet value. Wait until the core temperature Is stabilized. Produce hot brine and steam from the core. Measure the resistivity of the produced water at the end of each production stage. Close the outlet valve and reheat the core until the core temperature reaches the initial temperature. Repeat production and reheating until the core becomes completely dry. Measure the capacitance probe signal during the run.

6. RESULTS AND DISCUSSION

This chapter presents the results of this study. The first section covers the theoretical 'analysis and experimental calibration of the capacitance probe. Much of the theoretical analysis was developed by Denlinger (ref. 3). The second section presents the results of the steady, two-phase flow experiments. The third section consists of the temperature and saturation histories for the batch-type depletion experiments. The final section presents the results from the brine experiments.

6-1 Calibration

The dielectric constant of a sant pack filled with a steam-water mixture can be estimated by the modified Lichtnecker and Rother equation (ref. 23). The equation may be written as:

$$\varepsilon = [(1-\phi)\ \varepsilon_{ma}{}^{c} + S_w\phi\varepsilon_w{}^{c} + (1-S_w)\phi\ \varepsilon_s{}^{c}]^{\frac{1}{c}} \qquad (6\text{-}1)$$

where ε = dielectric constant of the media

ε_{ma} = dielectric constant of the matrix

ε_w = dielectric constant of water

ε_s = dielectric constant of steam

ϕ = total porosity

S_w = water saturation

c = the formation dielectric cementation and polarization factor. It depends on the grain size, shape, and orientation in the formation.

The total capacitance of the probe can be expressed as follows:

$$C_P = C_1 + C_2 \qquad (6\text{-}2)$$

where C_p = total capacitance of the probe

C_1 = capacitance of the "head on" cylinder (the silver plated glass tube and the copper tube)

C_2 = capacitance of the cylindrical capacitor (brass rod and silver plating)

Because the values of C_1 and C_2 for the subject probe are 0.5ε and 25.0 picofarad (1 p.f. = 10-12 farad), respectively, Eq. 6-2 becomes:[3]

$$C_p = 0.5\varepsilon + 25 \qquad (6\text{-}3)$$

Referring to Fig. 6-1, the total capacitance of the oscillator with the probe can be written as

$$\frac{1}{C} = \frac{1}{C_p+15} + \frac{1}{100} \qquad (6\text{-}4)$$

or

$$C = \frac{(C_p+15)100}{C_p+115} \qquad (6\text{-}5)$$

Substituting Eq. 6-3 into Eq. 6-5 yields:

$$C = \frac{(0.5\varepsilon+40)100}{0.5\varepsilon+140} \qquad (6\text{-}6)$$

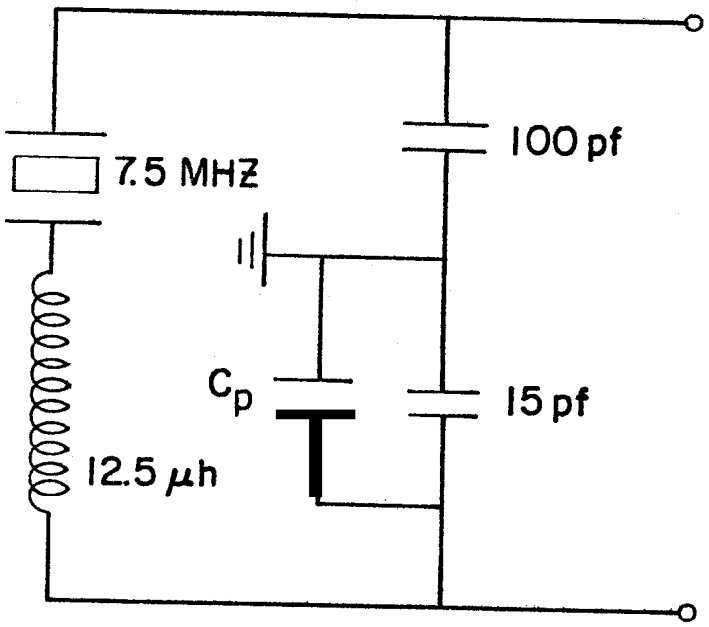

FIGURE 6-1. PORTION OF SCHEMATIC CIRCUIT DIAGRAM OF THE OSCILLATOR WITH PROBE

The resonant frequency of the oscillator with the probe can be calculated by:Eq. 6-7 for a series LC circuit.

$$(f_r)_2 = \frac{10^6}{2\pi\sqrt{LC}} \qquad (6\text{-}7)$$

where $(f_r)_2$ = resonant frequency of the oscillator with the probe, Hz

L = inductance of the oscillator, henries

C = capacitance of the oscillator, p. f.

The capacitance circuit measures the difference between the resonant frequencies of the two oscillators. The resonant frequency of the standard oscillator is fired. Thus, the frequency differ-nce is directly proportional to the resonant frequency of the oscillator containing the probe. The amplitude of the D.C. voltage obtained from the digital to analog converter is also proportional to the difference of the resonant frequencies. Therefore a theoretical calibration curve can be constructed by assigning a value for the water content, and the dielectric cementation and polarization factor of the porous media. (See Fig. 2 for specified values.) The theoretical calibration curves so found are shown on Fig. 6-2.

Referring to Fig. 6-2, the $(f_r)_s$ is the resonant frequency of the oscillator for the probe immersed in the core filled with steam. $(f_r)_w$ is the resonant frequency of the oscillator for the probe immersed in a core filled with water, and (f_r) is the resonant frequency of the oscillator for the probe immersed in a core filled with a steam-water mixture.

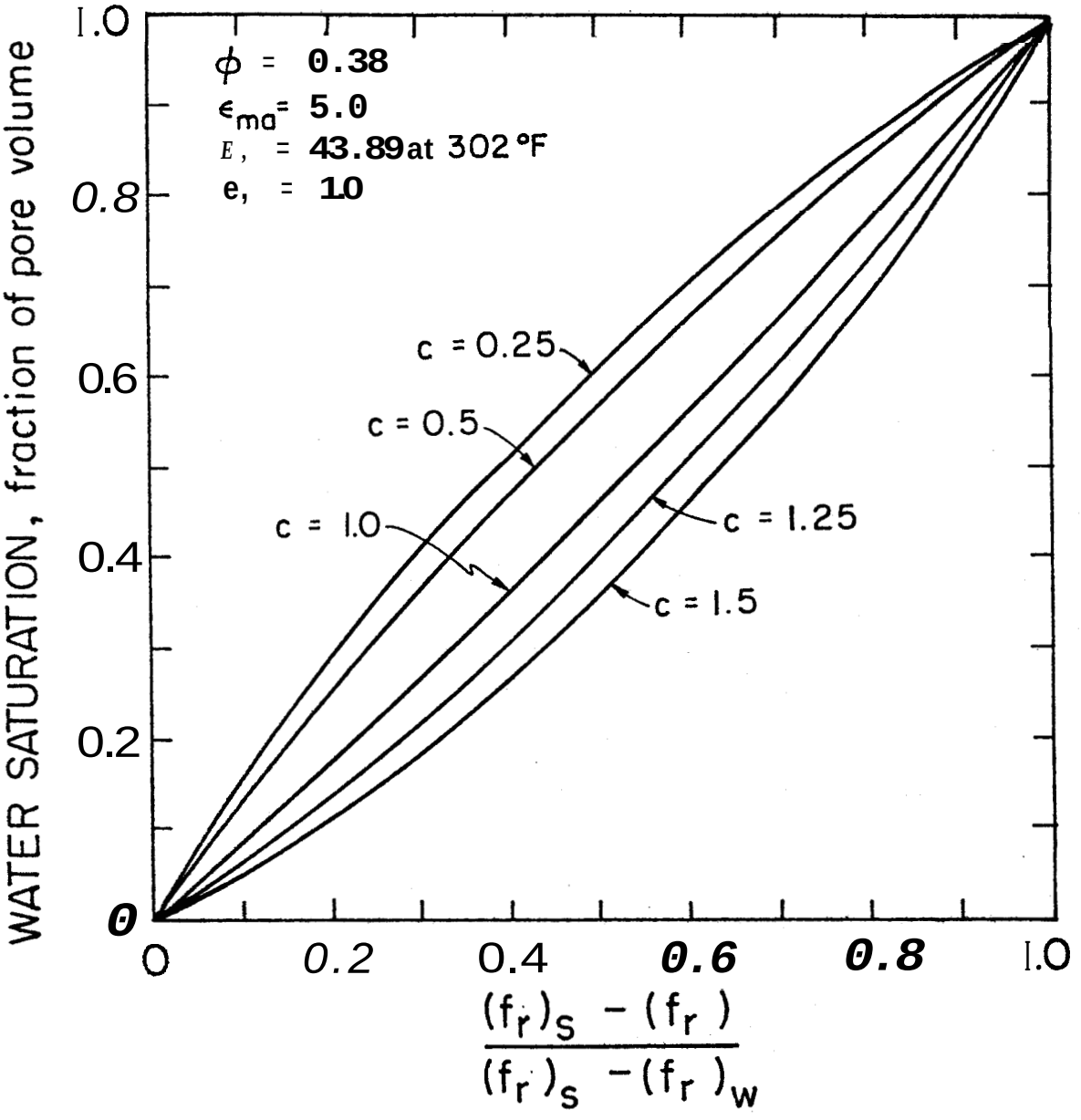

FIGURE 6-2. THEORETICAL CALIBRATION CURVES FOR THE CAPACITANCE PROBE

The details of the calculation of the calibration curve are presented in Appendix B.

Meador, et al.[23], indicated that the value of c, the formation dielectric cementation and polarization factor, might range from nearly zero to nearly two for most dielectric logging applications. Thus c values of 0-25, 0.5, 1.0, 1.25, and 1.5 were used in the calculation of the theoretical curves on Fig. 6.2.

Fig. 6-2 shows that the frequency shift of the probe is sensitive to the water saturation change, no matter what c value is used. Thus the capacitance probe may be used to measure water content (saturation) in the porous media.

In order to test the feasibility of the capacitance probe for measuring water saturation in porous media, and to see how the porous media-type and operating temperature level affect the probe calibration, actual calibrations of the probe were performed in synthetic consolidated sandstone cores filled with air-water mixtures at room temperature, and in sand packs filled with steam-water mixtures at elevated temperatures.

Because the dielectric constants of air and steam are nearly identical for a wide temperature range, the normalized static calibration of the probe in a core filled with air and water should also reflect the response of the probe in a core

filled with a steaa-water mixture. The water content (saturation, or volume fraction of pore volume) in a short synthetic consolidated sandstone core was calculated using the relation:

$$S_w = \frac{V_w}{V_p} = \frac{(W-W_d)/\rho_w}{(W_w-W_d)/\rho_w} = \frac{W-W_d}{W_w-W_d} \qquad (6-8)$$

where S_w = water saturation, volume fraction of pore volume

V_w = volume of water in core, cc

V_p = pore volume of core, cc

W = weight of partially-saturated core, gm

W_d = weight of dried core, gm

W_w = weight of fully water-saturated core, gm

ρ_w = density of water, gm/cc

The experimental results of static calibrations are presented in Appendix D-1. Typical results from static calibration testing in synthetic consolidated sandstone cores filled with air-water mixtures are shown in Fig. 6-3. Although the data show scattering in the high water saturation region, the relation between water saturation and the absolute probe signal (mV) is clear. Referring to Fig. 6-3 for a water saturation Less than E percent, the relationship is nearly linear. For water saturations above 60 percent, the calibration curve appears to fit a parabolic curve.

The scatter may be caused by the inhomogeneity of the test cores. An inhomogeneity effect an dielectric constant for a core was also reported by Meador, et al.[23]

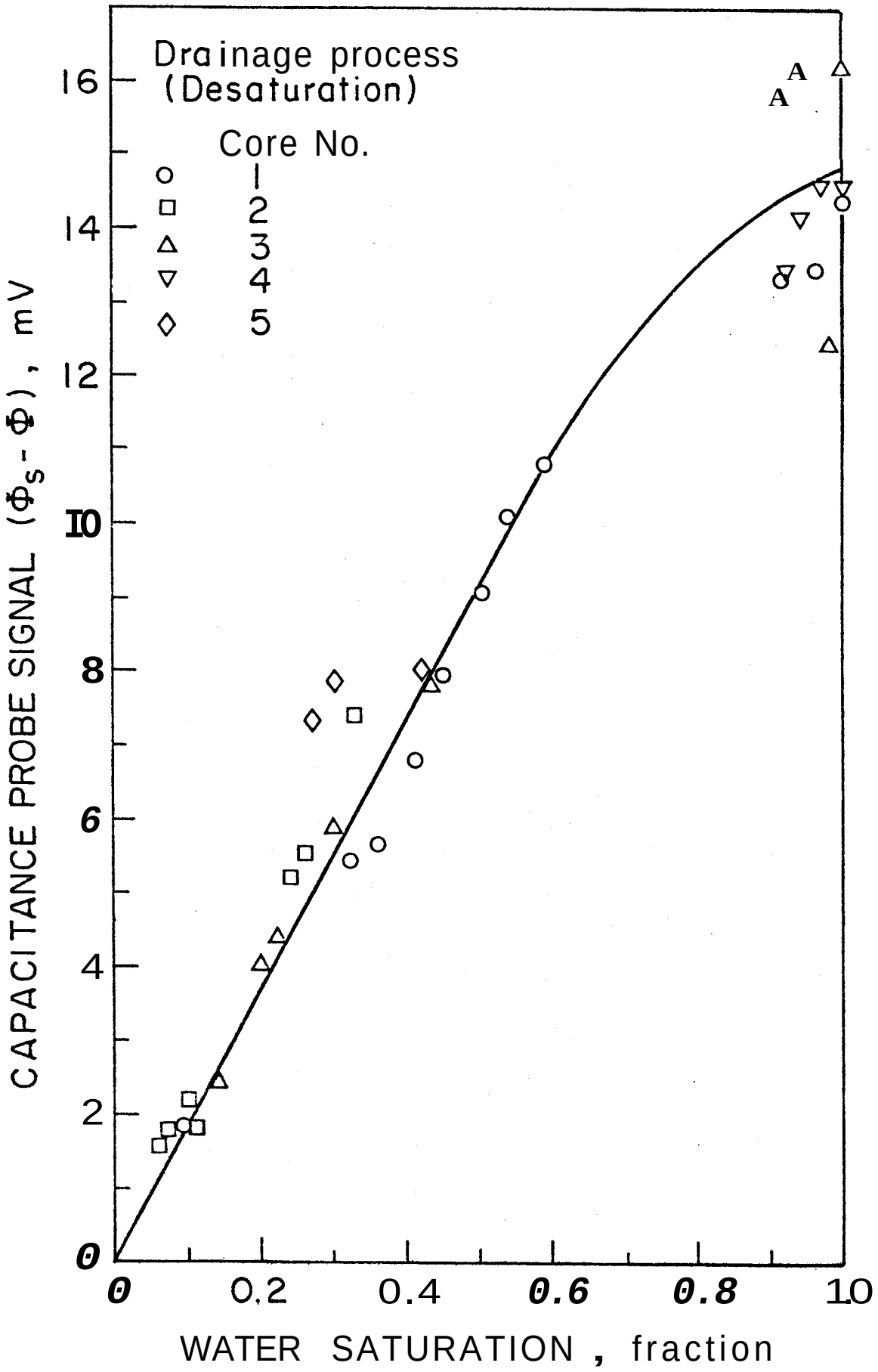

FIGURE 6-3. WATER SATURATION VS. CAPACITANCE PROBE SIGNAL IN A SYNTHETIC CONSOLICATED SANDSTONE CORE FILLED WITH AIR AND WATER AT ROOM TEMPERATURE (25°C)

The scatter at high water contents on Fig. 6-3 suggests the need for a normalized graph of the form of Fig. 6-2. Because the data for only cores No. 1, 3, and 4 in Fig. 6-3 included the probe signal ($\Phi_s - \Phi_w$) for 100 percent water saturation, the data for these cores were regraphed as water saturation vs. normalized probe signal. The normalized signal was defined as the ratio of the difference of probe signal from a dry core and a partially-saturated cone, to the difference of the probe signal from a dry core and fully water-saturated core. This is similar to the frequency ratio used on Fig. 5-2.

$$\Phi^* = \frac{\Phi_s - \Phi}{\Phi_s - \Phi_w} \qquad (6-9)$$

where Φ^* = normalized signal, fraction

Φ_s = probe signal from a core filled with air or steam, mv

Φ = probe signal from a core filled with air or steam and water mixture, mv

Φ_w = probe signal from a fully water-saturated core, mv

The result is shown in Fig. 6-4. Results are graphed in the manner of Fig. 5-2 because the calibration curves will be used to determine water saturation and to aid comparison. As can be seen, the data for the three cores agree well at all water saturations.

Next, two additional factors were studied. It was decided to use unconsolidated sand cores to study lithology

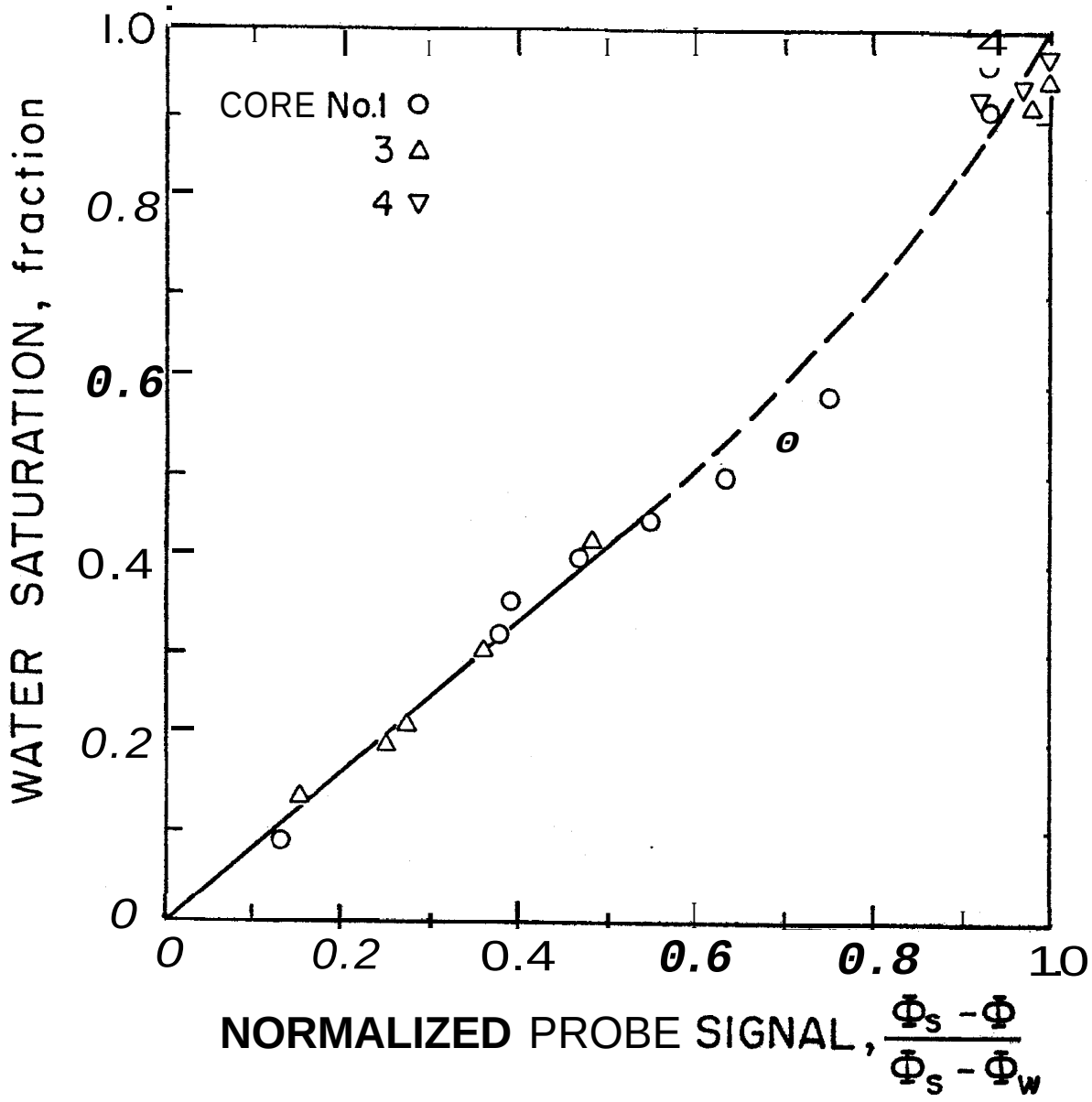

FIGURE 6-4. WATER SATURATION VS. NORMALIZED PROBE SIGNAL IN SYNTHETIC CONSOLIDATED SANDSTONE CORE AT ROOM TEMPERATURE (25°C)

effects and to avoid problems with heterogeneity, and then to perform calibrations at elevated temperatures to check the temperature effect on the calibration.

Calibrations were made in two different sand packs. One had a grain size ranging from 18 to 20 Tyler mesh, the other had a grain size ranging from 20 to 80 Tyler mesh. Sand was packed into a 2.7 inch diameter by 24 inch long tube p-sitioned horizontally in an air bath. Because the sand pack was fixed in a high temperature air bath, the weight of the core filled with a steam-water mixture could not be obtained by direct weighing on a balance; Eq. 6-8 could not be used to calculate the water saturation in the core. A new equation based on mass balance was derived for calculating water saturation in a core filled with a steam-water mixture at high temperatures. The derivation of this equation is presented in Appendix C. The result is:

$$S_w = \frac{v_w}{v_s - v_w} \left(\frac{v_s m}{V_p} - 1\right) \qquad (6\text{-}10)$$

where S_w = water saturation, volume fraction of pore volume

v_w = specific volume of water, cu ft/lb

v_s = specific volume of steam, cu ft/lb

m = total mass of the steam-water mixture in the core, lb

V_p = pore volume of the core, cu ft

To use Eq. 6-10, it is necessary to measure V_p, temperature (or pressure) and determine m by a mass balance.

Calibration curves were constructed by graphing water saturation vs. normalized probe signal (Eq. 6-9). Typical

results of static calibration testing with a large sand grain size are shown in Fig. 6-5. Typical results with a small sand grain size core are shown in Fig. 6-6. The scatter in the data for both Figs. 6-5 and 6-6 may be caused by gravity segregation in the high permeability sand packs.

The result of superposition of the two calibration curves from Figs. 6-5 and 6-6 is shown on Fig. 6-7. The resulting curve indicates that the probe calibration is nearly independent of sand grain size for the two sands used.

We can explore both the effects of temperature level and sandstone type by further comparisons. Fig. 6-8 shows the results of static calibration testing in a synthetic consolidated sandstone core filled with air and water at room temperature superimposed on the results of static calibration in a small sand grain, unconsolidated core filled with steam and water at high temperatures. One conclusion which may be drawn from Fig. 6-8 is that the normalized probe calibration curve is nearly independent of the operating temperature, and the type of sandstone porous medium surrounding the probe. However, the porosity range covered was limited: 34 to 38%. Even so, this is a remarkable result, and one of the most important findings of this study. This conclusion indicates the high potential of this device for geothermal experimental work.

Another important result is that the shape of the normalized calibration curves on all figures (Nos. 6-4 to 6-8) is similar to the computed curves for a dielectric cementation factor from 1 to 1.5 on Fig. 6-2, and appears linear over most of the water saturation range.

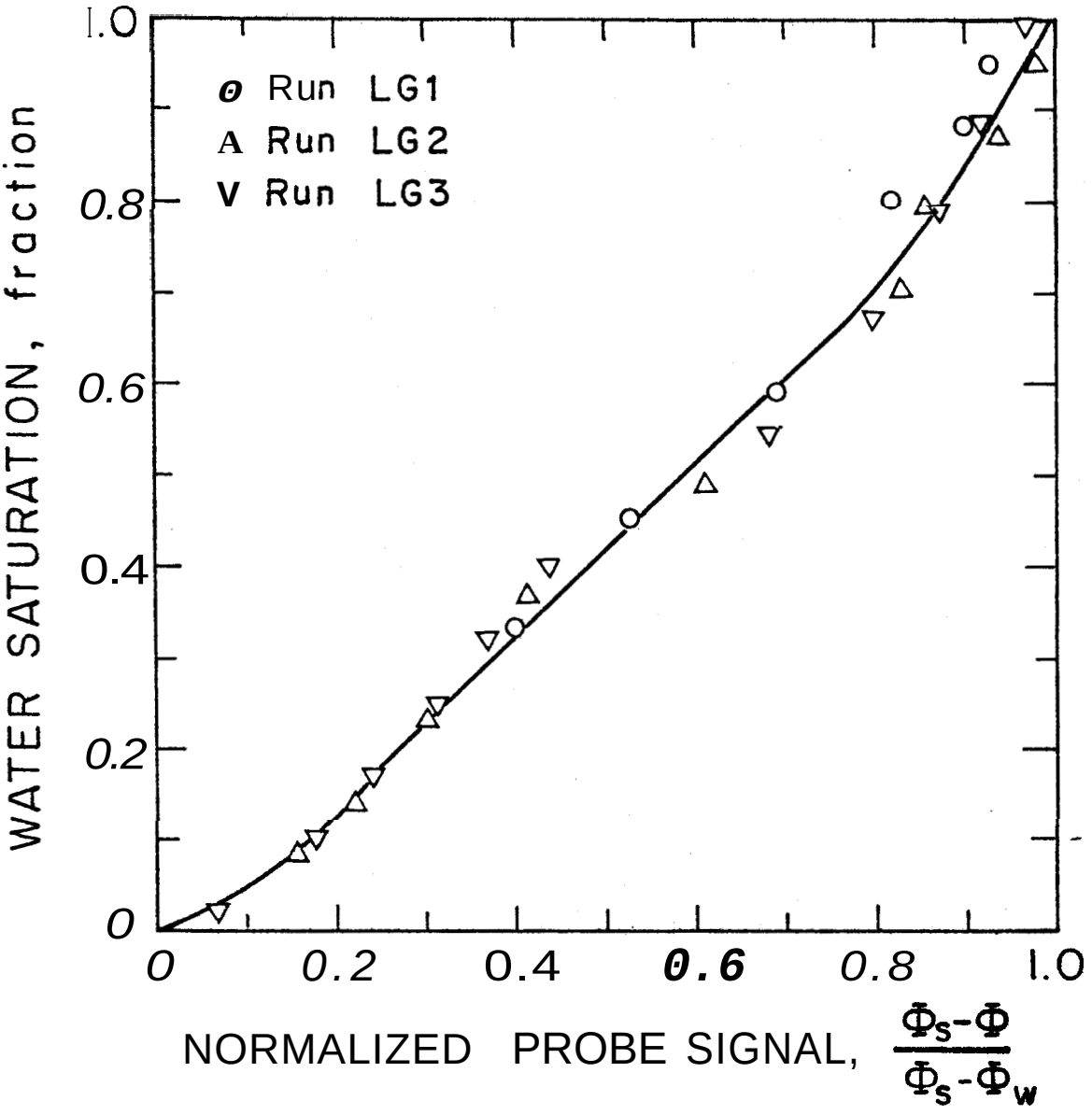

FIGURE 6-5. CALIBRATION CURVE FOR THE PROBE IN A SAND PACK OF 18-20 MESH GRAIN SIZE AT 300-310°F

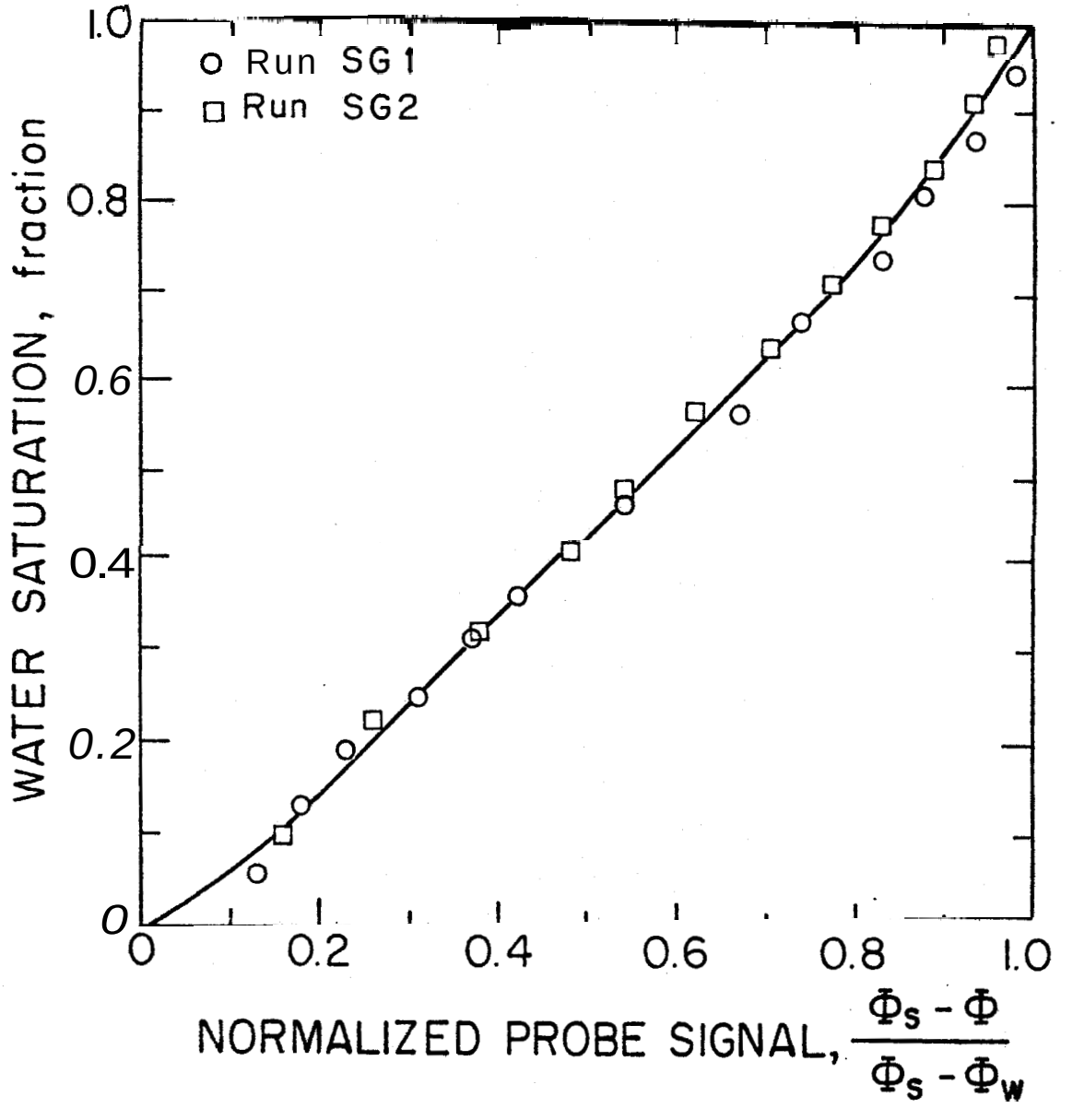

FIGURE 6-6. CALIBRATION CURVE FOR THE PROBE IN A SAND PACK OF 20-80 MESH GRAIN SIZE AT 300°F

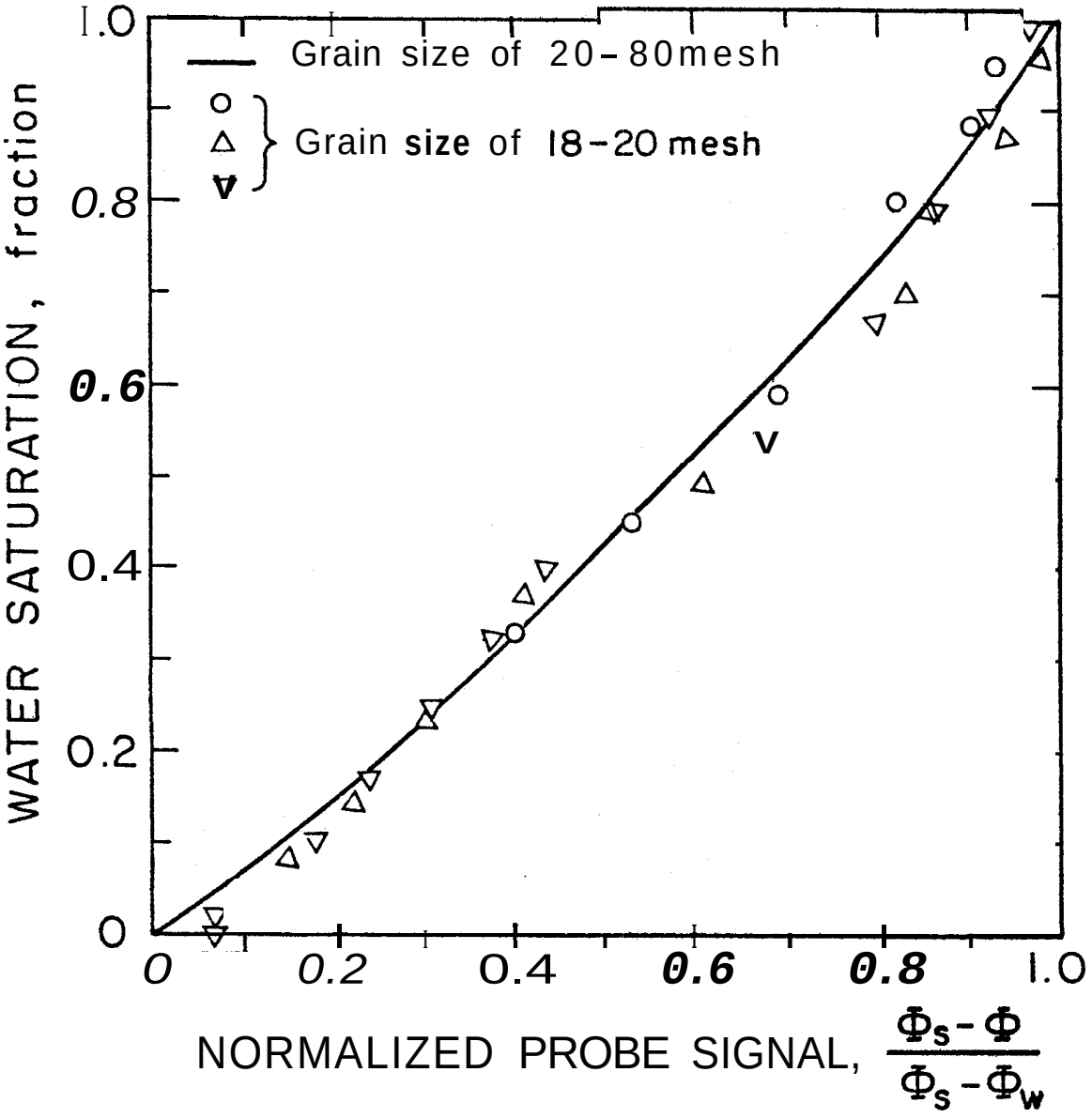

FIGURE 6-7. CALIBRATION CURVE FOR THE PROBE IN SAND PACKS OF DIFFERENT GRAIN SIZE AT HIGH TEMPERATURES (300-310°F)

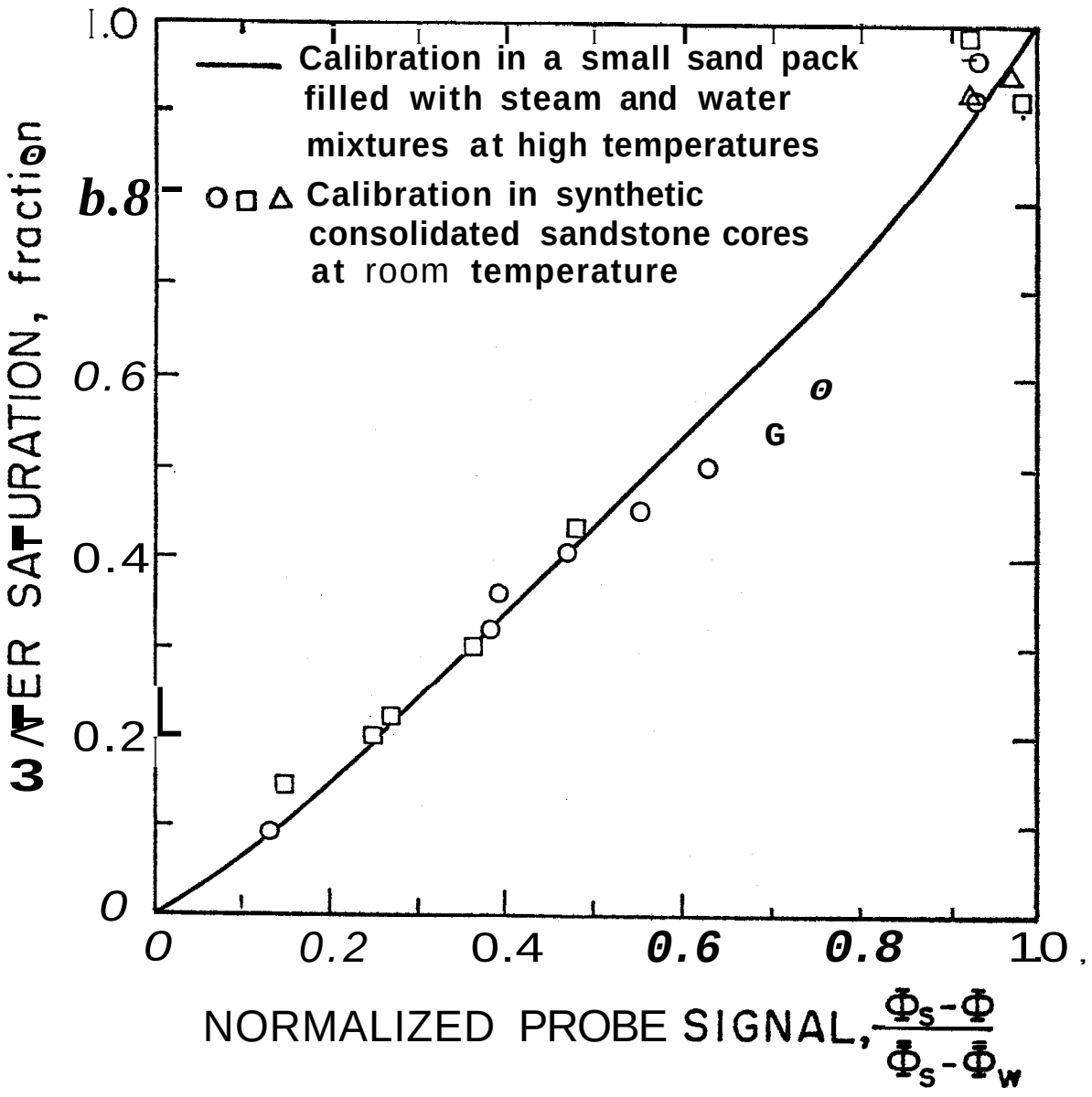

TIGURZ 6-8. COMPARISON OF THE **CALIBRATION** OF THE PROBE IN DIFFERENT MEDIA AND AT DIFFERENT OPERATING TEMPERATURES

These findings deserve further comment. An overlay comparison of the computed curves on Fig. 6-2 with the calibrations on Fig. 6-8 indicates good comparison with the curves on Fig. 6-2 for a "cementation" factor, c, of unity to 1.25. Although it is reassuring that such a good check between a computed and measured calibration was obtained, some problems remain. One calibration curve was obtained for both unconsolidated and consolidated media--indicating a single value of the cementation factor between unity and 1.25. This suggests the factor "c" is misnamed, and that although the form of the analytical equation is correct, the physical identification of paranetric dependence nay not be correct.

Another pertinent observation is apparent independence of the calibration from temperature level dependence. It is possible that one explanation may be a tendency toward temperature compensation inherent in the probe design. As temperature rises, the axial brass rod expands more than the plated glass sheath. This causes a detectable increase in the gap between the brass end cap and the silver-plated glass sheath. Details of a calibration of the probe in air *as* a function of temperature are given in Appendix D, Fig. D-1-1. This effect appears in opposite direction from the change in dielectric constant of water (liquid) with temperature change. Investigation of the nature of this effect was beyond the objectives of this study, but appear interesting enough to serve as an objective in a continuation of the study of the dielectric probe. Other interesting objectives will be presented later.

Attempts were also made to perform static calibration tests in the two-foot long synthetic consolidated sandstone cores filled wit'. steam and water. These tests were unsuccessful. The problem was that large saturation gradients developed in the low-permeability cores when steam and water were produced to generate different water saturations.

Because the calibration curves showed that the capacitance probe worked satisfactorily at high temperatures, the probe was used to neasure water saturation in steady, two-phase flow and depletion experiments with a synthetic consolidated sandstone core. The results of steady, two-phase flow experiments will be presented in the following section.

6-2 Steady, Two-Phase Flow Experiments with Synthetic Consolidated Sandstone Core. The steady, two-phase flow experiments were performed at two different ambient temperatures (295 and 336°F). The temperature profiles, saturation profiles, mass flow rate, and inlet and outlet pressures were recorded during the experiments. The experimental results are presented in Appendix 2-2. Typical temperature profiles are shown in Figs. 6-9 and E-IC, while typical water-saturation profiles are shown in Figs. 6-11 and 6-12.

As would be expected, the results agree with the concept that. flow of compressed water (single phase) in the porous media should be isothermal. Fig. 6-11 indicates a water saturation of unity to about 16 inches from the inlet end of the core, for Run No. 1, while Fig. 6-9 indicates almost constant

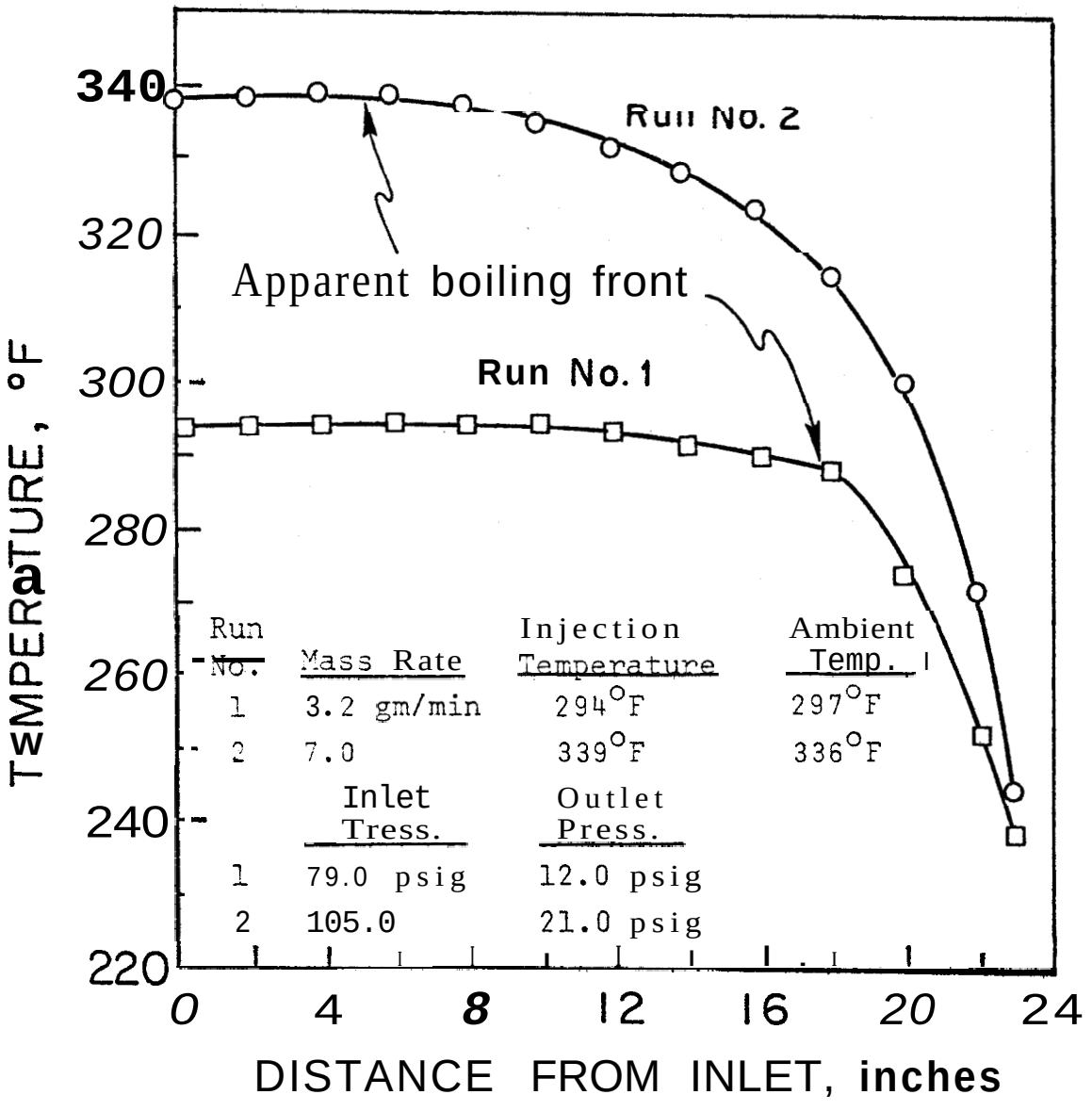

FIGURE 6-9. TEMPERATURE VS. DISTANCE FOR STEADY, TWO-PHASE FLOW EXPERIMENTS (RUNS 1 & 2) WITH SYNTHETIC CONSOLIDATED SANDSTONE CORE

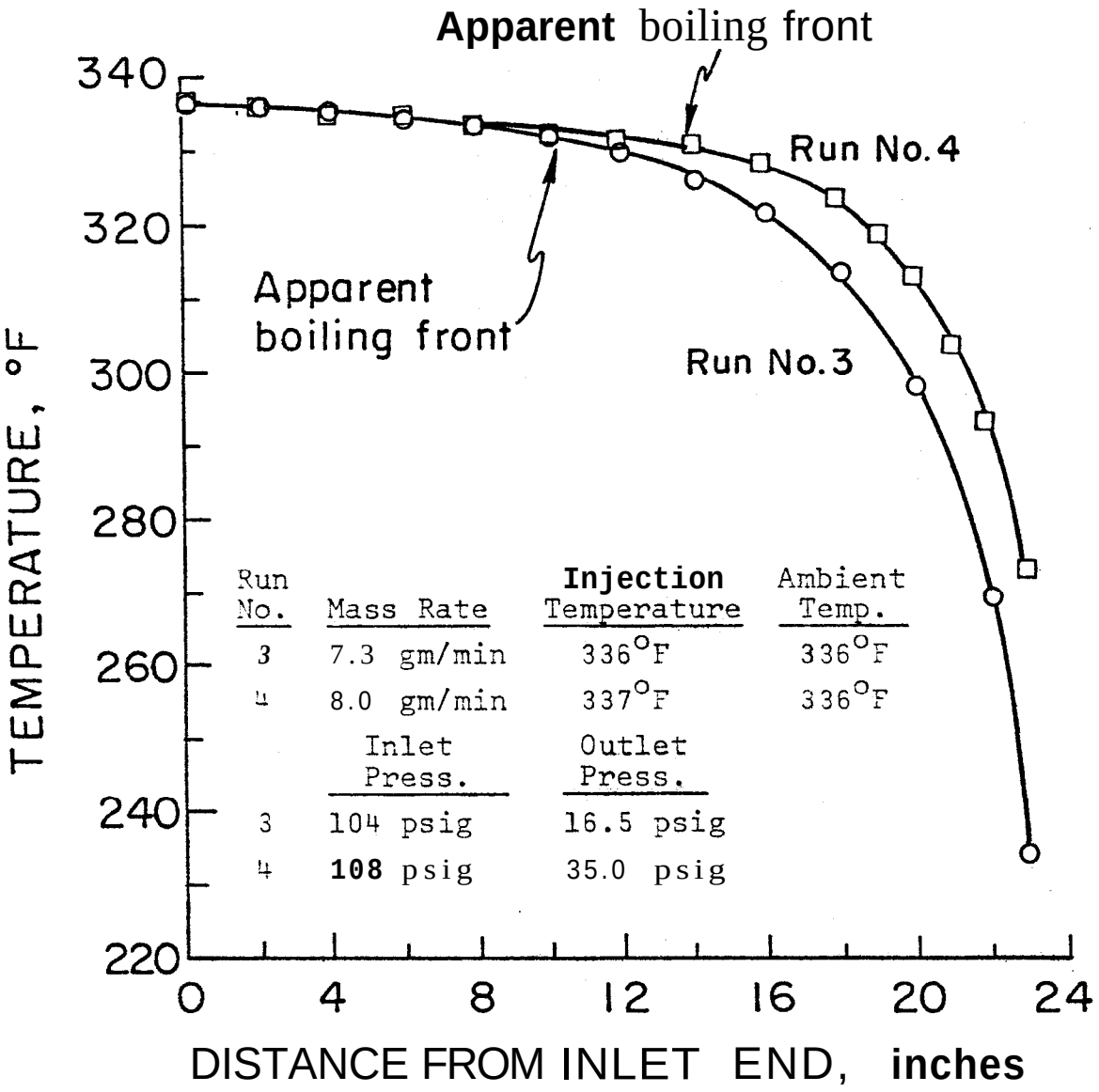

FIGURE 5-10. TEMPERATURE VS. DISTANCE FOR STEADY, TWO-PHASE FLOW EXPERIMENTS (RUNS 3 & 4) WITH SYNTHETIC CONSOLIDATED SANDSTONE CORE

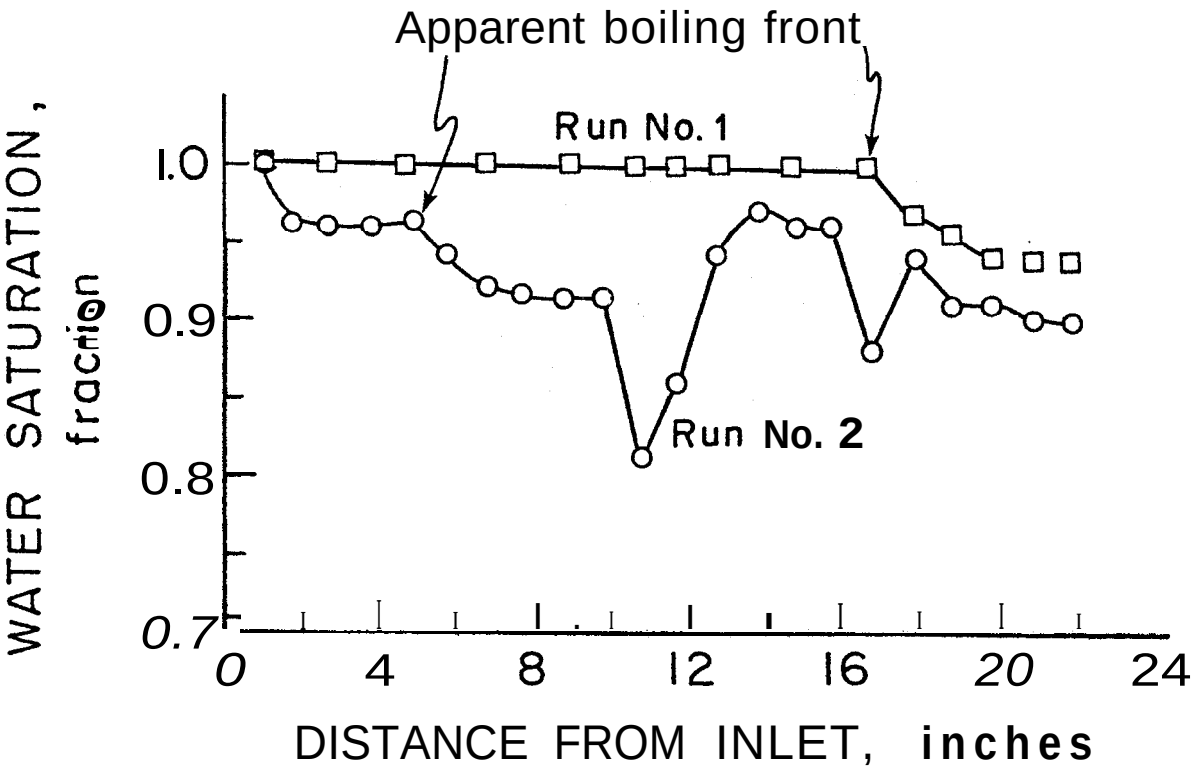

FIGURE 6-11. **WATER SATURATION VS [redacted] FOR** STEADY, TWO-PHASE FLOW EXPERIMENTS (RUNS 1 & 2) WITH SYNTHETIC CONSOLIDATED SANDSTONE **CORE**

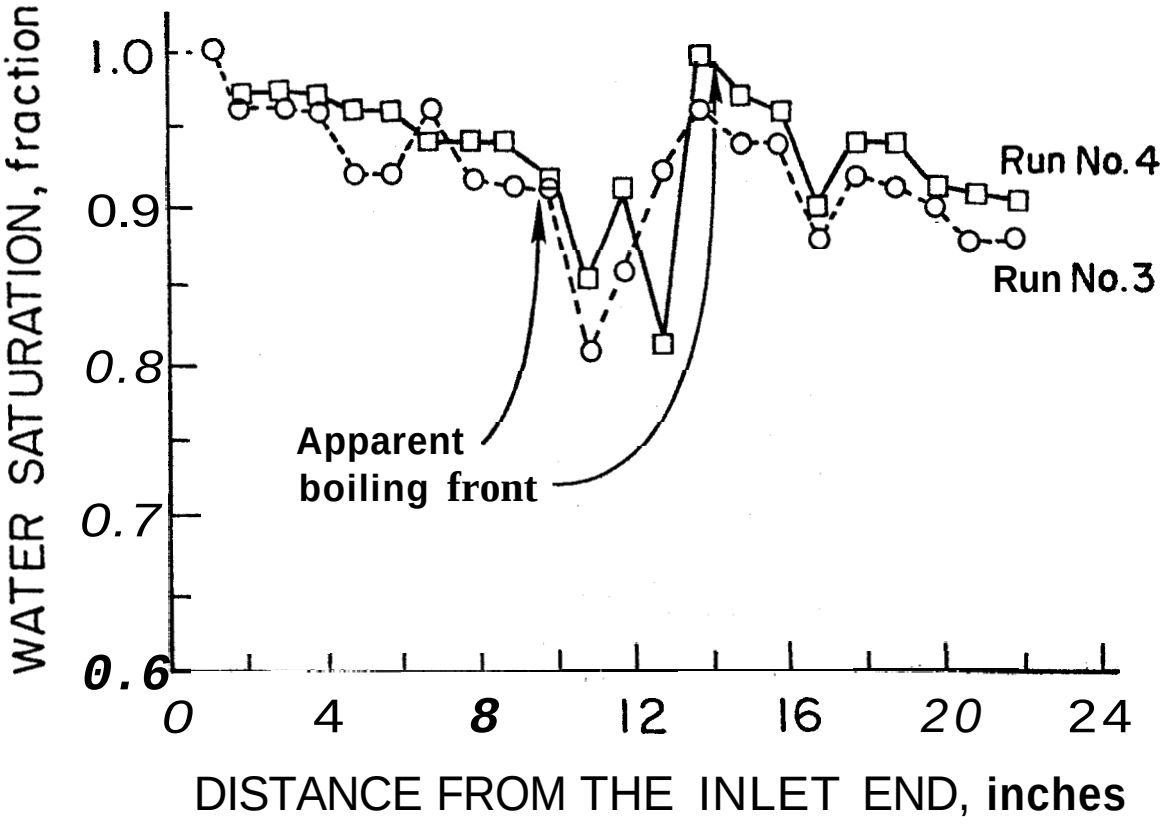

FIGURE 6-12. WATER SATUPATION VS. DISTANCE FOR STEADY, TWO-PHASE FLOW EXPERIMENTS (RUNS 3 E 4) WITH SYNTHETIC CONSOLIDATED SANDSTONE CORE

temperature to the same distances for Run No. 1. Fig. 6-9 indicates isothermal behavior to a distance of 6 inches from the inlet for Run No. 2; Fig. 6-11 indicates a water saturation of about 0.95 to unity for the first 4-5 inches of the core. This indicates that the sensitivity of water saturation determination may be on the order of ±5 percent of pore volune water content.

On the other hand, significant change in teaperature within the two-phase boiling flow region is characteristic for all runs. Referring to Fig. 6-11, the vapor saturation increases beyond the boiling front. The vapor saturation at the end increases with- initial reservoir temperature.

A strange drop in apparent water saturation at 11 inches fron the inlet is evident for Runs 2, 3, and 4 on Figs. 6-18 and 6-19. This nay be due to inhomogeneity of the synthetic consolidated sandstone core, because this corresponded to permeability change of the core (see Fig. 6-19).

Based on the assumptions of an isenthalpic process for steady, two-phase flow, and no vapor pressure lowering at high water 'saturations, the temperature profiles shown in Figs. 6-9 and 6-10 (and vapor pressures from. steam tables) were used to calculate the relative permeabilities to steam and water. The relative permeability ratio is given by (see Eq. 2-11):

$$\frac{k_w}{k_s} = \frac{\mu_w v_w}{\mu_s v_s} \left(\frac{1-f}{f}\right) \qquad (6\text{-}11)$$

where $f = \frac{h-h_w}{h_s-h_w}$ (see Eq. 2-61

and f is the mass fraction of the total flow stream which is vapor.

Introducing the absolute permeability, k, of the core. filled with water, Eq. 6-11 may be written as:

$$\frac{k_w}{k} = \frac{\mu_w v_w}{\mu_s v_s} \left(\frac{1-f}{f}\right) \frac{k_s}{k} \qquad (6\text{-}12)$$

In the two-phase flow region, the following equation is also valid (see Eq. 2-10):

$$\frac{k_w/k}{\mu_w v_w} + \frac{k_s/k}{\mu_s v_s} = -\frac{w}{Ak\frac{dp}{dx}} \qquad (6\text{-}13)$$

Introducing $\frac{k_w}{k}$ from Eq. 6-12 into Eq. 6-13 and rearranging, the result is:

$$\frac{k_s}{k} = 14.0 \frac{wf}{Ak} \cdot \frac{\mu_s v_s}{\left(-\frac{dp}{dx}\right)} \qquad (6\text{-}14)$$

where w = mass flow rate, gm/min

H = viscosity, cp

v = specific volune, cc/gm

A = cross sectional area, cm^2

x = distance, cm

k = absolute permeability, md

p = core pressure in two-phase region, atm

Table 6-1. Calculation of Steam and Water Relativity Permeabilities for a Synthetic Sandstone Core, Run No. 2.

x cm	T °F	p psia	dp/dx psi/cm	hw Btu/lb	hs Btu/lb	f, Mass fr.	μ_s, cp	μ_w, cp	v_s Cu ft/lb	v_w Cu ft/lb	k_s/k	k_w/k	S_w
0	339	114 9											
5.08	339												
10.16	339												
15.24	399												
20.32	338	114.8											
25.40	335	110.3											
30.48	332	105.9											
35.56	329	101.6	-1.28	299.81	1188.2	0.0118	0.0149	0.17	4.369	0.0177	0.092	0.357	0.97
40.64	324	94.8	-1.97	294.6	1186.8	0.0176	0.0149	0.17	4.665	0.0177	0.095	0.231	0.96
45.72	315	83.5	-2.76	285.3	1184.4	0.0278	0.0146	0.18	5.262	0.0176	0.119	0.175	0.94
50.80	300	67.0	-3.54	2647	1180.2	0.0445	0.0143	0.19	6.472	0.017	0.178	0.138	0.91
55.88	272	43.2	-5.90	241.0	1171.6	0.0744	0.0139	0.21	9.762	0.0172	0.262	0.088	0.90

Note: w = 7.0 gm/min
k = 35.6 md
h_{inlet} = 310.3 Btu/lb

Because all parameters on the right-hand side of Eq. 6-14 are known, the relative permeability to steam can be calculated. The relative permeability to water can be obtained from Eq. 6-12. To demonstrate this technique for measuring relative permeabilities to steam and water in 2-foot long consolidated sandstone cores, the data for Run No. 2 was selected for calculation because it had a large saturation variation. Table 6-1 presents the calculation results for Run No. 2 for a synthetic consolidated sandstone core. Thus, combining this data with the measured water saturations, relative permeability curves for steam and water flow can be constructed. The relative permeability curves so constructed are for a drainage process because the liquid water saturation decreased due to an increase in the steam flow.

The results in Table 6-1 deserve further discussion. It is not obvious that one can simply graph the relative permeabilities vs. water saturation in the conventional manner. The increase In steam saturation in the two-phase flow region was a result of a pressure and attendant temperature drop. Thus each relative permeability value in Table 6-1 is for a different temperature. Because it has been shown that relative permeabilities in sandstones are functions of temperature level, it is likely that each point in Table 6-1 is a point from a line different from that of the other points. It is possible to explore the nature of relative permeability curves by using known equations for drainage flow processes. First, we will review briefly some pertinent studies.

Corey[42] indicated that far all relative permeabilities, Burdine's Equation (Ref. 43) for tortuosity can be combined with the Kozeny-Karman equations to express the relative permeability to water as:

$$k_{rw} = \left(\frac{S_w - S_{wi}}{1 - S_{wi}}\right)^2 \frac{\int_0^{S_w} \frac{dS_w}{p_c^2}}{\int_0^1 \frac{dS_w}{p_c^2}} \qquad (6\text{-}15)$$

where S_{wi} = irreducible water saturation, fraction of pore volume

p_c = capillary pressure of the core corresponding to water saturation, S_w

For the relative permeability to gas:

$$k_{rg} = \left(1 - \frac{S_w - S_{wi}}{S_m - S_{wi}}\right)^2 \frac{\int_{S_w}^1 \frac{dS_w}{p_c^2}}{\int_0^1 \frac{dS_w}{p_c^2}} \qquad (6\text{-}16)$$

The S_m was defined as:

$$S_m = 1 - S_{gc} \qquad (6\text{-}17)$$

where S_{gc} = critical gas saturation

If S_{gc} is assumed negligible, or if S_m is assumed to be unity, Eq. 6-16 becomes

$$k_{rg} = \left(1 - \frac{S_w - S_{wi}}{1 - S_{wi}}\right)^2 \frac{\int_{S_w}^{1} \frac{dS_w}{P_c^2}}{\int_{0}^{1} \frac{dS_w}{P_c^2}} \qquad (6\text{-}18)$$

Defining $S_w^* = \frac{S_w - S_{wi}}{1 - S_{wi}}$, Eqns. 6-15 and 6-18 become

$$(k_{rw})_{dr} = (S_w^*)^2 \frac{\int_{0}^{S_w^*} \frac{dS_w^*}{P_c^2}}{\int_{0}^{1} \frac{dS_w^*}{P_c^2}} \qquad (6\text{-}19)$$

and

$$(k_{rg})_{dr} = (1 - S_w^*)^2 \frac{\int_{S_w^*}^{1} \frac{dS_w^*}{P_c^2}}{\int_{0}^{1} \frac{dS_w^*}{P_c^2}} \qquad (6\text{-}20)$$

where $(k_{rw})_{dr}$ = relative permeability to water for a drainage process

$(k_{rg})_{dr}$ = relative permeability to gas for a drainage process

The integrals in Eqs. 6-19 and 6-20 can be evaluated for a known pore size distribution index, λ. This work, originated by Corey and co-workers[49], was summarized by Standing[44]. The results are:

For the water:

$$(k_{rw})_{dr} = (S_w^*)^{\frac{2+3\lambda}{\lambda}} \qquad (6\text{-}21)$$

For the gas:

$$(k_{rg})_{dr} = (1-S_w^*)^2 \left[1-(S_w^*)^{\frac{2+\lambda}{\lambda}}\right] \qquad (6\text{-}22)$$

For a pore size distribution index, λ of 2 as used by Corey, Eqs. 6-21 and. 6-22, become

$$(k_{rw})_{dr} = (S_w^*)^4 \qquad (6\text{-}23)$$

$$(k_{rg})_{dr} = (1-S_w^*)^2 (1-S_w^{*2}) \qquad (6\text{-}24)$$

Eqs. 6-23 and 6-24 are known as the "Corey Equations." The relative permeability to gas can be obtained from Eq. 6-22 if a relationship between gas permeability at irreducible water saturation and absolute permeability is known. Standing[44] presented an emperical equation for irreducible water saturation values between 0.2 and 0.5. The result for the relative permeability to gas is:

$$k_{rg} = 1.08 - 1.11\, S_{wi} - 0.73\, (S_{wi})^2 \qquad (6\text{-}25)$$

Based on the experimental relative permeability and water saturation data from this study, the irreducible water

saturation can be calculated by using Eq. 6-21 and the definition of S_w^* for determining a value of X. Because for a wide range of pore size the distribution index, X, is known to range from 0.5 to 2, distribution indices, X, of 0.5, 0.75, and 2.0 were used for calculations. The results of these calculations are shown in Table 6-2.

The results indicate that the irreducible water saturation for the synthetic, consolidated sandstone core appear- to be very large (greater than 60 percent). Many recent studies have observed an increase in irreducible water saturation with temperature increase. Poston, et al.[45], reported that practical irreducible water saturation increased with increasing temperature for oil-water flow in unconsolidated sandstones. Weinbrandt, et al.[46], also found that the irreducible water saturation increased with increasing temperature for oil-water flow in consolidated Boise sandstones. Cassé and Ramey[47], and later, Aruna[48], reported that the absolute permeability of sandstones to water decreased with increasing temperature. It appears that the sandstone becomes more water wet at high tenperatures. This agreed with findings by Sinnokrot[50,51]

Although the results of this study appear to agree in principle with previous studies, i.e., that S_{wi} increases with increasing temperature, no specific information was found in the literature for steam-water systems. The results in Table 6-2 must be considered preliminary, but they are also unique. It is possible to proceed further toward development of complete relative permeability curves for specific temperature levels.

Table 6-2. Calculation of Irreducible Water Saturation from Experimental Relative Permeability and Saturation Data

			T=300°F S_w=0.91		T=315°F S_w=0.94		T=324°F S_w=0.96		T=329°F S_w=0.97	
λ	$\frac{2+3\lambda}{\lambda}$	$\frac{2+\lambda}{\lambda}$	k_{rw}	S_{wi}	k_{rw}	S_{wi}	k_{rw}	S_{wi}	k_{rw}	S_{wi}
0.5	7	5	0.138	0.64	0.175	0.73	0.231	0.79	0.357	0.67
0.75	5.67	3.67	0.138	0.71	0.175	0.77	0.231	0.83	0.357	0.82
2.0	4	2	0.138	0.77	0.175	0.83	0.231	0.87	0.357	0.87

Note: S_w = water saturation

S_{wi} = irreducible water saturation

Based on the calculated irreducible water saturation, relative permeability curves were calculated using Corey's equations ($\lambda=2$). The experimental relative permeability curves for steam and water so obtained are shown on Fig. 6-13 by the solid and dashed lines. Some data points from Table 6-1 are also shown. A reasonable comparison results.

Development of the relative permeability curves shown on Fig. 5-13 was not an objective of the present study. It did seem worthwhile to explore one possible way to develop such information when the opportunity arose, because it was the intention to obtain such information in the next phase of this research project. If this method is pursued further, several steps could lead to improvements. First, it would be desirable to measure capillary pressure curves for desaturation of core samples with steam over a range in temperature. These curves could be used to obtain the pore size distribution index,, X. Second, it would be desirable to obtain information over a broader steam saturation range. This might be achieved by using porous media with lower irreducible water saturations, and by operating with a larger pressure difference.

It is clear that the apparent high irreducible water saturations obtained from the information on Fig. 6-13 may not be real. Capillary pressure measurements should go a long way toward settling this question.

Another obvious conclusion is that the steady-state, two-phase flow experiments used to obtain Fig. 6-13 may not be the best way to obtain relative permeability data for steam-water systems. One alternate way would be by calculation from the Brooks and Corey[49] method with capillary pressure information.

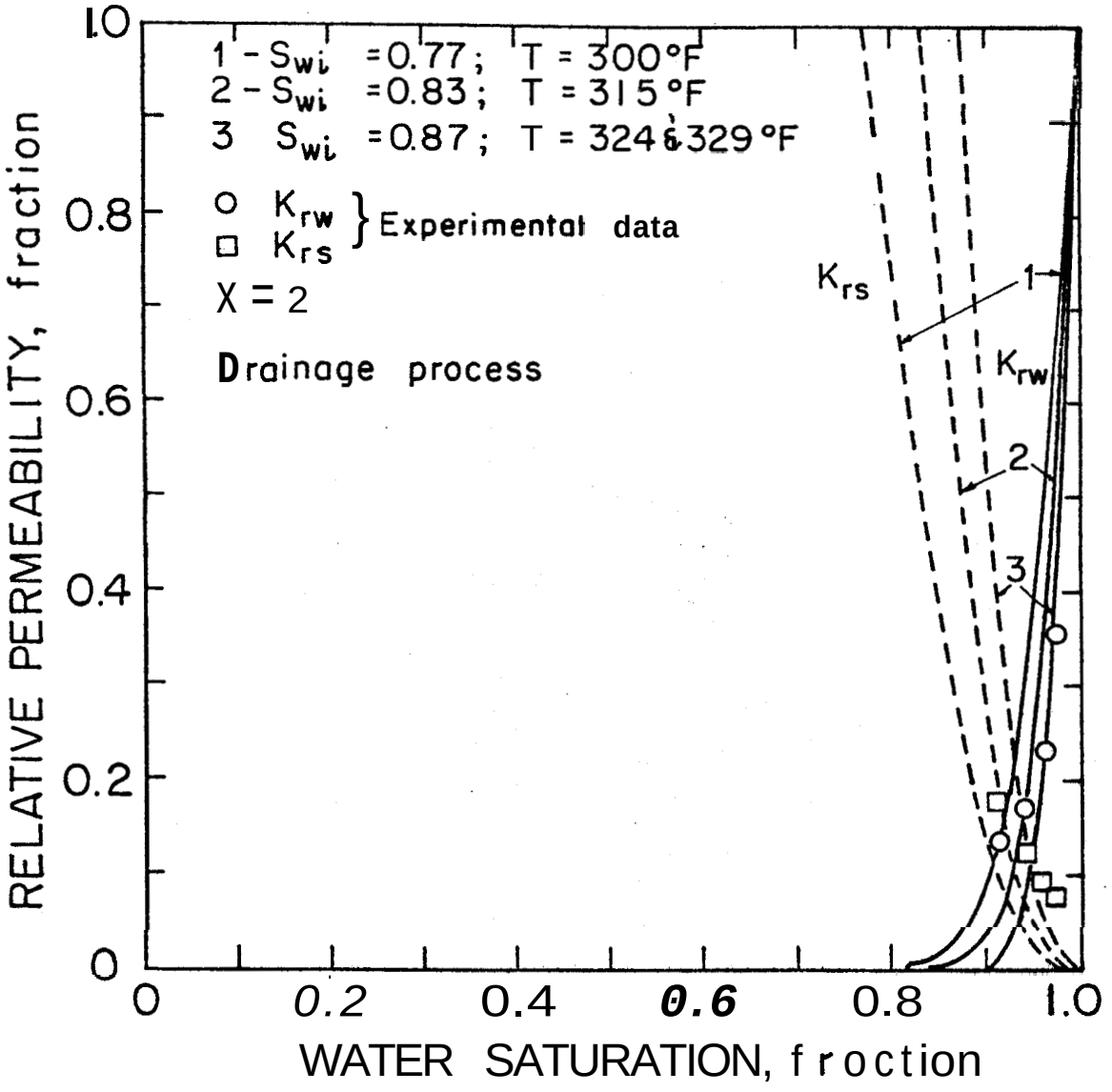

FIGURE 6-13. RELATIVE PERMEABILITY TO STEAM AND WATER VS. WATER SATURATION FOR A SYNTHETIC CONSOLIDATED SANDSTONE CORE

Perhaps an interesting way to calibrate the dielectric constant probe would be by immersing it in a core in a steam-water capillary pressure desaturation experiment.

We turn now to consideration of the results of the bate:?-type depletion experiments.

6-3 Depletion (Batch) Experiments

Two experiments were performed with initial core temperatures of 295°F (Run No. 1), and 340°F (Run No. 2). The experimental procedure was presented in Section 5.5. The experimental data (temperature, saturation, cumulative water production, and inlet and outlet pressures) are presented in Appendix D-3. Temperatures inside the core are shown in Figs. 6-14 and 6-15. The saturation histories are shown in Figs. 6-15 and 6-17. Referring to Figs. 6-16 and 6-17, boiling starts at the producing end (extreme right), and gradually spreads to the closed end of the core (extreme left). At longer production times, a steam zone forms near the producing end. Sometimes a small region of high vapor saturation forms at the closed end due to heat conduction through the end plug.

Regarding the temperature profiles (Figs. 6-14 and 6-15), tenperature decreases at the closed end during the early production period. The temperature near the producing end tends to increase toward the initial (or ambient) temperature during long production times, also due to heat conduction through the end plug. This is more apparent in Fig. 6-15 than in Fig. 6-14. The steam zone indicated from saturation measurements agrees well with inferences from temperature measurements. The main objective of these experiments was to supply

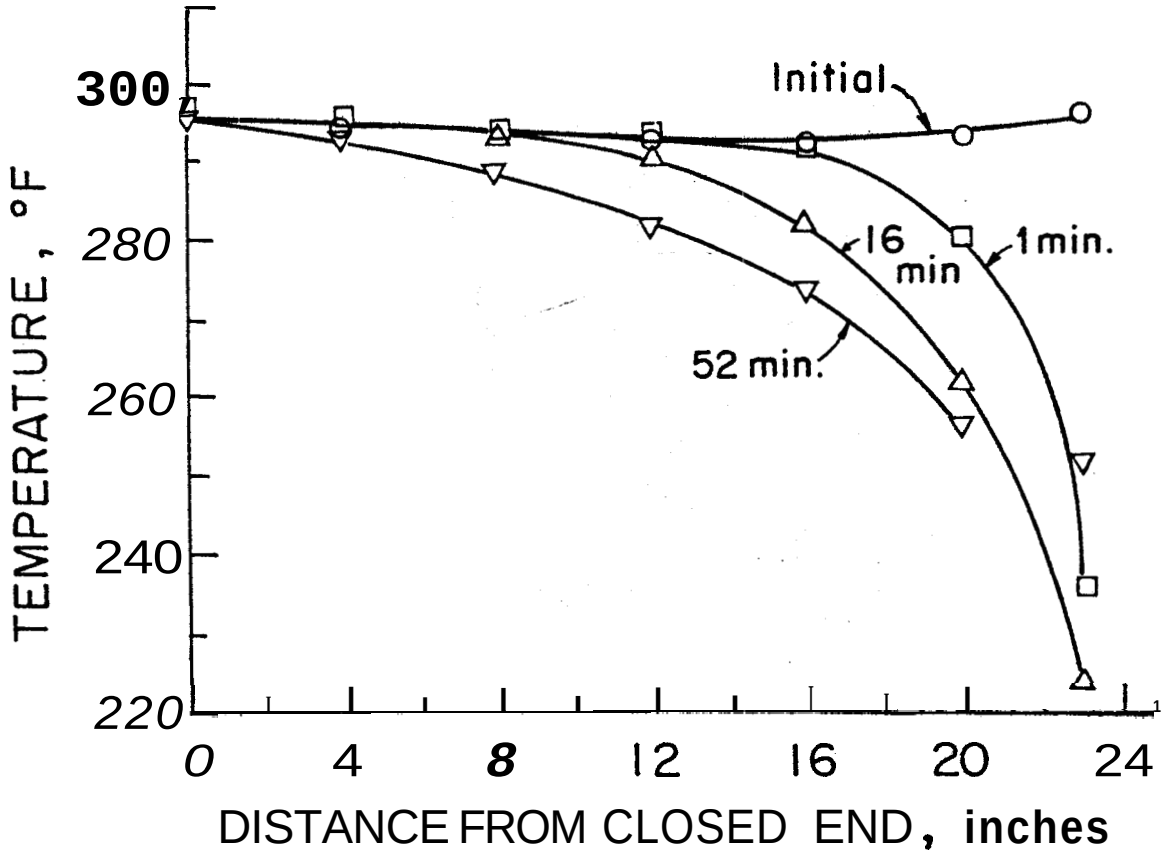

FIGURE 6-14. TEMPERATURE VS. DISTANCE FOR DEPLETION EXPERIMENT RUN NO. 1 (T_i = 295°F) WITH A SYNTHETIC CONSOLIDATED SANDSTONE CORE

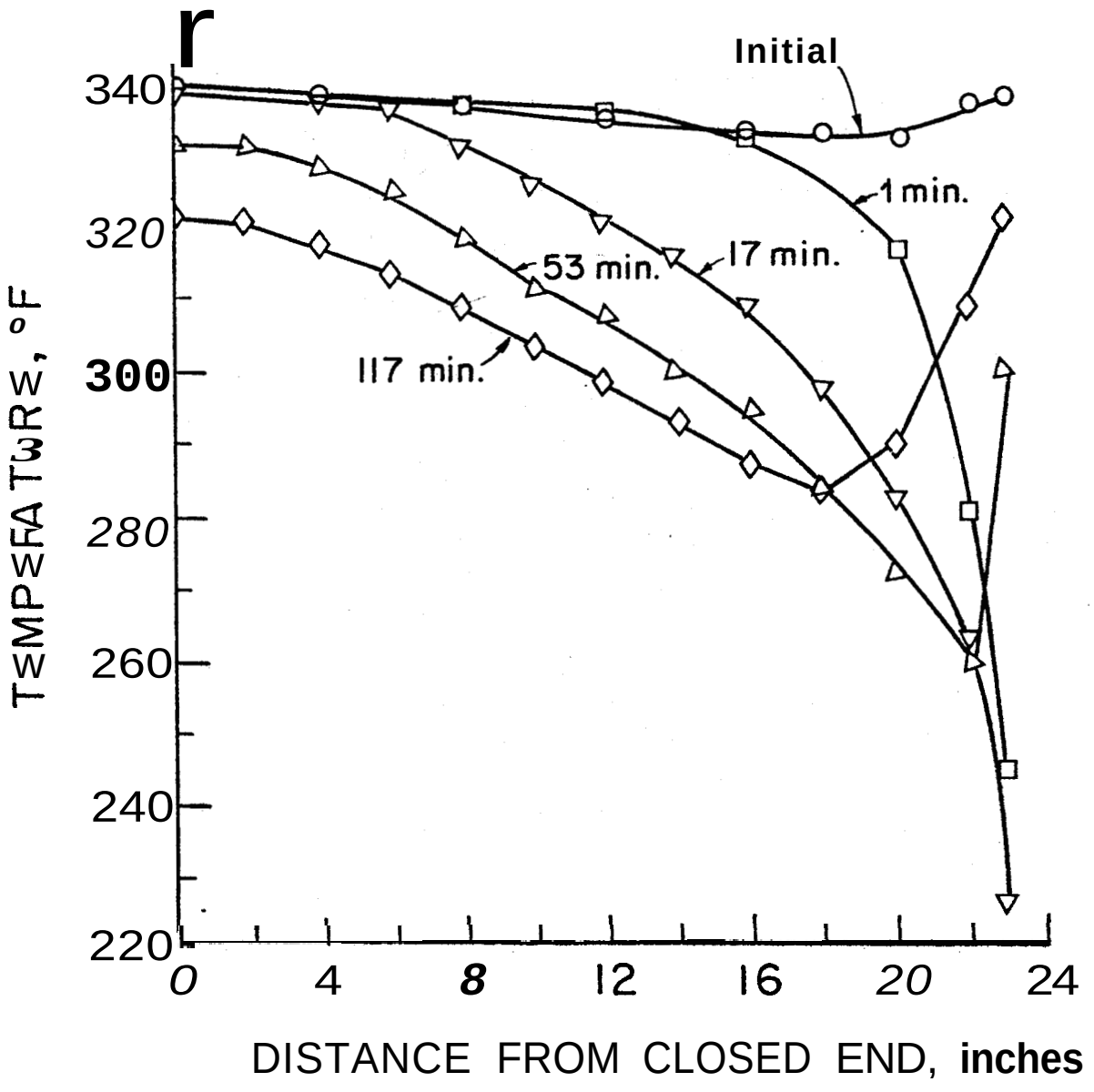

FIGURE 6-15. TEMPERATURE VS. DISTANCE FOR DEPLETION EXPERIMENT RUN NO. 2 (T_i = 340°F) WITH A SYNTHETIC CONSCLICATED SANDSTONE CORE

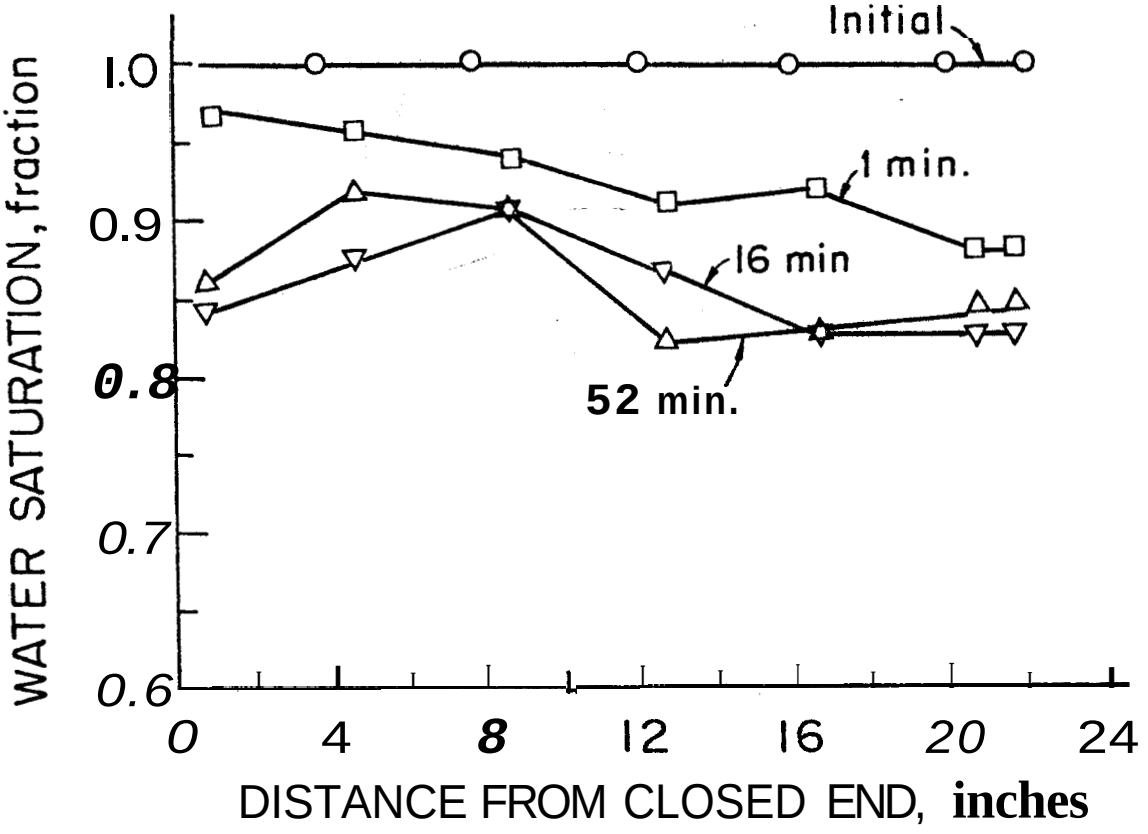

FIGURE 6-16. WATER SATURATION VS. DISTANCE FOR DEPLETION EXPERIMENT RUN NO. 1 (T_i = 295°F) WITH A SYNTHETIC CONSOLIDATED SANDSTONE CORE

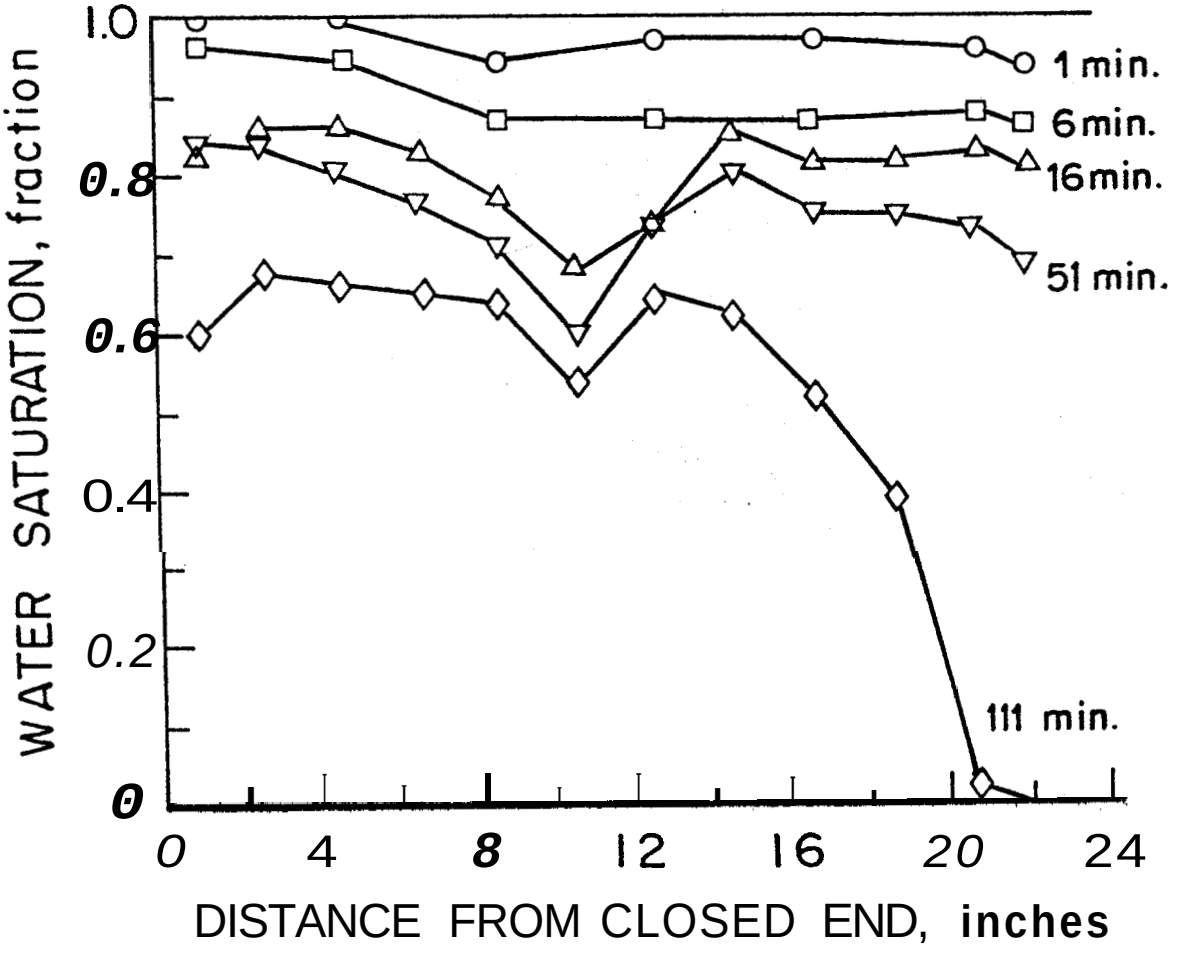

FIGURE 6-17. WATER SATURATION VS. DISTANCE FOR DEPLETION EXPERIMENT RUN NO. 2 (T_i = 340°F) WITH A SYNTHETIC CONSOLIDATED SANDSTONE CORE

physical data for comparison with numerical model solutions for saturation and temperature profiles. No similar saturation measurements for steam-water flow have been made in consolidated sandstone to our knowledge.

One other unique experiment was performed to aid planning for the next phase of this research project. A batch experiment with production of steam from a brine reservoir was performed. This experiment was intended to permit a preliminary study of the important characteristics of operating batch production experiments when the core initially contained a brine.

6-4 Brine Experiment

The experimental procedure was presented in Section 5-6. For convenience, the procedure involved filling the core with a 12,000 ppm sodium chloride solution and then producing it as in the batch depletion experiments. In addition, the resistivity of the produced liquid was measured during the run with a dip cell conductivity meter. After an initial depletion run, the core was reheated and another production cycle followed. At the end of the experiment, the core was dry. The core was then cut into eleven two-inch sections and the permeability to nitrogen measured with precipitated salt in place and again after removal of the salt by circulation in deionized water and drying.

The amount of salt deposited in each core plug was determined by first measuring the resistivity of each pore volume of the injected deionized water effluent. Then a calibration curve of salt concentration vs. dip cell conductivity

meter reading *was* used. Finally, the total deposited salt in the core was obtained by summing up the salt in each pore volume of the injected. water effluent. The calibration curve is shown in Appendix D-4, Fig. D-4-1. The salt content of effluent in Fig. D-4-1 was obtained by evaporating the injected water effluent and weighing the deposited salt. The experimental procedures for measuring gas permeability and salt content are presented in Appendix E. The detailed results of this experiment are presented below.

The resistivity of the produced water is shown in Fig. 6-18, and is also presented in Appendix D-4. Results show that the produced water becomes fresher after each. production run. This is not surprising because the steam carries little salt. Thus the results also indicate that more steam was produced in each succeeding production run.

The gas permeability of the core with deposited salt in place is shown in Fig. 6-19. The results of the gas permeability neasurements for the core containing salt and after salt extraction are presented in Table 6-3. The permeability results indicate that the permeability of the core is not affected by salt deposition for the given system. This is not greatly surprising. The largest salt concentration measured at the outflow end of the core was 0.011 gm/cc pore space. Since the specific gravity of salt is 2.163, this corresponds to a salt "saturation" of 0.005 fraction of pore volume.

The amount of salt deposited in the core is shown in Fig. 6-20, and is also presented in Appendix D-4. This result shows that most salt deposits near the producing end, as would be expected.

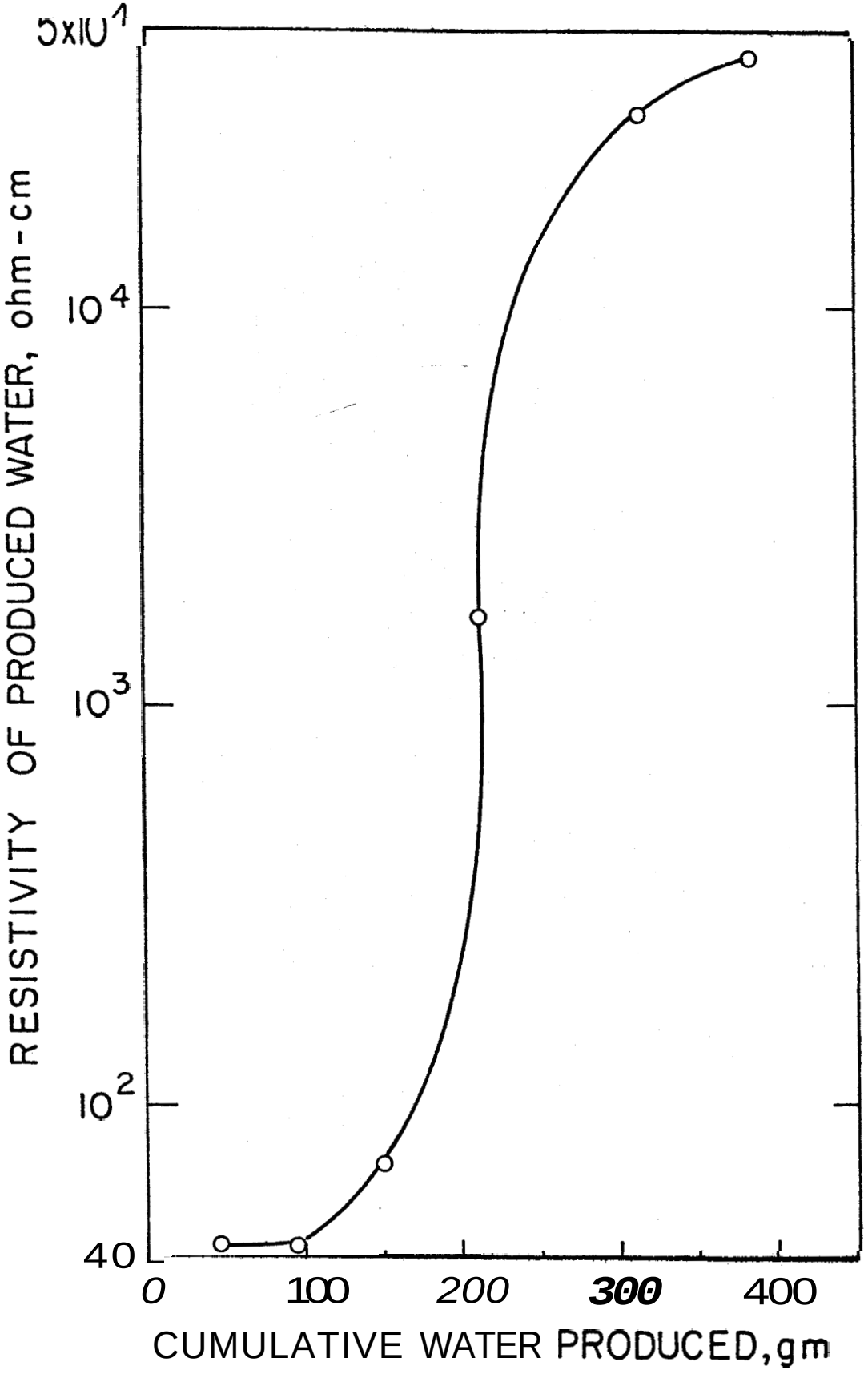

FIGURE 6-18. RESISTIVITY OF PRODUCED WATER

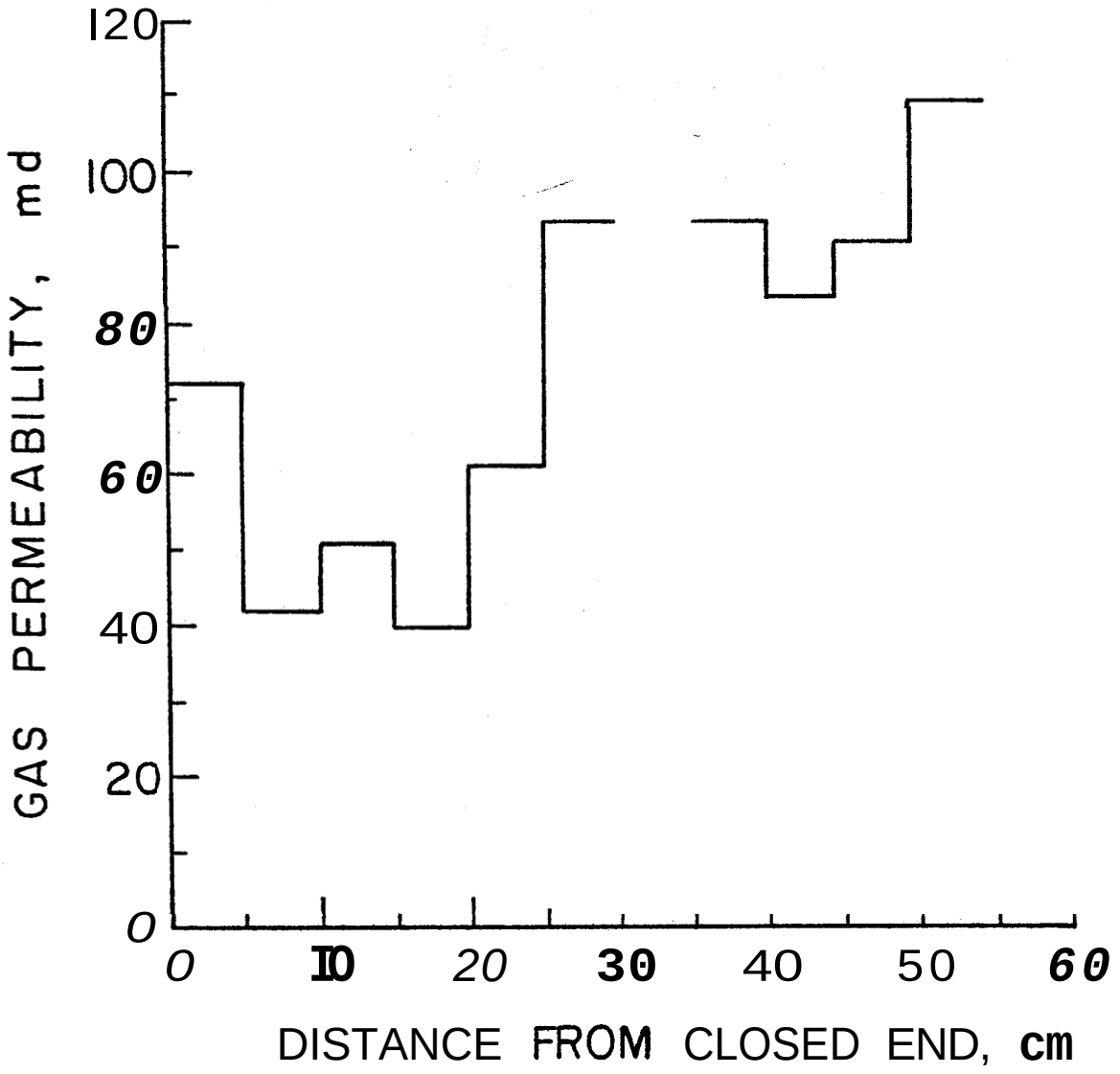

FIGURE 6-19. GAS PERMEABILITY OF A CORE CONTAINING SALT PRECIPITATE

Table 6-3. Gas Permeability of the Core with Salt Precipitate and after Salt Extraction

Sample No.	Salt Concentration gm/cu cm pore volume x 10^3	Permeability to Nitrogen, md	
		with Salt	Salt Free
1	4.824	72.7	63.1
2	-	42.5	-
3	4.391	50.9	51.5
4	5.500	39.9	-
5	-	61.3	-
6	6.167	94.0	89.8
7	-	-	-
8	7.000	94.2	-
9	7.547	84.2	84.8
10	7.433	91.8	91.2
11	11.126	110.0	110.3

Note: Sample No. 1 is located at closed end of the brine experiment core.

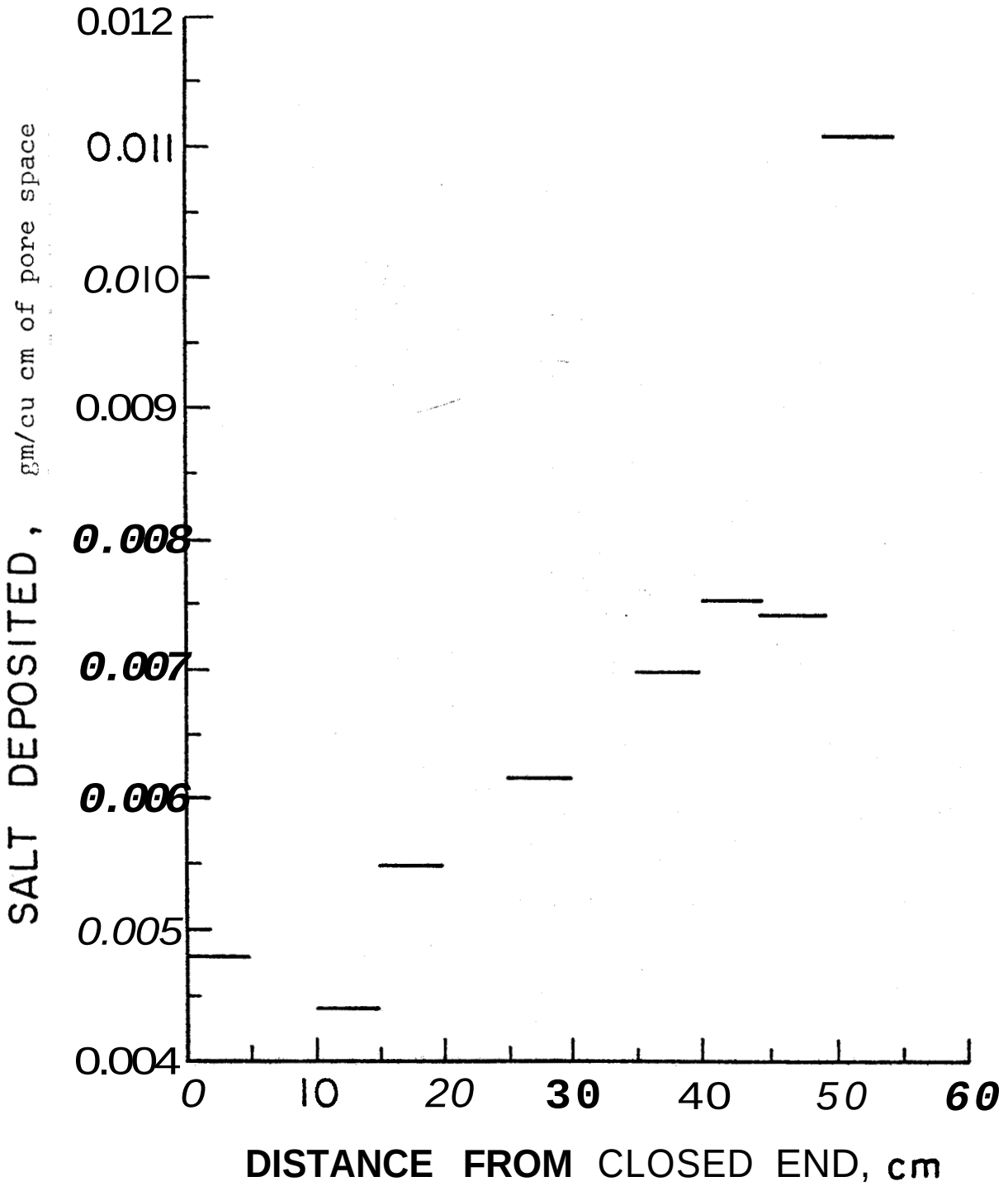

FIGURE 6-20. SALT DISTRIBUTION IN THE CORE

Fig. 6-21 shows the salt distribution and gas permeability of the core. It may be seen from Fig. 6-21 that the salt deposition in the core does not depend on core permeability. An investigation of the effect of salt deposition on core permeability for high concentration brines will become an important objective of continuing work on this project.

Finally, attempts were made to measure liquid content with the probe during the brine production experiment. Unfortunately; the results were poor, and are not presented herein. This sort of measurement will be pursued in the next phase of this project. Theoretically, the probe calibration should hardly be affected by brine concentration, but erratic results suggested some dependence on brine concentration.

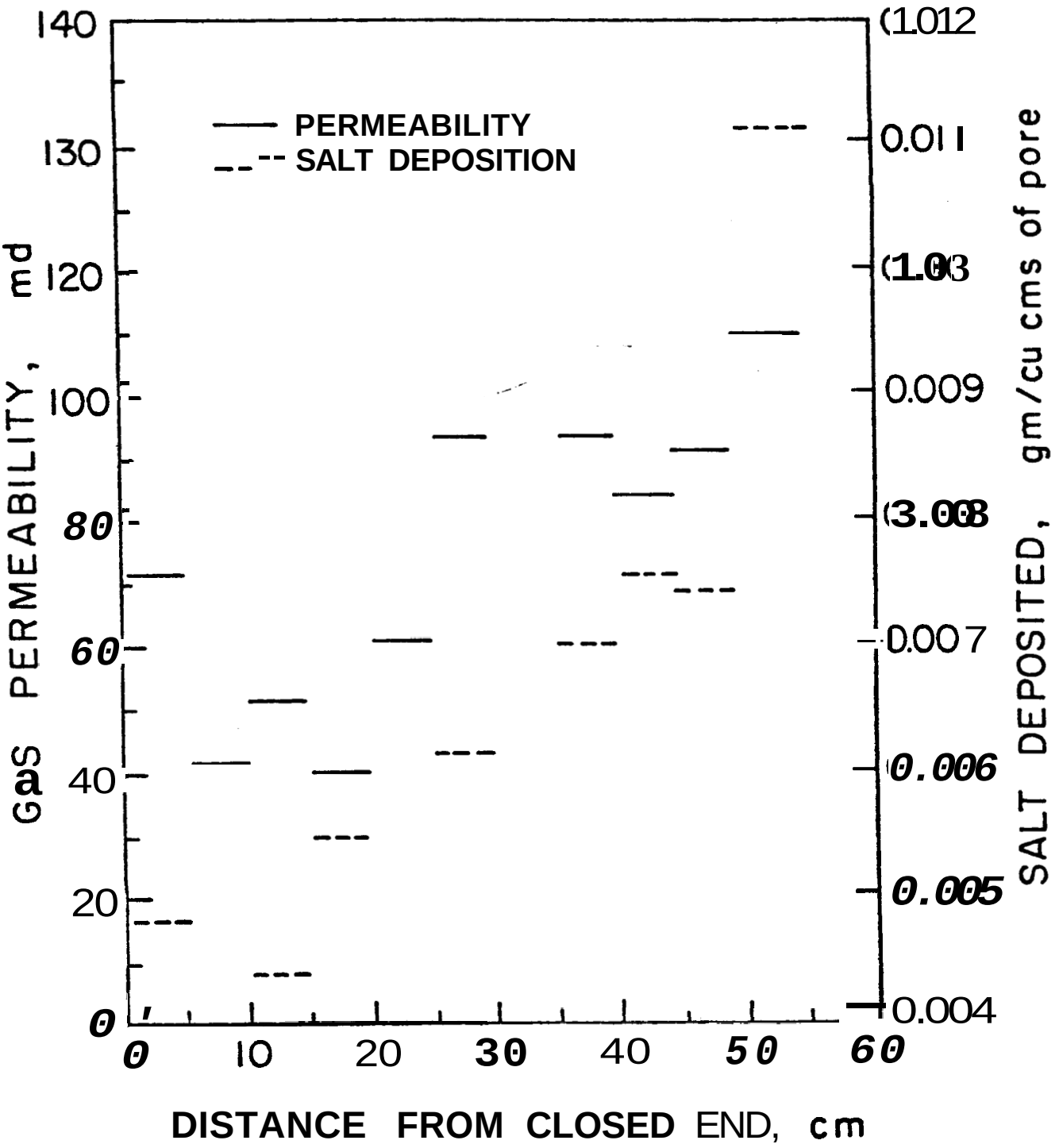

FIGURE 6-21. GAS PERMEABILITY AND SALT DISTRIBUTION FOR THE SYNTHETIC CONSOLIDATED CORE

7. CONCLUSIONS

Based on the experimental and calculated results, the conclusions of this study are as follows:

(1) The normalized probe calibration curve is nearly independent of either the operating temperature or the type of sandstone porous media surrounding the probe. (This remarkable result indicates the high potential of this device for geothermal experimentation both in the lab and in the field.)

(2) The shape of the experimental normalized calibration curve is similar to a computed calibration curve, and appears almost linear over most of the saturation range.

(3) As observed by Arihara[2], a large temperature gradient was found in the two-phase flow regime in both steady and batch experiments in the synthetic, consolidated-sandstone core.

(4) The vapor saturation in the steady, two-phase flow regime increased downstream from the boiling front. The higher the initial reservoir temperature, the greater the vapor saturation near the producing end.

(5) The irreducible water saturation appeared to be very large (64 to 87% of pore volume) for steam-water flow in the synthetic consolidated sandstone core. Irreducible water saturation as inferred from data matching with Corey-type equations appeared to increase with temperature, and relative

permeability curves computed from Corey's equations were temperature dependent.

(6) Determination of relative permeability from steady flow experiments with in-place water saturation measurement gave satisfactory results, 3ut it is likely that an optimum experiment was not performed in this study. Capillary pressure measurements for steam desaturation of a water-filled core nay yield better, or complementary, results.

(7) When steam and water were produced from. *a* synthetic consolidated core initially filled with hot compressed water, boiling occurred at the producing end of the core and gradually spread to the closed end of the core. A dry steam zone formed near the producing end after long production times.

(8) In batch experiments initially containing 12,000 ppm brine, salt deposition increased with increasing distance from the close5 end of the core.

(9) The permeability of the core to gas did not appear to be affected by salt deposition for the subject system. The maximum salt deposit formed was 0.011 gm/cc pore space, corresponding to a volume saturation of only 0.005 fraction of pore volume.

NOMENCLATURE

English

A	= area, cm^2
C	= capacitance of electric circuit, picofarad
C_p	= total capacitance of the probe
c	= formation dielectric concentration and polarization factor (see Eq. 6-1)
E	= internal energy
f	= mass fraction of total flow stream which is vapor
f_r	= resonant frequency
g	= acceleration due to gravity
h	= enthalpy, Btu/lb
k	= permeability, millidarcys
k_r	= relative permeability
K_m	= thermal conductivity of rock, liquid and vapor mixture
L	= inductance of circuit, henry
m	= mass transfer rate from liquid to vapor phase
m	= mass
n	= concentration (see Eq. 2-2)
p	= pressure
p_c	= capillary pressure
S	= saturation, volume fraction of pore volume
t	= time
T	= temperature, ^oF
T_i	= initial temperature, ^oF
u	= flow velocity

English, continued

V = volume

V_p = pore volume of the core

v = specific volume of fluid

W = weight

w = weight rate

x = distance in the direction of flow

Greek

ε = dielectric constant of materials or phases

ε_o = dielectric constant of pure water

ρ = density

μ = viscosity

ϕ = porosity

Φ = probe signal, mv

Φ^* = normalized signal, fraction (see Eq. 6-9)

∇ = gradient

λ = pore size distribution factor

Subscripts

dr = drainage process (desaturation)

1 = practical irreducible

ℓ = liquid

ma = natrix of rock

s = steam

w = water

REFERENCES

1. Baker, P.E.: "Effect of Pressure and Rate on Steam Zone Development in Steam Flooding," Soc. Pet. Engr. J. (Oct. 1973), 274-284; Trans. AIME (1973) 255.

2. Arihara, N.: "A Study of Non-Isothermal Single and Two-Phase Flow through Consolidated Sandstones," Ph.D. Dissertation, Stanford University (November 1974). See also SGP-TR2.

3. Denlinger, R.P.: "An Evaluation of the Capacitance Probe as a Technique for Determining Liquid Saturations in Laboratory Flow Experiments," Master Report, Departments of Geophysics and Petroleum Engineering, Stanford University, (June 1975).

4. Muskat, M., Wyckoff, R.D., Botset, H.G., and Meres, M.W.: "Flow of Gas-Liquid Mixtures through Sands," Trans. AIME (1937), 123, 69-96.

5. Botset, H.G.: "Flow of Sas-Liquid Mixtures through Consolidated. Sand," Trans. AIME (1940), 136, 91-105.

6. Leverett, M.C.: "Flow of Oil-Water Fixtures through Unconsolidated Sands," Trans. AIME (19391, 132, 149-171.

7. Boyer, R.L., Morgan, F., and Muskat, M.: "A New Method for Measurement of Oil Saturation in Cores," Trans. AIME (1947), 170, 15-33.

8. Morgan, F., McDowell, J.M., and Doty, E.C.: "Improvements in the X-Ray Saturation Technique of Studying Fluid Flow," Trans. AIME (1950), 189, 183-194.

9. Laird, A.D.K., and Putnam, J.A.: "Fluid Saturation in Porous Media by X-Ray Technique," Trans. AIME (1951), 192, 275-284.

10. Brunner, E., and Mardock, E.S.: "A Neutron Method for Measuring Saturation in Laboratory Flow Experiments," Trans. AIME (1946), 165, 133-143.

11. Visvalingam, M., and Tandy, J.D.: "The Neutron Method for Measuring Soil Moisture Content--A Review," J. Soil Sci. (1972), 23, No4, 499-511.

12. Parsons, R.W.: "Microwave Attenuation--A New Tool for Monitoring Saturatians in Laboratory Flooding Experiments," Trans. AIME (19751, 259-11, 302-310.

13. Saraf, D.N., and Fatt, I.: "Three-Phase Relative Permeability Measurement Using a Nuclear Magnetic Resonance Technique for Estimating Fluid Saturation," Trans. AIME (1967) 240-II, 235-242.

14. Whalen, J.W.: "A Magnetic Susceptibility Method for the Determination of Liquid Saturation in Porous Materials," Trans. AIME (1954), 201, 203-208.

15. McDonald, J.: "An Experimental Study of Boiling Flow Through Porous Media," Ph.D. Dissertation, University of Alabama, 1970.

16. Anderson, A.B.C., and Edlefsen, N.E.: "The Electrical Capacity of the 2-Electrode Plaster of Paris Block as an Indicator of Soil-Moisture Content," Soil Sci. (1942), 54, 35-46.

17. Anderson, A.B.C.: "A Method of Determining Soil-Moisture Content Based on the Variation of the Electrical Capacitance of Soils at a Low Frequency, with Moisture Content," Soil Sci. (1943), 56, 29-41.

18. Willihan, E.F.: "Studies of the Dielectric Method of Measuring Soil Moisture," Soil Sci. Soc. Amer. Proc. (1945), 39-40.

19. Leach, D.F.: "Design of a Single-Electrode Capacitor for Use with Moisture Meters and Similar Apparatus," J. Sci. Instrum. (1960), 37, 77-80.

20. Thomas, A.M.: "In-Situ Measurement of Moisture in Soil and Similar Substances by 'Fringe' Capacitance," J. Sci. Instrum. (19661, 43, 21-27.

21. Gregory, G.A., and Mattar, L.: "An In-Situ Volume Fraction Sensor for Two-Phase Rows of Mon-Electrolytes," J. of Canad. Pet. (April-June 1973), 48-52.

22. Bilhartz, E.L.: "Fluid Production from Geothermal Steam Reservoirs, MS Report, Stanford University (Spring 1971).

23. Meador, R.A., and *Sox*, P.T.: "Dielectric Constant Logging, A Salinity Independent Estimation of Formation Water Volume," Paper No. SPE 5504, 50th Annual Fall Meeting, SPE of AIME, Dallas Texas, September 28-October 1, 1975.

24. Akerlof, G.C., and Oshry, H.I.: "The Dielectric Constant of Water at High Temperatures and in Equilibrium with Its Vapor," J. Amer. Chem. Soc. (1950), 72, 2844-2847.

25. Warren, W.J.: "BS&W Measurement--Principles and Practices," J. Pet. Tech. (Nov. 1972), 1207-1212.

25. Parkhomenko, E.K.: Electrical Properties of Rocks, translated and edited by G.V. Keller, 1967, Plenus Fress, New York.

27. Gray, D.E.: American Institute of Physics Eandbook, Second Edition, 1963, McGraw-Hill, New York.

28. Keller, G.V.: "Electrical Properties of Rocks and Minerals," Handbook of Physical Constants, Geol. Soc. Am. Mem. (1966), 97, 553-578.

29. Keller, G.V., and Licastro, P.H.: "Dielectric Constant and Electrical Resistivity of Natural State Cores," U.S. Geol. Surv. Bull. 1052H (1959), 257-286.

30. Luikov, A.V.: Heat and Mass Transfer in Capillary Porous Bodies, translated by P.W.B. Harrison, Pergamon Press, Oxford, 1966.

31. Miller, F.G.: "Steady Flow of Two-Phase Single-Component Fluids through Porous Media," Trans. AIME (1951), 192, 205-216.

32. Kruger, P., and Ramey, H.J. Jr.: "Stirnulati-on and Reservoir Engineering of Geothermal Fesources," Stanford Geothermal Program Report No. 3 (June 1974).

33. Garg, S.K., Pritchett, J.W., and Brownell, D.H. Jr.: "Transport of Mass and Energy in Porous Media." The paper was distributed at Second United Nations Symposium on the Development and Use of Geothermal Resources, San Francisco, California, May 20-29, 1975. Authors may be contacted at System, Science and Software, P.O. Box 1620, La Jolla, California, 92038.

34. Cady, G.V.: "Model Studies of Geothermal Fluids Production," Ph.D. Dissertation, Stanford University (November 1969).

35. Strobel, C.J.: "Model Studies of Geothermal Fluids Production from Consolidated Porous Media," Engineer's Thesis, Stanford University (July 1973).

36. Chicoine, S.D.: "A Physical Model of a Geothermal System--Its Design and Construction and Its Application to Reservoir Engineering," Engineer's Thesis, Stanford University, June 1975.

37. Jones, S.C., Marathon Oil Co., Denver Res. Center, personal communication.

38. Wygal, R.J.: "Construction of Models that Simulate Oil Reservoirs," Soc. Pet. Engr. J. (Dec. 1973), 281-286.

39. Heath, L.J.: "Variation in Perneability and Porosity of Synthetic Oil Reservoir Rock--Method of Control," Soc. Pet. Engr. J. (Dec. 1965), 329-332.

48. Evers, J.F., Preston, F.W., Sadiq, S., and Swift, G.W.: "Preparation and Testing of Low Permeability Porous Media to Meet Scaling Requirements for Gas Reservoir Modeling," Soc. Pet. Eng. J. (June 19671, 189-194.

41. Saker, P.E., personal communication.

42. Corey, A.T.: "The Interrelation between Gas and Oil Relative Permeabilities," Producers' Monthly, Nov. 1954, 38-41.

43. Burdine, N.T.: "Relative Permeability Calculations from Pore Size Distribution Data," Trans. AIME (1953), 98, 71-78

44. Standing, M.B.: "Notes on Relative Permeability Relationships," Lecture Notes, Petroleum Engineering Department, Stanford University, California, 1975.

45. Poston, S.W., Ysrael, S., Hossain, X.K.J.S., Montgomery, E.F., 111, and Ramey, P.J., Jr.: "The Effect of Temperature on Irreducibie Water Saturation and Relative Permeability of Unconsolidated Sands," Soc. Pet. Eng. J. (June 19701, 171-180.

46. Weinbrandt, R.M., Ramey, H.J., Jr., and Cassé, F.J.: "The Effect of Temperature on Relative Permeability of Consolidated Rocks," Soc. Pet. Eng. J. (Oct. 19751, 376.

47. Cassé, F.J., arid Ramey, H.J. Jr.: "The Effect of Temperature and Confining Pressure on Single Phase Flow in Consolidated Rocks," Paper No. 5877, 46th Annual California Regional Meeting, SPE of AIME, Long Beach, California, April 8-9, 1976.

48. Aruna, M.: "The Effects of Temperature and Pressure on Absolute Permeability of Sandstones," Ph.D. Dissertation, Stanford University, May 1976.

49. Brooks, R.H., and Corey, A.T.: "Properties of Porous Media Affecting Fluid Flow," J. of the Irrigation and Drainage Div., Proc. ASCE (1966), 92, No. IR2, 61-88.

50. Sinnokrot, A.A.: "The Fffect of Temperature on Oil-Water Capillary Pressure Curves of Limestone and Sandstones, Ph.D. Dissertation, Stanford University, August 1969.

51. Sinnokrat, A.A., Ramey, H.J., Jr., Marsden, S.S., Jr.: "Effect of Temperature Level upon Capillary Pressure Curves," Soc. Pet. Eng. J. (March 1971), 13-22.

APPENDIX A

PHYSICAL DATA FOR THE CORES

1. Unconsolidated Sand Pack

   a. Monterey Sand

      Grain size - 18 20 mesh

      Permeability - 246 darcies

      Porosity - 0.38 fraction bulk volume

   b. White Sand

      Grain size - 20-80 mesh

      Permeability - 853 millidarcys

      Porosity - 0.36 fraction bulk volume

2. Synthetic Consolidated Sandstone

   Length - 23.1 inch

   Diameter - 2.0 inch

   Sand (80-170 mesh) weight % - 80

   Cement ($CaO \cdot AL_2O_3$ weight % - 20

   Blending water weight 17 gm

   Porosity fraction bulk volume - 0.34

   Permeability, millidarcies - 35.4

APPENDIX B

CALCULATION OF THEORETICAL CALIBRATION CURVES FOR THE CAPACITANCE PROBE

The calculation procedure is as follows:

Step 1: Calculate the dielectric constant of the core surrounding the probe using a Modified Lichtnecker and Rother Equation (Ref. 23).

$$\varepsilon = [(1-\phi)\ \varepsilon_{ma}{}^{c} + S_w \phi \varepsilon_w{}^{c} + (1-S_w)\phi \varepsilon_s{}^{c}]^{\frac{1}{c}}$$

assume values for ϕ, ε_{ma}, ε_w, ε_s as follows:

ϕ = 0.33 (porosity of sand pack of grain size 18-20 mesh)

E_{ma} = dielectric constant of sandstone matrix, 5.0

E_w = dielectric constant of water, 43.89 at 302°F

E_s = 1.00 for steam

An expression for ε can be written as:

$$E = [0.62\ \varepsilon_{ma} + 0.38\ S_w\ (43.89)^{c} + 0.38\ (1-S_w)]^{\frac{1}{c}}$$

Since the values of c range from 0 to 2, the dielectric constant of the core, E, can be calculated by assigning any value ranging from zero to two.

Appendix **Q**, continued

Step 2: Calculate the resonant frequency of the oscillator with capacitance probe.

$$f_r = \frac{1}{2\pi\sqrt{LC}}$$

where f_r = resonant frequency of the oscillator with probe, Hz

L = inductance of the oscillator in Fig. **6-1,**

12.5μh = 12.5×10^{-6}h.

C = capacitance of the oscillator, in Fig. 6-1

$$= \left(\frac{0.5\varepsilon+40}{0.5\varepsilon+140}\right) \times 100 \text{ pf}$$

$$= \left(\frac{0.5\varepsilon+40}{0.5\varepsilon+140}\right) \times 10^{2} \times 10^{-12} \text{ f}$$

$$= \left(\frac{0.5\varepsilon+40}{0.5\varepsilon+140}\right) \times 10^{-10} \text{ f}$$

$$\text{Thus, } f_r = \frac{1}{2\pi\sqrt{LC}} = \frac{1}{2\pi\sqrt{12.5\times10^{-6}\left(\frac{0.5\varepsilon+40}{0.5\varepsilon+140} \times 10^{-10}\right)}}$$

$$= \frac{4.50158 \times 10^{6}}{\sqrt{\frac{0.5\varepsilon+40}{0.5\varepsilon+140}}}$$

Step 3: Normalize the frequency of the oscillator with probe.

$$fr^{*} = \frac{(f_r)_s - (f_r)}{(f_r)_s - (f_r)_w}$$

Appendix B, continued

where f_r^* = normalized resonant frequency

$(f_r)_s$ = resonant frequency of the oscillator with probe for the probe immersed in a core filled with steam

$(f_r)_w$ = resonant frequency of the oscillator with probe for the probe immersed in a core filled with water

(f_r) = resonant frequency of the oscillator with probe for the probe immersed in a core filled with a steam-water mixture

Step 4: Tabulate the calculation results. The results of calculation with c values of 0.25, 0.5, 1.0, 1.25, and 1.5 are shown in the following table.

Table B-1: Summary of Probe Calibration Calculation

	c = 0.25			c = 0.5		
S_w	ε	$f_r x10^{-6}$ Hz)	f_r^*	ε	$f_r x10^{-6}$	f_r^*
0	2.94	8.31439	0	3.13	8.30766	0
0.1	3.52	8.29395	0.06	3.94	8.27930	0.07
0.2	4.18	3.27099	0.13	4.83	8.24865	0.15
0.3	4.93	8.24525	0.21	5.82	8.21518	0.24
0.4	5.77	8.21686	0.29	6.90	8.17938	0.34
0.5	6.72	5.18530	0.39	8.07	8.14142	0.43
0.6	7.78	8.15075	0.49	9.33	8.10146	0.54
c.7	8.35	8.11309	0.60	10.68	8.05966	0.65
0.3	10.27	5.07286	0.72	12.12	8.01620	0.76
0.9	11.71	3.02846	0.86	13.66	7.97095	0.88
1.0	13.31	7.98113	1.00	15.27	7.92495	1.00

	c = 1.0			c = 1.25		
S_w	E	$f_r x10^{-6}$	f_r^*	ε	$f_r x10^{-6}$	f_r^*
C	3.48	8.29535	0	3.64	8.28976	0
0.1	5.11	8.23912	0.11	5.94	8.21117	0.15
0.2	6.74	8.18464	0.22	8.03	8.14270	0.27
0.3	8.37	8.13182	0.33	10.00	8.08059	0.38
0.4	10.00	8.08058	0 .44	11.87	8.02367	0.49
0.5	11.63	8.03086	0.54	13.67	7.97067	0.59
0.5	13.26	7.98259	0.63	15.42	7.92073	0.68
0.7	14.89	7.93569	0.73	17.11	7.87393	0.77
0.8	16.52	7,89011	3.82	18.76	7.82953	0.85
0.9	18.15	7.84580	**0.91**	20.38	7.78712	0.92
1.0	19.78	7.80269	1.00	21.97	7.74659	**1.00**

Table B-1, Continued

$c = 1.5$

S_w	E	$f_r \times 10^{-6}$	f_r^*
0	3.77	8.28522	0
0.1	6.95	8.17774	0.18
0.2	9.51	8.09583	0.32
0.3	11.76	8.02696	0.44
0.4	13.82	7.96633	0.54
0.5	15.73	7.91205	0.63
0.6	17.53	7.86251	0.72
3.7	19.24	7.81685	0.80
0.8	20.88	7.77426	0.87
0.9	22.46	7.73432	0.94
1.0	23.98	7.69684	1.00

APPENDIX C

DERIVATION OF WATER SATURATION EXPRESSION (EQ. 6-10)

The average water saturation in the core filled with steam and water can be calculated by mass balance.

mass balance:

$$m_s + m_w = m \qquad \text{(C-1)}$$

where m_s = mass of steam in the core, lb

m_w = mass of water in the core, lb

m = mass of a steam-water mixture in the core, 15

For a given core temperature and pore volume of the core, the mass of steam and water can be calculated from the following equations:

$$m_s = \frac{V_s}{v_s} = \frac{V_p(1-S_w)}{v_s} \qquad \text{(C-2)}$$

$$m_w = \frac{V_w}{v_w} = \frac{V_p S_w}{v_w} \qquad \text{(C-3)}$$

where V_s = volume occupied. by steam, cu ft

v_s = specific volume of steam, cu ft/lb

V_p = pore volume of the core, cu ft

S_w = water saturation, fraction

Appendix C, continued

V_w = volume occupied by water, cu ft

v_w = specific volume of water, cu ft/lb

Thus, total mass of a steam-water mixture in the core may be written as:

$$m = m_{..} + m_{..} = \frac{V_p(1-S_w)}{v_{..}} + \frac{V_p S_w}{v_{..}} \qquad \text{(C-4)}$$

or

$$m = V_p \left(\frac{1}{v_w} - \frac{1}{v_s}\right) S_w + \frac{V_p}{v_s} \qquad \text{(C-5)}$$

Dividing Eq. C-5 by $\frac{V_p}{v_s}$, the result is:

$$m \frac{v_s}{V_p} = v_s \left(\frac{1}{v_w} - \frac{1}{v_s}\right) S_w + 1 \qquad \text{(C-6)}$$

or

$$m \frac{v_s}{V_p} = \left(\frac{v_s - v_w}{v_w}\right) S_w + 1 \qquad \text{(C-7)}$$

Solving for S_w from Eq. C-7,

$$S_w = \left(\frac{v_w}{v_s - v_w}\right) \left(\frac{m v_s}{V_p} - 1\right) \qquad \text{(C-8)}$$

$\bar{V}_p$ cap "V" sub "p"

APPENDIX D

TABULATED DATA

This appendix contains all of the pertinent data obtained through the course of the experimental work. The data collected will follow the order of calibration; steady, two-phase flow experiments; depletion experiments; and brine experiments.

D-1 Calibration of Capacitance Probe

The data in this section includes the calibration performed in short, synthetic consolidated sandstone cores with air-water mixtures at room temperature (25°C), and in sand packs with steam-water mixtures at high temperatures. The identification of the tables is formed by one letter and three digits. The letter D represents the Appendix 3. The number 1 in the first digit refers to calibration data. The number 1 in the second digit refers to the calibration made in short, synthetic consolidated sandstone cores at room temperature. The number 2 is the calibration performed in large grain diameter sand packs filled with steam-water mixtures. The number 3 is the calibration made in the small grain diameter sand pack. The last digit represents the order of the calibration in each category. The subletter (a or b) behind the last digit refers to the data of mass in-place, temperature and water saturation, or probe signal and water saturation.

D-1-1 Calibration of the Capacitance Probe in Short, Synthetic Consolidated Sandstone Cores with Air-Water Mixtures at Room Temperature

(1) Core No. 1

Weight of dry core = 255.4 gm
Weight of water saturated core = 314.1 gm
Porosity = 0.38

Date	Weight of Core	S_w, fraction	$\Phi_s - \Phi$, mv	Φ^*
2/27/75	314.1	1.00	14.44	1.00
2/27/75	311.8	0.96	13.45	0.93
2/27/75	308.8	0.91	13.35	0.93
2/28/75	290.0	0.59	10.80	0.75
2/28/75	289.1	0.54	10.10	0.70
2/28/75	284.8	0.50	9.05	0.63
2/28/75	281.8	0.45	7.95	0.55
2/28/75	279.5	0.41	6.80	0.47
2/28/75	276.5	0.36	5.65	0.39
2/28/75	274.2	0.32	5.46	0.38
2/28/75	260.7	0.09	1.85	0.13
3/02/75	279.5	0.41	5.75	0.40
3/02/75	276.0	0.35	4.45	0.31

(2) Core No. 2

Weight of dry core = 293.1 gm
Weight of water saturated core = 358.6 gm
Porosity = 0.37

2/27/75	214.4	0.33	7.40
2/27/75	310.0	0.26	5.50
2/27/75	309.1	0.24	5.20
2/28/75	233.6	0.10	2.20
2/25/75	237.7	0.07	1.75
2/23/75	297.0	0.06	1.55
3/02/75	300.3	0.11	1.80

D-1-1, continued

(3) Core No. 3

Weight of dry core = 271.6 gm
Weight of water saturated core = 332.3 gm
Porosity = 0.37

Date	Weight of Core	S_w, fraction	$\Phi_s - \Phi, m_v$	Φ^*
2/27/75	289.5	0.30	5.89	0.36
2/27/75	284.9	0.22	4.44	0.27
2/27/75	253.6	0.20	4.04	0.25
2/28/75	332.3	1.00	16.20	1.00
2/28/75	328.7	0.94	16.18	1.00
2/28/75	326.8	0.91	15.80	0.98
2/28/75	312.9	0.68	14.70	0.91
3/91/75	297.7	0.43	7.75	0.48
3/32/75	280.1	0.14	2.40	0.15
3/03/75	331.1	0.98	12.45	0.92

(4) Core No. 4

Weight of dry core = 298.8 gm
Weight of water saturated core = 371.3 gm
Porosity = 0.39

3/02/75	371.3	1.0	14.60	1.00
3/02/75	369.1	0.97	14.55	1.00
3/32/75	367.1	0.94	14.2	0.97
3/02/75	365.8	0.92	13.5	0.92

(5) Core No. 5

Weight of dry core = 321.3 gm
Weight of water saturated core = 394.8 gm
Porosity = 0.37

3/28/75	343.3	0.30	7.85
3/28/75	341.3	0.27	7.30
3/02/75	352.2	0.42	7.93

D-1-2 Calibration of the Capacitance Probe In the Large Grain Diameter Sand Pack (18-20 Mesh) with Steam-Water Mixtures at High Temperatures

Table 9-1-2-1 (a): Mass In-Place, Temperature and Water Saturation for Calibration of Capacitance Probe

Run No. LGI
Date: 1/18/75
Pore Volume = 0.0301 cu ft
Initial Mass = 5.8770 lb

Mass In-Place lb	Operating Temperature °F	Average Water Saturation
1.6294	306	0.95
1.5139	306	0.88
1.3713	306	0.80
1.0095	306	0.59
0.7835	305	0.45
0.5681	305	0.33

Table D-1-2-1(b): Probe Signal and Water Saturation for Calibration of Capacitance Probe

Run No. LGI
Date: 01/18/76

Distance from Closed End in.	$S_w = 1.0$ Φ_s mv	Φ_w mv	$\Phi_s - \Phi_w$ mv	$S_w = 0.95$ Φ mv	$\Phi_s - \Phi$ mv	Φ^*
1.25	9.5	-8.9	18.4	-5.9	15.4	0.84
1.75	9.5	-8.8	18.3	-5.7	15.2	0.83
2.75	9.6	-8.9	18.5	-5.5	15.1	0.82
3.75	9.6	-8.4	18.0	-5.3	14.9	0.83
4.75	9.6	-7.2	16.8	-5.1	14.7	0.88
5.75	9.7	-6.8	16.5	-5.1	14.8	0.90
6.75	9.7	-6.4	16.1	-5.1	14.8	0.92
7.75	9.7	-6.2	15.9	-4.9	14.6	0.92
8.75	9.8	-6.1	15.9	-4.9	14.7	0.92
9.75	9.8	-5.9	15.7	-4.9	14.7	0.94
10.75	9.8	-6.2	16.0	-5.2	15.0	0.94
11.75	9.8	-6.4	16.2	-5.6	15.4	0.95
12.75	9.8	-6.5	16.3	-5.4	15.2	0.93
13.75	9.5	-6.4	15.9	-6.0	15.5	0.97
14.75	9.5	-6.6	16.1	-6.6	16.1	1.0
15.75	9.5	-7.0	16.5	-7.0	16.5	1.0
16.75	9.5	-7.1	16.6	-7.0	16.5	0.99
17.75	9.4	-7.1	16.5	-6.7	16.1	0.98
18.75	9.5	-6.6	16.1	-6.6	16.1	1.0
19.75	9.6	-6.3	15.9	-6.5	16.1	1.0
20.75	9.6	-E.2	15.8	-6.4	16.0	1.0
21.75	9.8	-6.2	16.0	-6.3	16.1	**1.0**
Average						**0.93**

Cont.

Table D-1-2-1(b), continued

Distance from Closed End in.	S_w = 0.88 Φ mv	$\Phi_s - \Phi$ mv	Φ^*	S_w = 0.80 Φ mv	$\Phi_s - \Phi$ mv	Φ^*
1.25	-5.4	15.9	0.86	-5.0	14.5	3.79
1.75	-6.0	15.5	0.85	-4.9	14.4	0.79
2.75	-5.2	14.8	0.83	-4.7	14.3	0.77
3.75	-5.4	15.0	0.83	-4.5	**14.1**	0.78
4.75	-5.4	**15.0**	0.89	-4.5	**14.1**	0.84
5.75	-4.9	14.6	0.88	-4.2	**13.9**	0.84
6.75	-4.5	14.2	0.88	-4.0	13.7	0.85
7.75	-3.8	13.5	0.85	-3.2	12.9	**0.81**
8.75	-4.4	**14.2**	0.89	-3.9	13.7	0.86
9.75	-4.2	14.0	0.89	-3.7	13.5	0.86
10.75	-4.3	**14.1**	0.88	-3.0	12.8	0.80
11.75	-4.7	14.5	0.90	-3.7	13.5	**0.83**
12.75	-4.9	**14.7**	0.90	-3.1	12.9	0.79
13.75	-5.3	14.8	0.93	**-3.1**	12.6	0.79
14.75	-5.7	**15.2**	0.34	**-3.3**	12.8	0.80
15.75	-6.1	15.E	0.95	-4.1	**13.6**	0.82
16.75	-5.5	**16.0**	0.96	-4.6	14.1	0.85
17.75	-6.5	15.9	0.96	-4.9	**14.3**	0.87
18.75	-6.2	15.7	0.98	**-4.3**	13.8	0.86
19.75	-5.4	15.0	0.94	-4.2	**13.8**	0.87
20.75	-5.8	15.4	0.97	-4.0	13.6	0.86
21.75	-4.1	13.9	0.87	**-3.0**	12.8	0.80
Average			0.90			0.82

Table D-1-2-1(b), continued

Distance from Closed End in.	S_w = 0.59 Φ mv	$\Phi_s - \Phi$ mv	Φ^*	S_w = 0.45 Φ mv	$\Phi_s - \Phi$ mv	Φ^*
1.25	-3.3	12.8	0.70	-0.7	10.2	0.55
1.75	-3.4	12.9	0.70	-0.6	10.1	0.55
2.75	-2.9	12.5	0.68	-0.2	9.8	0.53
3.75	-2.4	12.0	0.67	0.5	9.1	0.51
4.75	-2.7	12.3	0.73	0.4	9.2	0.55
5.75	-2.1	11.8	0.72	0.9	8.8	0.53
6.75	-1.7	11.4	0.71	0.9	8.8	0.55
7.75	-1.2	10.3	0.69	1.3	8.4	0.53
8.75	-1.1	10.9	0.69	1.5	8.3	0.52
9.75	-1.0	10.8	0.69	1.3	8.5	0.54
10.75	-1.1	10.9	0.68	1.4	8.4	0.53
11.75	-1.6	11.4	0.70	1.1	8.7	0.54
12.75	-1.3	11.1	0.68	1.0	8.8	0.54
13.75	-1.2	10.7	0.67	1.1	8.4	0.53
14.75	-1.6	11.1	0.69	0.7	8.8	0.55
15.75	-2.1	11.6	0.70	0.1	9.4	0.57
16.75	-2.1	11.6	0.70	0.2	9.3	0.56
17.75	-1.7	11.1	0.67	0.3	9.1	0.55
18.75	-1.3	10.8	0.67	0.8	8.7	0.54
19.75	-1.2	10.8	0.68	1.2	8.4	0.53
20.75	-0.6	10.2	0.65	2.0	7.6	0.48
21.75	0.2	9.6	0.60	2.7	7.1	0.44
Average			0.69			0.53

Table D-1-2-1(b), continued

Distance fron Closed End In.	$S_w = 0.33$ Φ mv	$\Phi_s - \Phi$ mv	Φ^*
1.25	1.9	7.6	0.41
1.75	2.0	7.5	0.41
2.75	2.2	7.4	0.40
3.75	2.6	7.0	0.39
4.75	2.8	6.8	0.40
5.75	3.2	6.5	0.39
E. 75	3.3	6.4	0.40
7.75	3.5	6.2	0.39
8.75	3.6	6.2	0.39
9.75	3.4	6.4	0.41
10.75	3.3	6.5	0.41
11.75	3.1	6.7	0.41
12.75	3.1	6.7	0.41
13.75	3.1	6.4	0.40
14.75	2.8	6.7	0.42
15.75	2.3	7.2	0.44
16.75	2.3	7.2	0.43
17.75	2.6	6.8	0.41
18.75	3.0	6.5	0.40
i9.75	3.3	6.3	0.40
20.75	3.7	5.9	0.37
21.75	4.1	5.7	0.36
Average			0.40

Table D-1-2-2(a): Mass In-Place, Operating Temperature and Average Water Saturation for Calibration

Run No. LG2
Date: 91/25/76
Pore Volume: 0.32940 Cu ft
Initial Mass: 1.8358 lb

Mass In-Place lb	Operating Temperature °F	Average Water Saturation
1.5884	309	0.95
1.4623	309	0.87
1.3287	309	0.79
1.1698	305	0.70
5.8331	306	0.49
0.6224	307	0.37
0.3979	308	0.23
0.2407	338	0.14
0.1424	307	0.08

Table D-1-2-2(b): Probe Signal and Water Saturation

Run No. LG2
Date: 01/25/76

Distance from Closed End In.	$S_w = 1.0$ Φ_s mv	Φ_w mv	$\Phi_s - \Phi_w$ mv	a mv	$S_w = 0.95$ $\Phi_s - \Phi$ mv	Φ^*
1.25	10.0	-7.7	17.7	-6.8	16.8	0.95
1.75	10.0	-7.5	17.5	-6.8	16.8	0.96
2.75	9.9	-7.5	17.4	-6.7	16.6	0.95
3.75	10.0	-7.3	17.3	-6.9	16.9	0.98
4.75	10.0	-7.4	17.4	-5.8	15.8	0.91
5.75	9.8	-7.4	17.2	-6.5	16.3	0.95
5.75	9.8	-7.8	17.6	-7.5	17.3	0.98
7.75	9.8	-8.3	18.7	-8.0	17.8	0.95
8.75	9.7	-9.1	18.8	-9.0	18.7	0.99
9.75	3.7	-9.5	19.2	-9.5	18.2	1.0
10.75	9.7	-9.4	19.1	-9.2	18.9	0.99
11.75	9.8	-8.9	18.7	-8.5	18.3	0.98
12.75	9.8	-9.3	19.1	-8.6	18.4	0.96
13.75	3.8	-9.2	19.0	-9.0	18.8	0.99
14.75	9.5	-9.3	18.8	-9.2	18.7	0.99
15.75	3.4	-10.0	19.4	-9.8	19.2	0.99
16.75	9.2	-10.2	19.4	-9.9	19.1	0.98
17.75	9.4	-10.7	20.1	-10.4	19.8	0.99
18.75	9.6	-10.5	20.1	-10.7	20.3	1.0
19.75	9.5	-10.9	20.4	-10.9	20.4	1.0
20.75	9.6	-10.8	20.4	-10.6	20.2	0.99
21.75	3.7	-11.9	21.6	-11.9	21.6	1.0
Average						0.98

Table D-1-2-2(b), continued

Distance from Closed End In.	S_w = 0.87			S_w = 0.79		
	Φ mv	$\Phi_s - \Phi$ mv	Φ*	Φ mv	$\Phi_s - \Phi$ mv	Φ*
1.25	-7.1	17.1	0.97	-6.3	**16.3**	0.92
1.75	-7.0	**17.0**	0.97	-6.1	**16.1**	0.92
2.75	-6.8	16.7	**0.96**	-5.7	***15.6***	0.90
5.75	-5.5	15.6	**0.90**	-5.4	**15.Y**	**0.89**
4.75	-5.2	**15.2**	0.87	**-4.6**	14.6	**0.84**
5.75	-6.1	15.9	**0.92**	-4.8	14.6	0.85
6.75	-5.3	16.1	**0.91**	**-5.6**	15.4	0.88
7.75	-6.5	**16.3**	0.87	**-5.6**	**15.4**	**0.82**
8.75	-7.5	17.3	0.92	**-6.2**	**15.9**	**0.85**
9.75	-8.0	17.7	**0.92**	-6.6	**16.3**	0.85
10.75	-7.4	17.1	**0.90**	-6.3	**16.0**	0.84
11.75	-7.6	17.4	**0.93**	-6.0	15.8	**0.84**
12.75	**-8.1**	17.9	*0.94*	-6.4	**16.2**	0.85
13.75	-8.4	18.2	0.96	***-6.5***	**16.3**	**0.86**
14.75	-8.7	**18.2**	**0.97**	**-6.6**	**16.1**	0.86
15.75	-9.5	18.9	0.97	-7.4	16.8	0.87
16.75	-9.6	18.8	0.97	-7.8	17.0	0.88
17.75	**-9.9**	**19.3**	**0.96**	***-7.8***	**17.2**	0.86
18.75	-9.6	**19.2**	**0.96**	-7.9	17.5	**0.87**
19.75	-9.3	**19.3**	**0.95**	-7.8	**17.2**	0.86
20.75	-9.9	**19.5**	**0.96**	**-7.9**	17.5	**0.86**
21.75	-10.0	10.7	0.91	**-7.3**	**17.0**	**0.79**
Average			0.94			0.86

Table D-1-2-2(b), continued

Distance from Closed End In.	S_w = 0.70 Φ mv	$\Phi_s - \Phi$ mv	Φ^*	S_w = 0.49 Φ mv	$\Phi_s - \Phi$ mv	Φ^*
1.25	-4.9	14.9	0.84	-0.3	10.3	0.58
1.75	-4.9	14.9	0.85	-0.7	10.7	0.61
2.75	-4.8	14.7	0.84	-1.2	11.1	0.64
3.75	-4.7	14.7	0.85	-0.4	10.4	0.60
4.75	-4.3	14.3	0.82	-0.4	10.4	0.60
5.75	-4.9	14.7	0.85	-1.2	11.0	0.64
6.75	-5.6	15.4	0.88	-2.3	12.1	0.69
7.75	-5.1	14.9	0.80	-1.3	11.1	0.59
8.75	-5.7	15.4	0.82	-1.9	11.6	0.62
9.75	-5.7	15.4	0.80	-1.9	11.6	0.60
10.75	-5.7	15.4	0.81	-1.8	11.5	0.60
11.75	-5.7	15.5	0.83	-1.9	11.7	0.63
12.75	-5.5	15.3	0.80	-2.1	11.9	0.62
13.75	-5.9	15.7	0.83	-1.2	11.0	0.58
14.75	-5.8	15.3	0.81	-1.4	10.9	0.58
15.75	-6.5	15.9	0.82	-1.7	11.0	0.57
16.75	-7.3	16.5	0.85	-3.1	12.3	0.63
17.75	-7.2	16.E	0.83	-3.0	12.4	0.62
18.75	-7.1	16.7	0.83	-2.1	11.7	0.58
19.75	-7.3	16.8	0.82	-2.6	12.1	0.59
20.75	-7.5	17.1	0.84	-3.2	12.8	0.63
21.75	-6.8	16.5	0.76	-2.1	11.8	0.55
Average			0.83			0.61

Table D-1-2-2(b), continued

Distance from Closed End In.	S_w = 0.37 Φ mv	Φ_s-I, mv	Φ^*	S_w = 0.23 Φ mv	Φ_s-a, mv	Φ^*
1.25	3.0	7.0	0.40	4.6	5.4	0.31
1.75	2.7	7.3	0.42	4.5	5.5	0.31
2.75	2.3	7.6	0.44	4.4	5.5	0.32
3.75	2.7	7.3	0.42	4.6	5.4	0.31
4.75	2.7	7.3	0.42	4.6	5.4	0.31
5.75	1.9	7.9	0.46	4.3	5.5	13.32
6.75	2.0	7.8	0.44	4.3	5.5	0.31
7.75	2.2	7.6	0.41	4.4	5.4	0.29
8.75	1.9	7.8	0.41	4.3	5.4	0.29
9.75	2.2	7.5	0.39	4.2	5.5	0.29
10.75	2.2	7.5	0.39	4.3	5.4	0.28
11.75	2.2	7.6	0.41	4.3	5.5	0.29
12.75	2.1	7.7	0.40	4.3	5.5	0.29
13.75	2.5	7.3	0.38	4.4	5.4	0.28
14.75	1.8	7.7	0.41	4.0	5.5	0.29
15.75	1.5	7.9	0.41	3.9	5.5	0.28
16.75	0.7	8.5	0.44	3.1	6.1	0.31
17.75	0.9	8.5	0.42.	3.2	6.2	0.31
18.75	1.7	7.9	0.30	3.5	6.1	0.30
19.75	1.4	8.1	0.43	3.4	6.1	0.30
20.75	1.3	8.3	0.41	3.3	6.3	0.31
21.75	2.0	7.7	0.36	3.7	6.0	0.28
Average			0.41			0.30

Table D-1-2-2(b), continued

Distance from Closed End In.	S_w = 0.14 Φ mv	$\Phi_s - \Phi$ mv	Φ^*	S_w = 0.08 Φ mv	$\Phi_s - \Phi$ mv	Φ^*
1.25	5.8	4.2	0.24	7.0	3.0	0.17
1.75	5.8	4.2	0.24	7.0	3.0	0.17
2.75	5.7	4.2	0.24	6.9	3.0	0.17
3.75	5.9	4.1	0.24	7.1	2.9	0.17
4.75	5.0	4.0	0.23	7.2	2.8	0.16
5.75	5.7	4.1	0.24	6.9	2.9	0.17
5.75	5.6	4.2	0.24	6.8	3.0	0.17
7.75	5.7	4.1	0.22	6.9	2.9	0.16
8.75	5.6	4.1	0.22	6.9	2.8	0.15
9.75	5.5	4.2	0.22	6.8	2.9	0.15
10.75	5.7	4.0	0.21	7.0	2.7	0.14
11.75	5.7	4.1	0.22	7.1	2.7	0.14
12.75	5.3	4.0	3.21	7.2	2.6	0.14
13.75	5.8	4.0	0.21	7.2	2.6	0.14
14.75	5.4	4.1	0.22	6.9	2.6	0.14
15.75	5.2	4.2	0.22	6.7	2.7	0.14
16.75	4.8	4.4	0.23	6.6	2.6	0.13
17.75	4.9	4.5	0.22	6.7	2.6	0.13
18.75	5.2	4.4	0.22	6.9	2.7	0.13
19.75	5.1	4.4	0.22	7.0	2.5	0.12
20.75	5.1	4.5	0.22	7.1	2.5	0.12
21.75	5.4	4.3	0.20	7.2	2.5	0.12
Average			0.22			0.15

Table D-1-2-3(a): Mass In-Place, Temperature and Water Saturation

Run No. LG3
Date: 01/28/76
Pore Volume: 0.0291 cu ft
Initial Mass: 1.8170 lb

Mass In-Place lb	Operating Temperature °F	Average Water Saturation
1.6343	312	0.99
1.4522	311	0.89
1.3175	311	0.79
1.1036	310	0.67
0.8995	311	0.54
0.6638	304	0.40
0.5386	310	0.32
0.4195	309	0.25
0.2873	306	0.17
0.1649	310	0.10
0.0298	270	0.02

Table D-1-2-3(b): Probe Signa1 **and** Water Saturation

Run No. LG3
Date: 01/28/76

Distance from Closed End	$S_w = 1$			$S_w = 0.99$		
	a_s	Φ	$\Phi_s - \Phi_w$	Φ	$\Phi_s - \Phi$	Φ^*
	mv	mv	mv	mv	mv	
1.25	10.4	-7.6	18.0	-5.8	16.2	**0.90**
1.75	10.3	-7.6	17.9	-5.5	15.8	0.88
2.75	10.3	-7.7	10.0	-5.4	15.7	0.87
3.75	10.4	-8.0	18.4	-5.8	16.2	0.88
4.75	10.3	-7.5	17.8	-6.0	**16.3**	0.92
5.75	10.2	-7.4	17.6	-5.7	15.9	0.90
6.75	10.2	-7.5	17.7	-6.7	16.9	0.95
7.75	10.2	-7.5	17.7	-6.7	17.2	0.97
8.75	10.1	-7.6	17.7	-7.6	17.7	**1.0**
9.75	10.1	-8.0	18.1	-8.0	18.1	**1.0**
10.75	10.1	-7.9	18.0	-7.9	**18.0**	**1.0**
11.75	10.1	-7.9	18.0	-7.9	18.0	1.0
12.75	10.1	-7.9	18.0	-8.0	18.1	**1.0**
13.75	10.1	-8.1	18.2	-8.1	**18.2**	**1.0**
14.75	10.0	-8.2	18.2	-8.3	**18.3**	**1.0**
15.75	9.8	-8.5	18.3	-8.5	18.3	1.0
16.75	9.4	-8.3	17.7	-8.2	17.6	0.99
17.75	3.4	-8.7	18.1	-8.7	**18.1**	**1.0**
18.75	9.5	-8.6	18.1	-8.6	**18.1**	**1.0**
19.75	9.5	-8.7	18.2	-8.7	18.2	**1.0**
20.75	9.6	-8.6	18.2	-8.7	**18.3**	**1.0**
21.75	9.8	-9.7	19.5	-9.9	19.7	**1.0**
Average						0.97

Table D-1-2-3(b), continued

Distance from Closed End In	S_w = 0.89			S_w = 0.79		
	Φ mv	$\Phi_s - \Phi$ mv	Φ^*	Φ mv	$\Phi_s - \Phi$ mv	Φ^*
1.25	-5.7	16.1	0.89	-4.9	15.3	0.85
1.75	-5.3	15.6	0.87	-5.0	15.3	0.85
2.75	-5.0	15.3	0.85	-4.6	**14.9**	0.83
3.75	-4.8	15.2	0.83	-4.5	14.9	0.81
4.75	-4.9	15.2	0.85	-4.5	**14.8**	0.83
5.75	-4.9	15.1	0.86	-4.8	15.0	0.85
6.75	-6.0	16.2	0.92	-5.8	16.0	0.90
7.75	-6.2	16.4	0.93	-5.4	15.6	0.88
8.75	-5.1	15.2	0.86	-5.1	15.2	0.86
9.75	-5.7	15.8	0.87	-5.5	15.6	0.86
10.75	-5.4	15.5	0.86	-5.4	15.5	0.86
11.75	-6.9	17.0	0.94	-5.5	15.6	0.87
12.75	-6.4	16.5	0.92	-5.0	15.1	0.84
13.75	-5.4	16.5	0.91	-5.4	15.5	0.85
14.75	-7.3	17.3	0.95	-5.9	15.9	0.87
15.75	-7.6	17.4	0.95	-6.3	**16.1**	0.88
16.75	-8.2	17.6	0.99	-6.4	**15.8**	0.90
17.75	-8.1	17.5	3.97	-6.5	15.9	0.88
18.75	-8.4	17.9	0.99	*-6.8*	**16.3**	0.90
13.75	-8.7	18.2	1.0	-6.8	16.3	0.90
20.75	-8.1	17.7	0.97	-7.3	**16.9**	0.93
21.75	-8.8	18.6	0.95	-7.4	17.2	0.88
Average			0.92			0.87

Table D-1-2-3(b), continued

Run No. 012876

Distance from Closed End In	S_w = 0.67			S_w = 0.54		
	Φ mv	$\Phi_s - \Phi$ mv	Φ^*	Φ mv	$\Phi_s - \Phi$ mv	Φ^*
1.25	-3.2	13.6	0.76	-0.7	11.1	0.62
1.75	-3.6	13.9	0.78	-1.1	11.4	0.64
2.75	-3.3	13.6	0.76	-1.0	11.3	0.63
3.75	-3.0	13.4	0.73	-0.6	11.0	0.60
4.75	-3.1	13.4	0.75	-0.9	11.2	0.63
5.75	-3.7	13.9	0.79	-1.6	11.8	0.67
6.75	-4.7	14.9	0.84	-2.6	12.8	0.72
7.75	-4.3	14.5	0.82	-1.9	12.1	0.68
8.75	-3.9	14.0	0.79	-2.0	12.1	0.68
9.75	-4.4	14.5	0.80	-2.2	12.3	0.68
10.75	-4.4	14.5	0.81	-2.2	12.3	0.68
11.75	-4.8	14.9	0.83	-2.3	12.4	0.69
12.75	-4.2	14.3	0.79	-2.4	12.5	0.69
13.75	-4.5	14.6	0.80	-1.9	12.0	0.66
14.75	-5.1	15.1	0.83	-2.8	12.8	0.70
15.75	-5.2	15.0	0.82	-2.7	12.5	0.68
16.75	-5.7	15.1	0.85	-3.6	13.0	0.73
17.75	-5.5	14.9	0.82	-3.4	12.8	0.71
18.75	-5.4	14.9	0.82	-2.2	11.7	0.65
19.75	-5.5	15.0	0.82	-3.1	12.6	0.69
20.75	-6.3	15.9	0.87	-4.2	13.8	0.76
21.75	-5.8	15.6	0.80	-3.1	12.9	0.66
Average			0.80			0.68

Table D-1-2-3(b), continued

Distance from Closed End In	S_w = 0.40			S_w = 0.32		
	Φ mv	$\Phi_s - \Phi$ mv	Φ^*	Φ mv	$\Phi_s - \Phi$ mv	Φ^*
1.25	3.3	7.1	0.39	4.5	5.9	0.33
i.75	3.0	7.3	0.41	4.2	6.1	0.34
2.75	2.7	7.6	0.42	4.1	6.2	0.34
3.75	3.0	7.4	0.40	4.2	6.2	0.34
4.75	3.0	7.3	0.41	4.2	6.1	0.34
5.75	2.2	8.0	0.45	3.6	6.6	0.38
5.75	2.2	8.0	0.45	3.6	6.6	0.37
7.75	2.4	7.8	0.44	3.8	6.4	0.36
8.75	2.2	7.9	0.45	3.4	6.7	0.38
9.75	2.3	7.8	0.43	3.5	6.6	0.36
10.75	2.3	7.8	0.43	3.6	6.5	0.36
11.75	2.2	7.9	0.44	3.4	6.7	0.37
12.75	2.1	8.0	0.44	3.4	6.7	0.37
13.75	2.5	7.6	0.42	3.7	6.4	0.35
14.75	1.5	8.5	0.47	3.0	7.0	0.38
i5.75	1.4	8.4	0.46	2.7	7.1	0.39
16.75	0.4	3.0	0.51	1.9	7.5	0.42
17.75	0.6	8.8	0.49	2.2	7.2	0.40
18.75	1.5	8.0	0.44	2.7	6.8	0.38
19.75	1.1	8.4	0.46	2.5	7.0	0.38
20.75	0.9	8.7	0.48	2.4	7.2	0.40
21.75	1.6	8.2	0.42	2.9	6.9	0.35
Average			0.44			0.37

Table D-1-2-3(b), continued

Distance from Closed End In	S_w = 0.25			S_w = 0.17		
	Φ mv	$\Phi_s - \Phi$ mv	Φ^*	Φ mv	$\Phi_s - a$ mv	Φ^*
1.25	5.3	5.1	0.28	6.3	4.1	0.23
1.75	5.1	5.2	0.29	6.2	4.1	0.23
2.75	5.0	5.3	0.29	6.1	4.2	0.23
3.75	5.0	5.4	0.29	6.2	4.2	0.23
4.75	5.0	5.3	0.30	6.2	4.1	0.23
5.75	4.6	5.6	0.32	5.9	4.3	0.24
6.75	4.5	5.7	0.32	5.8	4.4	0.25
7.75	Q.6	5.6	0.32	6.0	4.2	0.24
8.75	4.4	5.7	0.32	5.8	4.3	0.24
9.75	4.4	5.7	0.31	5.7	4.4	0.24
10.75	4.4	5.7	0.32	5.7	4.4	0.24
11.75	4.4	5.7	0.32	5.6	4.5	0.25
12.75	4.5	5.6	0.31	5.7	4.4	0.24
13.75	4.6	5.5	0.30	5.8	4.3	0.24
14.75	4.1	5.9	0.32	5.4	4.6	0.25
15.75	3.8	6.0	0.33	5.4	4.4	0.24
16.75	3.3	6.1	0.34	5.0	4.4	0.25
17.75	3.4	6.0	0.33	5.0	4.4	0.24
18.75	3.8	5.7	0.31	5.0	4.5	0.25
19.75	3.7	5.8	0.32	4.9	4.6	0,25
20.75	3.5	5.1	0.34	4.7	4.9	0.27
21.75	4.0	5.8	0.30	5.0	4.8	0.25
Average			0.31			0.24

Table D-1-2-3(b), continued

Distance from Ciosed End In	S_{wi} = 0.10			S_w = 0.02		
	Φ mv	$\Phi_s - \Phi$ mv	Φ^*	Φ mv	$\Phi_s - \Phi$ mv	Φ^*
1.25	7.3	**3.1**	0.17	9.1	**1.3**	0.07
1.75	7.2	3.1	0.17	9.1	1.2	0.07
2.75	7.2	3.1	0.17	9.1	1.2	0.07
3.75	7.2	3.2	0.17	9.2	**1.2**	0.07
4.75	7.2	3.1	0.17	9.2	**1.1**	0.06
5.75	7.0	3.2	0.18	9.0	1.2	0.07
6.75	6.8	3.4	0.19	9.0	**1.3**	0.07
7.75	6.9	3.3	0.19	9.1	**1.1**	0.06
8.75	5.8	3.3	0.19	9.0	**1.1**	0.06
9.75	6.8	3.3	**0.18**	9.0	**1.1**	0.06
10.75	6.8	3.3	**0.18**	9.0	**1.1**	0.06
11.75	6.8	3.3	0.18	9.0	**1.1**	0.06
12.75	5.8	3.3	0.18	9.0	1.1	0.06
13.75	6.8	3.3	0.18	8.9	1.2	0.07
14.75	6.5	3.5	0.19	8.4	**1.6**	0.09
15.75	6.2	3.6	0.20	8.5	**1.3**	0.07
16.75	6.0	3.4	0.19	8.2	1.2	0.07
17.75	6.0	3.4	0.19	8.3	**1.1**	0.06
18.75	6.1	3.4	0.19	**8.4**	1.1	0.06
19.75	6.1	3.4	**0.19**	8.4	1.1	0.06
20.75	6.1	3.5	0.19	8.4	**1.2**	0.07
21.75	6.3	3.5	0.18	8.5	1.3	0.07
Average			0.18			0.07

D-1-3. Calibration of the Capacitance Probe in the Small Grain Diameter Sand Pack (20-80 Mesh) with Steam-Water Mixtures at High Temperatures

Table D-1-3-1(a): Mass In-Place, Temperature and Water Saturation

Run No. : SG1
Date: 02/73/76
Pore Volume: 0.0280 cu ft
Initial Mass: 1.7456 lb

Mass In-Place lb	Operating Temperature °F	Average Water Saturation
1.5038	302	0.94
1.3957	302	0.87
1.3023	302	0.81
1.2015	302	0.74
1.0776	302	0.67
0.9253	302	0.57
0.7606	301	0.47
0.6058	301	0.37
0.5247	300	0.32
0.4341	300	0.26
0.3278	300	0.20
0.2325	301	0.14
0.1206	300	0.07

Table D-1-3-1(b): Probe Signal and Water Saturation

Run No. SG1
Date: 02/13/76

Distance from Closed End In	$S_w = 1.0$ Φ_s mv	Φ_w mv	$\Phi_s - \Phi_w$ mv	$S_w = 0.94$ Φ mv	$\Phi_s - \Phi$ mv	Φ^*
1.25	9.9	-7.8	17.7	-6.6	16.5	0.93
1.75	9.9	-7.9	17.8	-7.1	17.0	0.96
2.75	9.9	-8.3	18.2	-7.9	17.8	0.98
3.75	10.0	-8.1	18.1	-7.7	17.7	0.98
4.75	5.9	-8.0	17.9	-7.2	17.1	0.96
5.75	9.9	-8.2	18.1	-8.2	18.1	1.00
5.75	3.9	-8.6	18.5	-8.6	18.5	1.00
7.75	9.8	-8.7	18.5	-8.7	18.5	1.00
3.75	3.8	-8.5	18.3	-8.5	18.3	1.00
9.75	9.8	-8.7	18.5	-8.5	18.3	0.99
10.75	9.8	-8.9	18.7	-8.8	18.6	0.99
11.75	9.9	-3.1	13.0	-8.7	18.6	0.98
12.75	9.9	-8.3	19.2	-9.1	19.0	0.99
13.75	9.9	-3.5	19.4	-9.4	19.3	0.99
14.75	3.9	-9.6	19.5	-9.5	19.4	0.99
15.75	S.8	-9.5	19.3	-9.3	19.1	0.99
16.75	9.8	-10.5	20.3	-10.0	19.8	0.98
17.75	3.8	-11.0	20.8	-10.3	20.1	0.97
18.75	9.8	-12.3	22.1	-11.7	21.5	0.97
19.75	9.9	-13.4	23.3	-12.9	22.8	5.98
20.75	10.0	-13.6	23.6	-13.1	23.1	0.98
21.75	10.0	-15.4	25.4	-14.5	24.5	0.96
Average						0.98

Table D-1-3-1(b), continued

Run No. SG1

Distance from Closed End In	S_w = 0.74 Φ mv	$\Phi_s - \Phi$ mv	Φ^*	S_w = '0.67 Φ mv	$\Phi_s - \Phi$ mv	Φ^*
a.25	-4.5	14.4	0.81	-2.5	12.4	9.70
1.75	-4.6	14.5	0.81	-3.0	12.9	9.72
2.75	-4.7	14.E	0.80	-3.1	13.0	0.71
3.75	-2.7	12.7	0.70	-0.7	10.7	0.59
4.75	-3.5	13.4	0.75	-2.1	12.0	0.67
5.75	-5.7	15.6	0.86	-4.2	14.1	0.78
6.75	-6.0	15.9	0.86	-3.7	13.6	0.74
7.75	-7.1	16.9	0.91	-4.7	14.5	0.78
8.75	-7.3	17.1	0.93	-4.4	14.2	0.78
9.75	-7.5	17.3	0.94	-5.3	15.1	9.82
10.75	-7.4	17.2	0.92	-5.2	15.0	0.80
11.75	-5.9	15.8	0.83	-3.8	13.7	0.72
12.75	-7.0	16.9	0.88	-5.3	15.2	0.79
13.75	-7.2	17.1	0.88	-5.6	15.5	0.80
14.75	-6.3	16.2	0.83	-4.7	14.6	0.75
15.75	-8.0	17.8	0.92	-6.5	16.3	0.84
16.75	-8.0	17.8	0.88	-6.8	16.6	0.82
17.75	-7.4	17.2	0.83	-5.9	15.7	0.75
18.75	-7.7	17.5	0.79	-6.7	16.5	0.75
19.75	-7.6	17.5	0.75	-6.5	16.4	0.70
20.75	-6.7	16.7	0.71	-5.5	15.5	0.66
21.75	-5.3	16.3	0.64	-4.4	14.4	9.57
Average			0.83			0.74

Table D-1-3-1(b), continued

Distance from Closed End In	S_w = 0.57			S_w = 0.47		
	Φ mv	$\Phi_s - \Phi$ mv	Φ^a	Φ mv	$\Phi_s - \Phi$ mv	Φ^*
1.25	-2.1	12.0	0.68	-0.6	**10.5**	**0.59**
1.75	-2.7	12.6	0.71	**-1.1**	**11.0**	**0.62**
2.75	-2.3	12.2	0.67	-0.9	**10.8**	**0.59**
3.75	-0.1	10.1	0.56	1.2	8.8	**0.49**
4.75	-1.8	11.7	0.65	0.0	9.9	**0.55**
5.75	-3.7	13.6	0.75	**-1.8**	11.7	**0.65**
6.75	-3.0	12.9	0.70	**-1.3**	**11.2**	**0.61**
7.75	-3.9	13.7	0.74	-1.5	**11.3**	**0.61**
8.75	-3.7	13.5	0.74	-0.9	10.7	0.58
3.75	-4.8	14.6	0.79	-1.5	**11.3**	0.61
10.75	-4.1	13.9	0.74	-0.8	**10.6**	0.57
11.75	-2.3	12.2	0.64	0.6	**9.3**	0.49
12.75	-3.4	13.3	0.69	0.0	9.9	0.52
13.75	-3.2	13.1	0.68	0.0	9.9	**0.51**
14.75	-2.5	12.4	0.64	0.3	9.6	0.49
15.75	-4.4	14.2	0.74	**-1.2**	**11.0**	0.57
16.75	-3.7	13.5	0.67	-0.8	10.6	0.52
17.75	-2.6	12.4	0.60	**0.2**	9.6	0.46
18.75	-3.5	13.3	0.60	**-1.0**	**10.8**	0.49
19.75	-3.7	13.6	0.58	**-1.3**	**11.2**	0.48
20.75	-3.5	13.5	0.57	-1.7	**11.7**	0.50
21.75	-2.5	12.5	0.49	-0.5	10.5	**0.41**
Average			0.67			0.54

Table D-1-3-1(b), continued

Distance from Closed End In	S_w = 0.36 Φ mv	$\Phi_s - \Phi$ mv	Φ^*	S_w = 0.31 a mv	$\Phi_s - \Phi$ mv	Φ^*
1.25	1.8	8.1	0.46	3.1	6.8	**0.38**
1.75	1.6	8.3	0.47	2.9	7.0	0.39
2.75	1.6	8.3	0.46	**2.9**	7.0	0.38
3.75	3.0	7.0	0.39	4.0	6.0	0.33
4.75	2.3	7.6	0.42	**3.5**	6.4	0.36
5.75	1.1	8.8	0.49	2.3	7.6	0.42
6.75	1.5	8.4	0.45	2.7	7.2	0.39
7.75	1.5	8.3	0.45	2.7	7.1	0.38
8.75	1.7	8.1	0.44	2.8	7.0	0.38
9.75	1.3	8.5	0.46	2.4	7.4,	0.40
10.75	2.0	7.8	0.42	2.3	6.9	0.37
11.75	3.9	6.9	0.36	3.7	6.2	0.33
12.75	2.3	7-6	0.40	**3.1**	6.8	0.35
13.75	2.3	7.6	0.39	3.0	6.9	0.36
14.75	2.2	7.7	0.39	**3.1**	6.8	0.35
15.75	0.6	9.2	0.48	1.7	8.1	0.42
16.75	1.3	8.5	0.42	2.0	7.8	0.38
17.75	1.3	8.5	0.41	2.3	7.5	0.36
18.75	0	9.8	0.44	**1.6**	8.2	**0.37**
19.75	0.6	9.3	0.40	2.0	7.9	0.34
20.75	3.3	9.1	0.39	2.3	7.7	**0.33**
21.75	1.8	8.2	0.32	**3.3**	6.7	0.26
Average			0.42			0.37

Table D-1-3-1(b), Continued

Distance from Closed End In	S_w = 0.25			S_w = 0.13		
	Φ mv	$\Phi_s - \Phi$ mv	Φ^*	Φ mv	$\Phi_s - \Phi$ mv	Φ^*
1.25	4.2	5.7	0.32	6.6	3.3	0.19
1.75	4.1	5.8	0.33	6.5	3.4	0.19
2.75	4.0	5.9	0.32	6.4	3.5	0.19
3.75	4.8	5.2	0.29	6.9	3.1	0.17
4.75	4.4	5.5	0.31	6.8	3.1	0.17
5.75	3.4	6.5	0.36	6.1	3.8	0.21
6.75	3.7	6.2	0.34	6.1	3.8	0.21
7.75	3.7	6.1	0.33	6.1	3.7	0.20
8.75	3.8	6.0	0.33	6.1	3.7	0.20
9.75	3.7	6.1	0.33	6.0	3.8	0.21
10.75	4.1	5.7	0.30	6.0	3.8	0.20
11.75	4.7	5.2	0.27	6.5	3.4	0.18
12.75	9.3	5.6	0.29	6.3	3.6	0.19
13.75	4.2	5.7	0.29	6.4	3.5	0.18
14.75	4.2	5.7	0.29	6.5	3.4	0.17
15.75	3.3	6.5	0.34	6.1	3.7	0.19
16.75	3.6	6.2	0.31	6.4	3.4	0.17
17.75	3.5	6.3	0.30	6.5	3.3	0.16
18.75	2.8	7.0	0.32	6.4	3.4	0.15
19.75	3.1	6.8	0.29	6.7	3.2	0.14
20.75	3.4	6.6	0.28	7.0	3.0	0.13
21.75	4.2	5.8	0.23	7.6	2.4	0.09
Average			0.31			0.18

Table D-1-3-1(b), continued

Distance from Closed End In	S_w = 0.06			S_w = 0.19		
	Φ mv	$\Phi_s - \Phi$ mv	Φ^*	Φ mv	$\Phi_s - \Phi$ mv	Φ^*
1.25	7.8	2.1	0.12	5.7	4.2	0.24
1.75	7.6	2.3	0.13	5.5	4.4	0.25
2.75	7.6	2.3	0.13	5.4	4.5	0.25
3.75	7.8	2.2	0.12	6.3	3.7	0.20
4.75	7.9	2.0	0.11	5.9	4.0	0.22
5.75	7.4	2.5	0.14	5.2	4.7	0.26
5.75	7.2	2.7	0.15	5.3	4.6	0.25
7.75	7.0	2.8	0.15	5.2	4.6	0.25
8.75	6.9	2.9	0.16	5.2	4.6	0.25
9.75	6.8	3.0	0.16	5.1	4.7	0.25
10.75	7.0	2.8	0.15	5.3	4.5	0.24
11.75	7.3	2.6	0.14	5.8	4.1	0.22
12.75	7.1	2.8	0.15	5.4	4.5	0.23
13.75	7.1	2.8	0.14	5.4	4.5	0.23
14.75	7.2	2.7	0.14	5.5	4.4	0.23
15.75	6.9	2.9	0.15	4.9	4.9	0.25
16.75	7.2	2.6	0.13	5.1	4.7	0.23
17.75	7.3	2.5	0.12	5.3	4.5	0.22
18.75	7.4	2.4	0.11	4.9	4.9	0.22
19.75	7.8	2.1	0.09	5.1	4.8	0.21
20.75	8.1	1.9	0.08	5.2	4.8	0.20
21.75	3.7	1.3	0.05	5.6	4.4	0.17
Average			0.13			0.23

Table D-1-3-2(a): Mass In-Place, Temperature and Water Saturation

Run No.: SG2
Date: 02/17/76
Pore Volume: 0.02719 cu ft
Initial Mass: 1.6976 lb

Mass In-Place lb	Operating Temperature °F	Average Water Saturation Fraction
1.5199	300	0.98
1.4165	301	0.91
1.3162	301	0.84
1.2110	301	0.78
1.1056	300	0.71
0.9958	300	0.64
0,8900	299	0.57
0.766%	296	0.49
0.6398	300	0.41
0.5027	296	0.32
0.3437	300	0.22
0.1543	298	0.10

Table D-1-3-2(b): Probe Signal an2 Water **Saturation**

Distance from Closed End In	S_w = 1.00 Φ_s mv	Φ_w mv	$\Phi_s - \Phi_w$ mv	S_w = 0.98 Φ mv	$\Phi_s - \Phi$ mv	Φ^*
1.25	9.5	-5.3	14.80	-4.2	13.7	0.93
1.75	9.6	-5.4	15.0	-4.7	14.3	0.95
2.75	9.6	-5.5	15.1	-4.8	14.4	0.95
3.75	9.6	-5.9	15.5	-4.5	14.1	0.91
4.75	9.6	-5.6	15.2	-4.6	14.2	0.93
5.75	9.6	-5.8	15.4	-5.2	**14.8**	0.96
6.75	9.6	-6.4	16.0	-5.5	15.1	0.94
7.75	9.6	-6.0	15.6	-5.8	15.4	0.99
8.75	9.6	**-6.1**	15.7	-6.1	15.7	1.00
9.75	9.5	-6.2	15.7	**-6.2**	15.7	1.00
10.75	9.5	-6.2	15.7	-6.2	15.7	1.00
11.75	9.5	-6.2	15.7	-6.2	15.7	1.00
12.75	9.5	-6.5	16.0	-6.2	**15.7**	0.98
13.75	9.5	-6.5	16.0	-6.5	16.0	**1.00**
14.75	9.5	-6.6	16.1	-6.6	16.1	1.00
15.75	9.4	-6.8	16.2	-6.7	16.1	0.99
16.75	9.4	-7.3	16.7	**-7.2**	16.6	0.99
17.75	Q.4	-7.9	17.3	-7.7	17.1	0.99
18.75	9.4	-8.8	18.2	**-8.1**	**17.5**	**0.96**
19.75	0.4	-9.2	18.6	**-9.1**	**18.5**	0.99
20.75	3.4	-9.8	19.2	-9.3	**18.7**	0.97
21.75	9.4	-11.4	20.8	-10.5	19.9	0.96
Average						0.96

Table D-1-3-2(b), continued

Distance from Closed End In	S_w = 0.87 Φ mv	$\Phi_s - \Phi$ mv	Φ^*	S_w = 0.81 Φ mv	$\Phi_s - \Phi$ mv	Φ^*
1.25	-5.4	15.3	0.86	-4.9	14.8	0.84
1.75	-5.5	15.4	0.87	-4.5	14.4	**0.81**
2.75	-5.8	15.7	0.86	-5.3	15.2	*0.84*
3.75	-4.4	14.4	0.80	-3.4	13.4	0.74
4.75	-4.6	14.5	**0.81**	-3.9	**13.8**	0.77
5.75	-6.8	16.7	0.92	-6.4	16.3	0.90
6.75	-7.5	17.4	0.94	-7.0	16.9	**0.91**
7.75	-7.8	17.6	0.95	-7.7	17.5	0.95
8.75	-8.3	18.1	0.99	-7.7	17.5	0.96
9.75	-8.3	18.1	0.98	-7.9	**17.7**	0.96
10.75	-8.3	18.1	0.97	-7.8	17.6	0.94
11.75	-7.7	17.6	0.93	-6.6	16.5	0.87
12.75	-8.5	18.4	0.96	-7.4	17.3	0.90
13.75	-9.1	19.0	0.98	-8.4	18.3	0.94
14.75	-9.4	19.3	0.99	-8.0	17.9	0.92
15.75	-9.3	**19.1**	0.99	-8.a	18.6	0.96
16.75	-9.6	19.4	0.96	-9.2	**19.0**	*0.34*
17.75	-9.8	19.6	0.94	-8.8	18.6	0.89
18.75	-10.0	19.8	0.90	-9.0	**18.8**	0.85
19.75	-11.3	21.2	0.91	-8.7	18.6	0.80
20.75	-12.0	-22.0	0.93	-9.4	19.4	0.80
21.75	-13.5	-23.5	0.93	-10.4	20.4	0.80
Average			0.93			0.88

Table D-1-3-2(b), continued

Distance from Closed End In	S_w = 0.91 Φ mv	$\Phi_s-\Phi$ mv	Φ^*	S_w = 0.84 Q mv	$\Phi_s-\Phi$ mv	Φ^*
1.25	-3.6	13.1	0.89	-3.0	12.5	0.84
1.75	-4.0	13.6	0.91	-3.7	13.0	0.87
2.75	-4.2	13.8	0.91	-3.6	13.2	0.89
3.75	-3.3	12.9	0.83	-2.3	**11.9**	0.77
4.75	-3.6	13.2	0.89	-2.8	**12.4**	0.82
5.75	-5.2	14.8	0.96	-4.1	13.7	0.89
6.75	-5.2	14.8	0.93	-4.6	14.2	0.89
7.75	-5.2	14.8	0.95	-5.3	14.9	0.96
8.75	-5.5	15.1	0.96	-5.4	15.0	0.96
9.75	-5.4	14.9	0.95	-5.0	14.5	0.92
10.75	-5.5	15.0	0.96	-5.0	14.5	0.92
11.75	-4.9	14.4	0.92	-4.0	13.5	0.86
12.75	-5.7	15.2	0.95	-5.4	14.9	0.93
13.75	-6.1	15.6	0.98	-5.8	**15.3**	0.96
14.75	-6.2	15.7	0.98	-5.3	14.8	0.92
15.75	-6.3	15.7	0.98	-6.4	15.8	0.98
16.75	-6.4	15.8	0.95	-6.3	15.7	0.94
17.75	-7.1	16.5	0.95	**-6.2**	15.6	0.90
18.75	-7.1	16.5	0.91	-6.6	**16.0**	0.88
19.75	-8.2	17.6	0.95	**-7.1**	16.5	0.89
20.75	-8.2	17.6	0.92	-6.9	16.3	0.85
21.75	-8.4	17.8	0.86	-6.8	16.2	0.78
Average			0.93			0.89

Table D-1-3-2(b), continued

Distance from Closed End In	$S_w = 0.78$ Φ mv	$\Phi_s - \Phi$ mv	Φ^*	$S_w = 0.71$ Φ mv	$\Phi_s - \Phi$ mv	Φ^*
1.25	-2.0	11.5	0.78	-1.9	11.4	0.77
1.75	-2.2	11.8	0.79	-2.1	11.7	0.78
2.75	-2.5	12.1	0.80	-2.3	11.9	0.79
3.75	-0.4	10	0.65	-0.4	10.0	0.65
4.75	-1.6	11.2	0.74	-1.6	11.2	0.74
5.75	-3.5	13.1	0.85	-2.8	12.4	0.81
5.75	-3.1	12.7	0.79	-2.6	12.2	0.76
7.75	-3.9	13.5	0.87	-3.0	12.6	0.81
8.75	-3.9	13.5	0.86	-2.9	12.5	0.80
9.75	-4.2	13.7	0.87	-3.3	12.8	0.82
10.75	-4.2	13.7	0.87	-2.6	12.1	0.77
11.75	-3.2	12.7	0.81	-1.6	11.1	0.71
12.75	-4.2	13.7	0.86	-2.8	12.3	0.77
13.75	-5.2	14.7	0.92	-2.8	12.3	0.77
14.75	-4.4	13.9	0.86	-2.5	12.0	0.75
15.75	-6.1	15.5	0.96	-4.6	14.0	0.86
16.75	-6.5	15.9	0.95	-5.5	14.9	0.89
17.75	-6.0	15.4	0.89	-4.8	14.2	0.82
18.75	-6.4	15.8	0.87	-5.1	14.5	0.80
19.75	-5.0	15.4	0.83	-4.9	14.3	0.77
20.75	-6.5	15.9	0.83	-4.3	13.7	0.71
21.75	-5.2	14.6	0.70	-3.4	12.8	0.62
Average			0.83			0.77

Table D-1-3-2(b), continued

Distance from Closed End In	S_w = 0.64 Φ mv	$\Phi_s - \Phi$ mv	Φ^*	S_w = 0.57 Φ mv	$\Phi_s - \Phi$ mv	Φ^*
1.25	-1.5	11.0	0.74	-0.5	10.0	0.68
1.75	-1.5	11.1	0.74	-0.8	10.4	0.69
2.75	-1.5	11.1	0.74	-0.8	10.4	0.69
3.75	0.4	9.2	0.59	-1.2	8.4	0.54
4.75	-0.7	10.3	0.68	0.2	9.4	0.62
5.75	-2.3	11.9	0.77	-1.2	10.8	0.70
6.75	-1.6	11.2	0.70	-0.6	10.2	0.64
7.75	-2.2	11.8	0.76	-1.2	10.8	0.69
8.75	-1.6	11.2	0.71	-0.3	9.9	0.63
9.75	-2.1	11.6	0.74	-1.0	10.5	0.67
10.75	-1.5	11.0	0.70	-0.3	9.8	0.62
11.75	-0.3	9.8	0.62	0.9	8.6	0.55
12.75	-1.4	1.0.9	0.68	0	9.5	0.59
13.75	-1.1	1.0.6	0.66	0.2	9.3	0.58
14.75	-1.1	1.0.6	0.66	0.3	9.2	0.57
15.75	-3.2	12.6	0.78	-1.6	11.0	0.68
16.75	-3.4	12.8	0.77	-1.4	10.8	0.65
17.75	-2.7	1.2.1	0.70	-0.9	10.3	0.60
18.75	-4.1	13.5	0.74	-2.3	11.7	0.64
19.75	-3.5	12.9	0.69	-2.0	11.4	0.61
20.75	-3.1	12.5	0.65	-1.7	11.1	0.58
21.75	-2.1	11.5	0.55	-0.7	10.1	0.49
Average			0.70			0.62

Table D-1-3-2(b), continued

Distance from Closed End In	S_w = 0.49			S_w = 0.41		
	Φ mv	$\Phi_s - \Phi$ mv	Φ^*	Φ mv	$\Phi_s - \Phi$ mv	&*
1.25	1.0	0.85	0.57	1.7	7.8	0.53
1.75	0.6	3	0.60	1.5	8.1	0.54
2.75	0.9	8.7	0.58	1.6	8	0.53
3.75	2.6	7	0.45	3.0	6.6	0.43
4.75	1.6	8	0.53	2.4	7.2	0.47
5.75	0.4	9.2	0.60	1.4	8.2	0.53
6.75	1.0	8.6	0.54	1.7	7.9	0.49
7.75	0.7	8.9	3.57	1.8	7.8	0.50
8.75	1.2	8.4	0.54	2.0	7.6	0.48
9.75	0.6	8.9	0.57	1.5	8.0	0.51
10.75	1.1	8.4	0.54	2.1	7.4	0.47
11.75	2.3	7.2	0.46	2.8	6.7	0.43
12.75	1.6	7.9	0.49	2.4	7.1	0.44
13.75	1.6	7.3	0.49	2.4	7.1	0.44
14.75	1.7	7.8	0.48	2.3	7.2	0.45
15.75	0	9.4	0.58	1.0	8.4	0.52
16.75	0.4	9.0	0.54	1.4	8.0	0.48
17.75	0.6	8.8	0.51	1.5	7.9	0.46
18.75	-0.7	10.1	0.55	0.4	9.0	0.49
19.75	-1.0	10.4	0.56	0.4	9.0	0.48
20.75	-1.5	10.9	0.57	0.8	8.6	0.45
21.75	-0.5	9.9	0.48	1.7	7.7	0.37
Average			0.54			0.48

Table D-1-3-2(b), continued

Distance from Closed End In	S_w = 0.32			S_w = 0.22		
	a mv	$\Phi_s - \Phi$ mv	Φ^*	Φ mv	$\Phi_s - \Phi$ mv	Φ^*
1.25	3.3	6.20	0.42	5.2	4.3	0.29
1.75	3.2	6.4	0.43	5.1	4.5	0.30
2.75	3.4	6.2	0.41	5.1	4.5	0.30
3.75	4.2	5.4	0.35	5.8	3.8	0.25
4.75	3.9	5.7	0.38	5.6	4.0	0.26
5.75	3.0	6.6	0.43	5.0	4.6	0.30
6.75	3.3	6.3	0.39	5.1	4.5	0.28
7.75	3.3	6.3	0.40	5.1	4.5	0.29
8.75	3.5	6.1	0.39	5.1	4.5	0.29
9.75	3.2	6.3	0.40	4.9	4.6	0.29
10.75	3.6	5.9	0.38	5.1	4.4	0.28
i1.75	4.3	5.2	0.33	5.6	3.9	0.25
12.75	3.9	5.6	0.35	5.3	4.2	0.26
13.75	3.8	5.7	0.36	5.3	4.2	0.26
14.75	3.8	5.7	0.35	5.4	4.1	0.25
15.75	2.7	6.7	0.41	4.9	4.5	0.28
16.75	2.8	6.6	0.40	5.0	4.4	0.26
17.75	3.0	6.4	0.37	4.9	4.5	0.26
18.75	2.2	7.2	0.40	4.5	4.9	0.27
19.75	2.3	7.1	0.38	4.5	4.9	0.26
20.75	2.5	6.9	0.36	4.7	4.7	0.24
21.75	3.3	6.1	0.29	5.1	4.3	0.21
Average			0.38			0.26

Table D-1-3-2(b), continued

$S_w = 0.10$

Distance from Closed End In	Φ mv	$\Phi_s - \Phi$ mv	Φ^*
1.25	7.0	2.5	0.17
1.75	7.0	2.6	0.17
2.75	7.0	2.6	0.17
3.75	7.3	2.3	0.15
4.75	7.2	2.4	**0.16**
5.75	6.9	2.7	0.18
5.75	6.8	2.8	0.18
7.75	5.6	3.0	0.19
8.75	6.6	3.0	0.19
9.75	6.5	3.0	0.19
10.75	6.6	2.9	0.18
11.75	6.8	2.7	0.17
12.75	6.7	2.8	0.18
13.75	6.6	2.9	0.18
14.75	6.8	2.7	0.17
15.75	6.6	2.8	0.17
16.75	6.7	2.7	0.16
17.75	6.8	2.6	0.15
18.75	6.8	2.6	0.14
19.75	7.1	2.3	0.12
20.75	7.2	2.2	0.11
21.75	7.4	2.0	0.10
Average			0.16

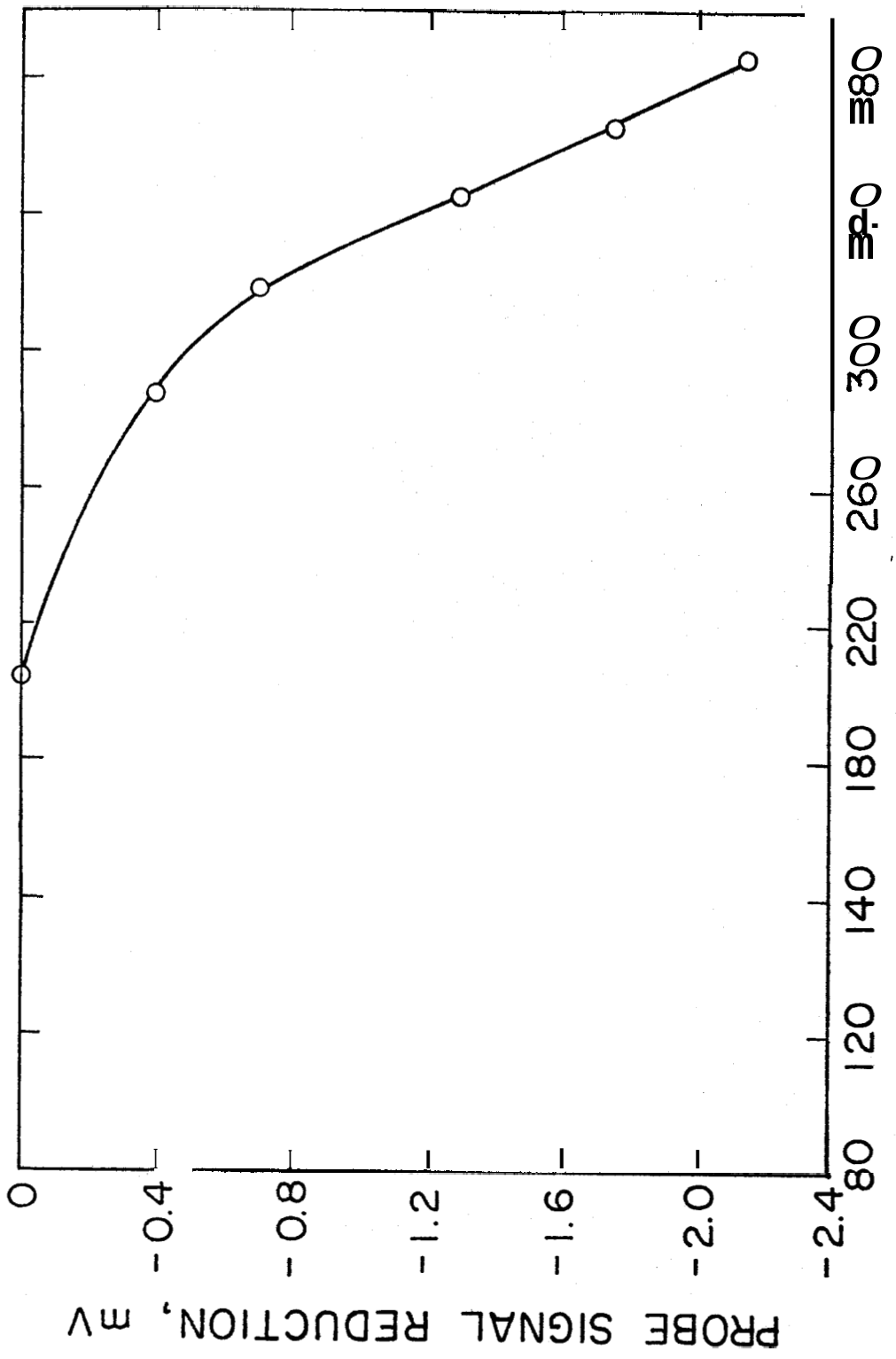

FIGURE D-1-1. TEMPERATURE EFFECT ON CAPACITANCE PROBE WITH THE PROBE IMMERSED IN THE AIR BATH

D-2. EXPERIMENTAL DATA FOR STEADY, TWO-PHASE FLOW EXPERIMENTS

The summaries of inlet and outlet pressure, mass flow rate, and inlet and outlet temperature are as follows:

Run No.	1	2	3	4
Inlet pressure, psig	79.0	105	104	108
Outlet pressure, psig	12.0	21	16.5	35
Mass flow rate, gm/min	9.7	7.0	7.9	8.0
Inlet temperature, ^{o}F	294	339	336	337
Outlet temperature, ^{o}F (at 23 in from inlet end)	238	244	234	273

The temperature and saturation profiles will be presented in the following tables.

Table D-2-1: Probe Signal and Saturation Profile for Steady, Two-Phase Flow, Run 1

x in	Φ_s mv	Φ_w mv	$\Phi_s-\Phi_w$ mv	Φ mv	$\Phi_s-\Phi$ mv	Φ^*	E_w
1.25	5.5	-10.6	16.2	**-10.5**	16.2	1.0	1.0
1.75	5.9	-10.8	16.7	-11.0	16.9	1.0	1.0
2.75	5.6	-10.6	16.2	**-10.6**	16.2	1.0	1.0
3.75	5.4	-10.6	16.0	-10.5	15.9	0.99	0.97
4.75	5.5	-10.1	15.6	-10.2	**15.7**	1.0	**1.0**
5.75	5.?	-9.9	15.6	-9.9	15.5	**1.0**	1.0
6.75	5.8	-9.7	15.5	-9.7	15.5	**1.0**	**1.0**
7.75	5.7	-9.8	15.5	-9.7	15.4	0.99	0.97
8.75	6.0	-9.2	15.2	-9.2	15.2	**1.0**	1.0
3.75	6.2	-8.8	15.0	-8.8	15.0	**1.0**	**1.0**
10.75	6.2	-7.8	14.0	-7.8	14.0	**1.0**	**1.0**
11.75	6.5	-7.5	14.3	-7.8	**14.3**	1.0	1.0
12.75	6.1	-6.9	13.0	-6.8	12.9	0.99	0.97
13.75	5.8	-6.6	12.4	-6.E	12.4	1.0	1.0
14.75	5.8	-7.0	12.8	-7.0	**12.8**	12.8	1.0
15.75	5.6	-8.2	13.8	-8.2	**13.8**	1.0	1.0
15.75	5.4	-9.1	14.5	-9.1	14.5	**1.0**	**1.0**
17.75	5.2	-9.7	14.9	-9.5	**14.7**	0.99	0.97
18.75	5.2	-10.0	15.2	-9.6	**14.8**	0.98	0.96
19.75	4.9	-10.4	15.3	-9.9	**14.8**	0.97	0.94
20.75	5.1	-10.5	15.7	-10.1	**15.2**	0.97	0.94
21.75	5.5	-10.6	16.1	-10.1	**15.6**	0.97	0.94

Note: X indicates the distance **from inlet** end.

Table D-2-2: Probe Signal and Saturation Profile for Steady, Two-Phase Flow

		RUN 2						RUN 3				RUN 4			
x_{tp} in	Φ_s	Φ_w	$\Phi_{\Delta 1}$ [2]	Φ	$\Phi_{\Delta 2}$ [3]	Φ^* [4]	S_w	Φ	$\Phi_{\Delta 2}$	Φ^*	S_w	Φ	$\Phi_{\Delta 2}$	Φ^*	S_w
1.25	4.8	-11.4	16.2	-11.4	16.2	1.0	1.0	-11.4	16.2	1.	1.0	-11.5	16.3	1.0	1.0
1.75	5.1	-11.6	16.7	-11.3	16.4	0.98	0.96	-11.2	16.3	0. 8	0.96	-11.4	16.5	0.99	0.97
2.75	4.6	-11.8	16.4	-11.5	16.1	0.98	0.96	-11.4	16.0	0. 8	0.96	-11.6	16.2	0.99	0.97
3.75	4.6	-11.7	16.3	-11.4	16.0	0.98	0.96	-11.4	16.0	0. 8	0.96	-11.6	16.2	0.99	0.97
4.75	4.6	-11.4	16.0	-11.0	15.6	0.98	0.96	-10.8	15.4	0. 6	0.92	-11.1	15.7	0.98	0.96
5.75	4.8	-11.2	16.0	-10.7	15.5	0.97	0.94	-10.6	15.4	0. 6	0.92	-10.8	15.6	0.98	0.96
6.75	4.9	-10.9	15.8	-10.3	15.2	0.96	0.92	-10.2	15.1	0. 8	0.96	-10.5	15.4	0.97	0.94
7.75	4.8	-10.7	15.5	-10.1	14.9	0.96	0.92	-9.9	14.7	0. 5	0.91	-10.3	15.1	0.97	0.94
8.75	5.2	-10.0	15.2	-9.3	14.5	0.95	0.91	-9.2	14.4	0. 5	0.91	-9.6	14.8	0.97	0.94
9.75	5.6	-9.6	15.2	-8.8	14.4	0.95	0.91	-8.8	14.4	0. 5	0.91	-9.0	14.6	0.96	0.92
10.75	5.5	-8.4	13.9	-6.6	12.1	0.87	0.81	-6.4	11.9	0. 6	0.80	-7.0	12.5	0.90	0.85
11.75	5.8	-7.0	12.8	-5.9	11.7	0.91	0.86	-5.8	11.6	0. 1	0.86	-6.3	12.1	0.95	0.91
12.75	5.6	-7.6	13.2	-7.2	12.8	0.97	0.94	-7.1	12.7	0. 6	0.92	-5.9	11.5	0.87	0.81
13.75	5.1	-8.2	13.3	-8.1	13.2	0.99	0.97	-8.0	13.1	0. 8	0.96	-8.3	13.4	1.01	1.0
14.75	5.0	-8.9	13.9	-8.6	13.6	0.98	0.96	-8.5	13.5	0. 7	0.94	-8.8	13.8	0.99	0.97
15.75	4.8	-9.1	13.9	-8.8	13.6	0.98	0.96	-8.7	13.5	0. 7	0.94	-8.8	13.5	0.98	0.96
16.75	4.9	-10.4	15.3	-9.4	14.3	0.93	0.88	-9.3	14.2	0. 3	0.88	-9.5	14.4	0.94	0.90
17.75	4.7	-10.4	15.1	-9.9	14.6	0.97	0.94	-9.8	14.5	0. 6	0.92	-9.9	14.6	0.97	0.94
18.75	4.9	-10.4	15.3	-9.7	14.6	0.95	0.91	-9.6	14.5	0. 5	0.91	-9.9	14.8	0.97	0.94
19.75	4.6	-10.5	15.1	-9.8	14.4	0.95	0.91	-9.6	14.2	0. 4	0.90	-9.8	14.4	0.95	0.91
20.75	4.7	-10.6	15.3	-9.7	14.4	0.94	0.90	-9.6	14.3	0 3	0.88	-9.8	14.5	0.95	0.91
21.75	5.2	-10.6	15.8	-9.6	14.8	0.94	0.90	-9.5	14.7	0 3	0.88	-9.6	14.8	0.94	0.90

Note: 1. x indicates the distance from inlet end.

2. $\Phi_{\Delta 1} = \Phi_s - \Phi_w$

3. $\Phi_{\Delta 2} = \Phi_s - \Phi$

4. $\Phi^* = \frac{\Phi_{\Delta 2}}{\Phi_{\Delta 1}}$

Table D-2-3: Temperature Profile for Steady, Two-Phase Flow

x-[1] in	Run 1	Run 2	Run 3	Run 4
	294	339	336	337
	294	339	336	336
4	294	339	336	335
6	294	339	335	335
8	294	338	334	334
10	294	335	332	333
12	293	332	330	332
14	292	329	327	331
16	290	324	322	329
18	233	315	314	324
19	-	-	-	319
20	275	300	298	313
21	-	-	-	303
22	252	272	265	293
23	238	244	234	273

Note 1: X indicates the distance from Inlet End

D.3. EXPERIMENTAL DATA FOR DEPLETION BATCH EXPERIMENTS

The experimental data for these experiments will include mass production, inlet and outlet pressure, and temperature profiles.

Table D-3-1: Mass Production and Temperature History for Depletion Experiment Run No. 1

(Ambient Temperature: 298°F)

Time min	Mass Produced gm	Core Pressure - psig Distance from Closed End, inches 0	23.5
0	0	109	108
1	34	46	20
6	51	43	13
16	80	43	9.5
46	124	41	10
52	130	41	10
72	150.7	41	9

Distance from Closed End In	Temperature °F Time, min 0	1	6	16	46	52	72
0	296	297	297	296	295	295	294
4	295	296	296	295	293	293	291
8	294	294	295	294	289	289	286
12	293	293	293	291	283	282	279
16	293	292	290	283	273	274	270
20	294	281	269	262	257	257	253
21	-	-	-	-	-	-	244
22	-	-	-	-	-	-	264
23	297	236	228	224	242	252	264

Table D-3-2: Mass Production and Temperature History for Depletion Experiment Run No. 2

(Ambient Temperature: 342°F)

Time min	Mass Produced gm	Core Pressure - psig, Distance from Closed End, inches: 0	23.5
0	0	212	213
1	47	100	45
6	80	100	25
16	121	97	21
31	158.8	93	20
51	195.7	88	18
111	291.0	72	14

Distance from Closed End In	Temperature °F, Time, min: 0	1	5	17	32	53	114
0	340	340	339	338	336	331	321
2	-	-	-	-	335	331	320
4	338	338	338	337	333	328	317
6		-	-	336	331	325	314
8	337	337	336	331	325	319	309
10	-	-	-	326	320	312	304
12	335	336	333	321	316	308	299
14	-	-	328	316	309	301	293
16	334	332	322	309	303	295	288
18	334	323	312	298	294	285	284
19	-	-	-	-	-	279	285
20	334	318	296	283	281	273	291
21	335	295	285	273	273	266	302
22	338	281	272	264	264	260	310
23	339	245	238	226	267	301	322

Table D-3-3: Probe Signal and Water Saturation for Depletion Experiment Run No. 1

	t = 0			t = 1 min				t = 16 min			
x	Φ_s	Φ_w	$\Phi_s-\Phi_w$	Φ	$\Phi_s-\Phi$	Φ^*	S_w	Φ	$\Phi_s-\Phi$	Φ^*	S_w
in	mv	mv	mv	mv	mv			mv	mv		
1.25	5.6	-10.8	16.4	-10.1	15.7	0.99	0.97	-9.4	15.0	0.91	0.86
4.75	5.5	-10.7	16.2	-10.3	15.8	0.98	0.96	-10.0	15.5	0.96	0.92
8.75	6.0	-9.4	15.4	-9.0	15.0	0.97	0.94	-8.7	14.6	0.95	0.91
12.75	6.1	-6.6	12.7	-6.0	12.1	0.95	0.91	-5.1	11.2	0.88	0.82
16.75	5.4	-9.0	14.4	-8.4	13.8	0.96	0.92	-7.4	12.8	0.89	0.83
20.75	5.1	-10.6	15.7	-9.5	14.6	0.93	0.88	-9.0	14.1	0.90	0.84
21.75	5.5	-10.5	16.0	-9.3	14.8	0.93	0.88	-8.8	14.4	0.90	0.84

Note: x = distance from closed end, in.

	t = 52 min			
x				
in				
1.25	-9.2	14.8	0.90	0.84
4.75	9.6	15.1	0.93	0.88
8.75	8.6	14.6	0.95	0.91
12.75	5.6	11.8	0.92	0.87
16.75	7.4	12.8	0.89	0.83
20.75	8.9	14.0	0.89	0.83
21.75	8.7	14.2	0.89	0.83

Table D-3-4: Probe Signal and Water Saturation for Depletion Experiment Run No. 2

	t = 0			t = 1 min				t = 6 min			
x^1	Φ_s	Φ_w^t	$\Phi_s-\Phi_w$	Φ	$\Phi_s-\Phi$	Φ^*	S_w	Φ	$\Phi_s-\Phi$	Φ^*	S_w
in	mv	mv	mv	mv	mv			mv	mv		
1.25	5.0	-11.3	16.3	-11.3	16.3	1.0	1.0	-10.9	15.9	0.98	0.96
2.75	4.7	-11.5	16.2								
4.75	4.7	-11.4	16.1	-11.4	16.1	1.0	1.0	-10.9	15.6	0.97	0.94
6.75	5.0	-10.9	15.9								
8.75	5.2	-10.6	15.8	-10.1	15.3	0.97	0.94	-9.3	14.5	0.92	0.87
10.75	5.6	-10.2	15.8								
12.75	5.7	-7.8	13.5	-7.6	13.3	0.99	0.97	-6.7	12.4	0.92	0.87
14.75	5.2	-8.5	13.7								
16.75	4.8	-9.6	14.4	-9.5	14.3	0.99	0.97	-8.4	13.2	0.92	0.87
18.75	4.5	-10.2	14.7								
20.75	4.4	-10.3	14.7	-10.0	14.3	0.98	0.96	-9.2	13.6	0.93	0.88
21.75	5.0	-10.3	15.3	-9.8	14.3	0.97	0.94	-9.1	14.1	0.92	0.87
22.0	5.5	-9.3	14.8	-8.9	14.3	0.97	0.94	-8.1	13.6	0.92	0.87

Note: x = distance from closed end, in.

Table D-3-4, continued

	t = 16 min				t = 51 min				t = 111 min			
x^1	Φ	$\Phi_s-\Phi$	Φ^*	S_w	Φ	$\Phi_s-\Phi$	Φ^*	S_w	Φ	$\Phi_s-\Phi$	Φ^*	S_w
in	mv	mv			mv	mv			mv	mv		
1.25	-9.3	14.3	0.88	0.82	-9.7	14.7	0.90	0.84	-6.0	11.0	0.67	0.60
2.75	-10.0	14.7	0.91	0.86	-9.8	14.5	0.90	0.84	-7.3	12.0	0.74	0.67
4.75	-10.0	14.7	0.91	0.86	-9.1	13.8	0.86	0.80	-7.1	11.8	0.73	0.66
6.75	-9.1	14.1	0.89	0.83	-8.2	13.2	0.83	0.76	-6.3	11.3	0.71	0.65
8.75	-8.1	13.3	0.84	0.77	-7.2	12.4	0.78	0.71	-5.9	11.1	0.70	0.63
10.75	-6.2	11.8	0.75	0.68	-4.8	10.4	0.66	0.59	-3.8	9.4	0.59	0.53
12.75	-5.3	11.0	0.74	0.81	-5.2	10.9	0.81	0.74	-4.0	9.7	0.72	0.65
14.75	-7.3	12.5	0.91	0.86	-6.7	11.9	0.87	0.81	-4.3	9.5	0.69	0.62
16.75	-7.8	12.6	0.88	0.82	-7.0	11.8	0.82	0.75	-3.6	8.4	0.58	0.52
18.75	-8.5	13.0	0.88	0.82	-7.6	12.1	0.82	0.75	-1.4	5.9	0.40	0.34
20.75	-8.8	13.2	0.90	0.84	-7.5	11.9	0.81	0.74	3.8	0.6	0.04	0.02
21.75	-8.5	13.5	0.88	0.82	-6.7	11.7	0.76	0.69	4.8	0.2	0.01	0
22.0	-7.4	12.9	0.87	0.81	-5.8	11.3	0.76	0.69	5.3	0.2	0.01	0

Note: x = distance from closed end, in.

D-4 EXPERIMENTAL DATA FOR BRINE EXPERIMENTS

The experimental data include the resistivities of produced water and deposited salt content in the core.

Table D-4-1: Resistivity of Water Produced for Brine Experiment

Water Produced gm	Dip Cell Meter Reading (m), Ω	Resistivity m ÷ 1.26 Ω - cm
47.5	56.3	44.7
97.5	56.3	44.7
149.6	88.0	69.8
211.9	2,140	1698.4
315.3	38,800	30793.6
326.6	52,800	41904.8
Brine @ 12000 ppm	49.2	39.0

Table D-4-2: Salt Deposition in the Core

Core No.	Salt Deposited gm	Salt per Tore Volume gm/cc X 10^3
1	0.1660	4.824
3	0.1418	4.391
4	0.1770	5.500
6	0.1982	6.167
8	0.2111	7.000
9	0.2434	7.547
10	0.2444	7.433
11	0.3596	11.126

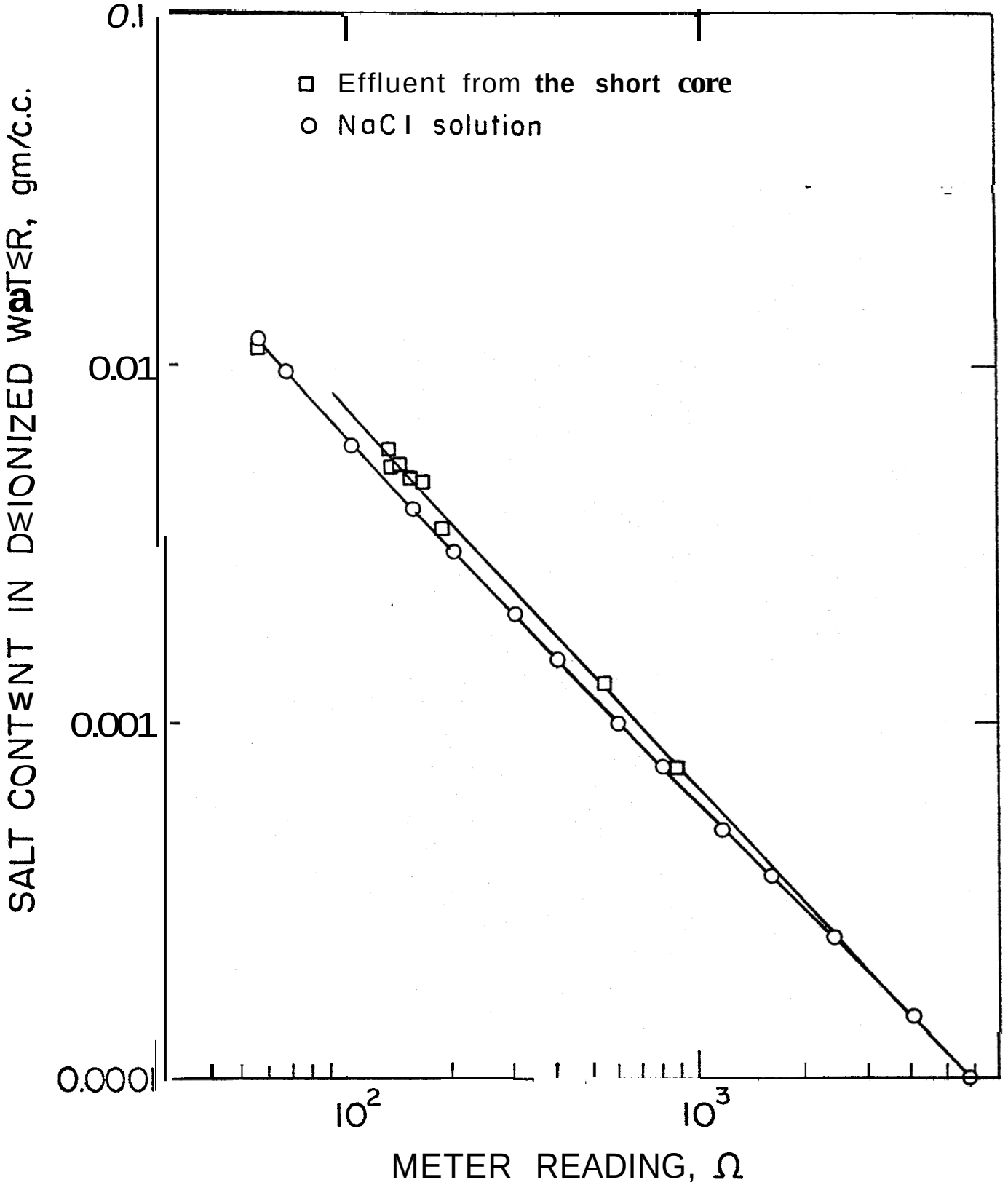

FIGURE 3-4-1. SALT CONCENTRATION VS. DIP CELL CONDUCTIVITY METER READING

APPENDIX E

PROCEDURE FOR DETERMINING SALT CONTENT AND PERMEABILITY CHANGE CAUSED BY SALT

1. Cut core into about 2-inch lengths using tungsten carbide hacksaw.
2. Measure length and diameter.
3. Cover outside diameter of the core with resin. Plug glass guide with rubber stopper and plug thermocouple well with epoxy. Core is wrapped with a heat shrinkable tubing. Slide the core with sleeve into a silicone rubber sleeve. Fasten ends with hose clamps.
4. Measure permeability to nitrogen using standard upstream pressure (1.031 atm to 1.032 atm) and standard downstream pressure (1.010 atm).
5. Flood with 3 pore volumes of deionized water.
6. Measure resistivity of the effluent at each pore volume.
7. Calibrate the dip cell conductivity meter in the range of salt concentration noted in 6.
8. Reduce water in the core by flooding with nitrogen.
9. Dry in oven.
10. Measure k_{N_2} again using same upstream and downstream pressure.